ABSTRACT

COMPUTATIONAL DETERMINATION OF LAMINAR FLOW
LOSS COEFFICIENTS IN A 90° CHANNEL BEND

by
Leonard Paul Parkin

Loss coefficients for laminar two dimensional incompressible channel (or duct) flow in a 90° bend are investigated using FEM software, FIDAP. This problem consists of a two dimensional duct with a 90° bend of constant radius flowing with water, at 70°F and atmospheric conditions. The bend radius to duct width ratios examined were 1.5 and 1.0. Both bend radius to duct width ratios were analyzed for Reynolds Number ranging from 50 to 1800. The pressure and velocity distributions were found and used to determine the pressure loss due to the bend. The results show the pressure loss effect due to the bend as a dimensionless coefficient plotted versus Reynolds Number.

It was found that the loss coefficient increases with decreasing Reynolds Number and increases with decreasing bend radius. The loss coefficient values ranged from 0.188 to 1.367 for a bend radius to duct width ratio of 1.5 and varied from 0.498 to 3.929 for a bend radius to duct width ratio of 1.0. These results can be compared with plots of existing pressure loss coefficients for like duct geometry. The results show a similar trend with existing empirical data.

COMPUTATIONAL DETERMINATION OF LAMINAR FLOW LOSS COEFFICIENTS IN A 90° CHANNEL BEND

by
Leonard Paul Parkin

A Thesis
Submitted to the Faculty of
New Jersey Institute of Technology
in Partial Fulfillment of the requirements for the Degree of
Master of Science

Department of Mechanical Engineering

October 1997

Blank Page

APPROVAL PAGE

COMPUTATIONAL DETERMINATION OF LAMINAR FLOW LOSS COEFFICIENTS IN A 90° CHANNEL BEND

Leonard Paul Parkin

Dr. Rong Yaw Chen, Thesis Advisor   Date
Professor of Mechanical Engineering, NJIT

Dr. Pasquale Florio, Committee Member   Date
Associate Chairman of Mechanical Engineering, NJIT

Dr. Pushpendra Singh, Committe Member   Date
Associate Professor of Mechanical Engineering, NJIT

BIOGRAPHICAL SKETCH

Author: Leonard Paul Parkin

Degree: Master of Science

Date: October 1997

Date of Birth: May 29, 1971

Place of Birth: Summit, New Jersey USA

Undergraduate and Graduate Education:

- Master of Science in Mechanical Engineering,
  New Jersey Institute of Technology, Newark, NJ, 1997

- Bachelor of Engineering in Mechanical Engineering
  Stevens Institute of Technology, Hoboken, NJ, 1994

Major: Mechanical Engineering

This thesis is dedicated to the memory of
Anne Dunne, William Dunne, William Dunne, Jr., and Leonard P. Parkin, Sr.

ACKNOWLEDGMENT

TABLE OF CONTENTS

TABLE OF CONTENTS
(Continued)

LIST OF TABLES

LIST OF FIGURES

Figure	Page

LIST OF FIGURES
(Continued)

LIST OF FIGURES

CHAPTER 1

INTRODUCTION

1.1 Applications

Advances in computer technology and computational modeling have made it possible to derive accurate solutions within the realm of fluid mechanics. The computational approach allows timely investigation of various model configurations under different physical conditions. This quick analysis reduces time costs in the design phases. With reduced design time, manufacturing processes for industry can become highly adept, and thus more competitive. With the evolution of the microcomputer, complex numerical analysis have become commonplace and a new paradigm in product evaluation has developed. Any industry not assimilating this technical approach will lack a competitive edge and struggle in this new fast paced environment.

Within research, the computational analysis approach has offered distinct advantages for laboratory experimental techniques. This approach has the dual advantage of eliminating disturbances that arise from measurement devices, as well as forming detailed information on all physical variables throughout the flow domain. Typically, computational and experimental techniques go hand in hand: A computational analysis is generally used for fine tuning the scope of laboratory techniques and confirming numerical solutions to complex problems. Historically, the engineering design approach has consisted of constructing a physical model, conducting laboratory experiments, and then interpreting the data for a verifiable relationship. With computational analysis, different models can be investigated then a good approximation can be decided upon for a physical

model. Acting as a gauge, researchers can also determine if their experimental results fit the theoretical trends, and if not, easily search for reasons for discrepancies.

For this project, the pressure loss will be determined in a two-dimensional channel bend for Reynolds numbers ranging from 50 to 1800. Within industry, study of pressure loss through tubes, pipes, and other closed conduits plays an important role for the design of many engineering applications. Although the main focus of this project is a numerical investigation, it is important to mention the practical applications of the present project. Some examples include

Heating, ventilating, and air conditioning (HVAC). Determining the proper duct work to transport volumes of air throughout dwellings involves accounting for various duct sizes, bends, entrances, and exits. With better understanding of the pressure losses resulting from these components, a more efficient system can be configured to satisfy the needs of the building. An optimum pump rating can than be determined for any system and allow for savings in operating costs.

Food and Beverage Industries. The manufacturing of food stuffs requires precision assembly line processes for maximum safety and efficiency. More importantly, care is required to avoid contamination of various products. Pressure development within hydraulic lines, supply lines and other critical medium needs to be understood to avoid equipment failure which may result in contamination. Problem areas near bends and other weak connections may be properly identified and eliminated from causing harm.

Power Industries (Nuclear, Coal, Gas, etc.): Power producing systems require transportation of water in various states through sometimes complex piping systems.

Pump requirements can be determined by realizing pressure loss components within the system. Concurrently, high pressure areas can be identified which may result in a sometimes fatal result. Flows of this type typically involve supersonic speeds within the pipes. This flow is almost impossible to solve analytically, and this is where the advantage of numerical analysis bears useful results.

1.2 Basic Concepts of Computational Finite-Element Analysis

The finite-element method (FEM) is well suited for work with a digital computer. The FIDAP fluid dynamics analysis package is a general purpose computer program that uses the finite-element method to simulate many classes of fluid flow models. FIDAP contains several program modules designed to model, solve, and post-process fluid flow problems. Analyses are limited in size only by practical considerations of computer time and the capacity of secondary storage devices. The FEM solution technique has a relatively short history in computational fluid mechanics. Known for its popularity in structural analyses, FEM is becoming a convincingly powerful tool in fluid mechanics as well.

For the problem presented in this writing the equations of continuity and momentum are solved with the finite-element package FIDAP. The model to be considered is a two-dimensional channel containing a 90° bend of constant radius. The flow is low in viscosity, steady in state and ranges in Reynolds number from 50 to about 1800, thus remaining in the laminar flow region. Typically, an analytical solution of this problem would provide numerical values at all points of the region of interest, while the numerical method gives values only at the nodal points contained in the FEM region.

However, an analytical solution of such a problem would require a large amount of time, and a solution is not always guaranteed. The FEM approach divides the flow domain into smaller, finite regions called elements. The partial differential equations of fluid mechanics that govern the fluid flow are approximated by the integral form of ordinary differential equations as algebraic equations in each element. These system of equations are then solved by proven numerical techniques to determine the velocities, pressures, and other desired quantities throughout the region. The conditions of these quantities at the boundary of the domain are known initially, and are used to find the state of the domain a small, finite distance away from the boundary.

1.3 Scope of Work

This project intends to use FIDAP to solve a viscous, laminar, steady-state, two-dimensional flow problem. The geometry of the model is described as follows:

- A 90° channel bend with constant radius

- A bend radius to duct width ratio of 1.5

- An inlet length of 5 duct widths

- An outlet length of at least 60 duct widths

FIDAP is an excellent computer driven numerical solver and will be utilized to compare previously established empirical data. Figure 1.3.1 shows a curve relating Reynolds Number to pressure loss due to various duct geometries. This experiment will concentrate

on comparing data to the curve for a 90° Ell. The flows considered will be of low Reynolds numbers ranging from 50 to 1800, and any realm dealing with turbulence will not be considered. The pressure distribution will be found for several different Reynolds Numbers. Once a pressure distribution profile is determined, a mean pressure loss will be calculated for each Reynolds number running through the bend. Using the Darcy relation for pressure differentials, a series of loss coefficients will then be calculated. The Reynolds number is the ratio of inertial forces to viscous forces, and in this case the velocity will be varied while the viscosity will remain constant. Each loss coefficient will be found for its corresponding Reynolds number, and then graphed to form a curve. This curve will be compared for congruence to experimental curves that have already been established.
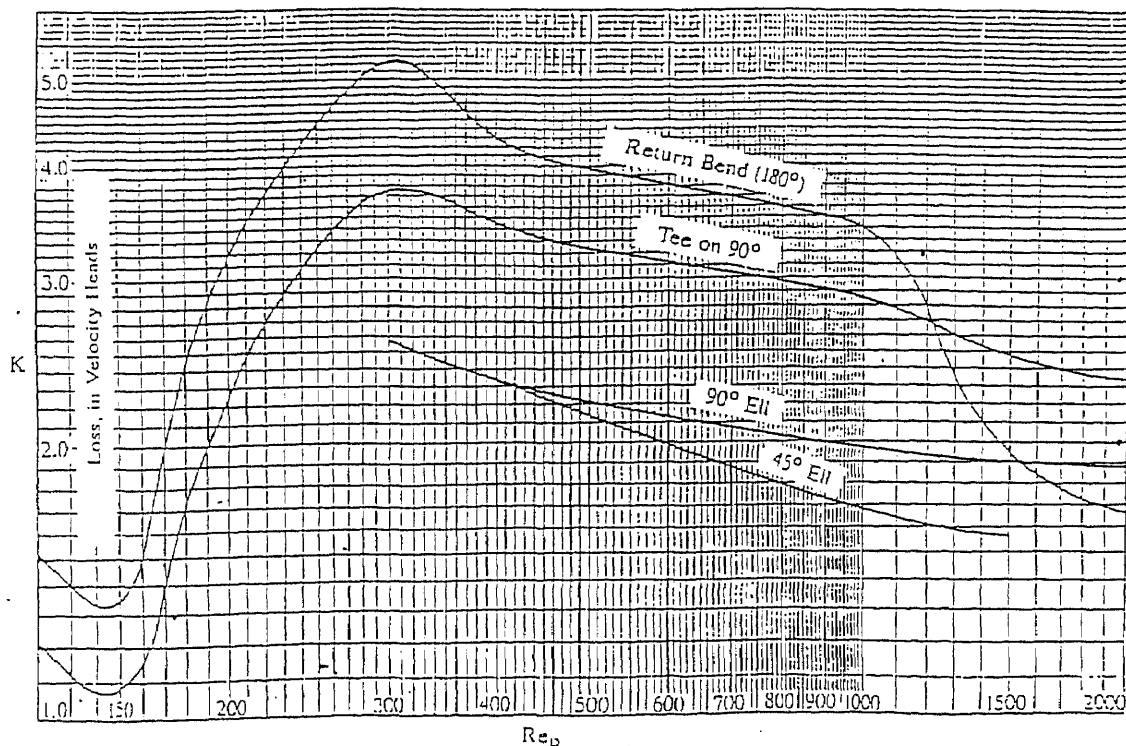
Figure 1.3.1
Bend Loss Coefficients in Various Streamline Fittings versus Reynolds Number

CHAPTER 2

LITERATURE SURVEY

The uses of duct flow systems in engineering are diverse. Distribution systems in heating, ventilating, and air conditioning; food and beverage industry; and the nuclear, coal, and gas industries are prevalent examples. Other applications include the chemical industry, hydraulic systems, civil engineering, and most types of vehicles. Internal flow systems performing a number of different functions have an important contribution in serving the overall performance of the design. The greatest enhanced attribute gained, with increased knowledge of pressure loss behavior, in industry is economical benefits. Available information on pressure loss in duct components is largely based on experimental work.

Pressure loss of fluids traveling through curved ducts and pipes is greater than that of flow through comparable straight sections. Determining these losses is complicated and less reliable than predictions for straight sections, due to a number of factors. These include, but are not limited to: entrance effects, dealing with non-uniformity, exit effects due to downstream components, amplification or dampening of inlet distortion due to the pipe bend, and inadequate empirical data on curved pressure losses [2]. The flow in a curved duct will be laminar or turbulent depending upon the value of the Reynolds number. The critical value, at which the transition from laminar to turbulent flow occurs, is influenced by the curvature of the bend. The importance of understanding transition lies in the increased effects on pressure distribution, which usually become random and unpredictable as the flow tends towards turbulence. This critical value is higher for bends than for straight ducts and increases as the radius of the bend to duct diameter ratio

decreases. For straight ducts the Reynolds number transition range lies between 1200 and 2500 with a limit of 2300 being approached by many experimenters [2]. For laminar flow through pipe bends, the excess pressure drop is the total pressure drop minus that for a straight duct. The magnitude of the excess pressure drop depends on the Reynolds number together with the diameter of the pipe and the curvature of the bend.

In experiments performed by White [12], certain features of the pressure loss were observed with a 90° duct bend. The variations in static pressure due to the presence of the bend begin to occur upstream of the bend at a value between 1 to 2 of the ratio of the upstream entrance to the duct height. Also occurring with this ratio value were distinct pressure distribution situations; an adverse pressure gradient develops on the outer surface of the bend and a favorable gradient forms on the inner surface. As the ratio of upstream entrance to duct height increases beyond 2, the pressure distribution on the outer wall becomes favorable, and the pressure gradients formed on the inner wall become adverse. Providing the downstream tangent is sufficiently long, the variation in static pressure at a cross-section was found to persist into the downstream tangent. The pressure distribution in the upstream tangent and over the upstream portion of the bend was determined independent of the inlet conditions for all bends tested [12].

Smith determined [5] for small values of downstream length to duct height (< 2), the outlet conditions had a very strong influence on the static pressure developed within the downstream portion of the bend, but for larger values of this ratio the pressure distribution within the bends were found to be independent of downstream length to duct height Considering those tangents in the range $0 < L_d/h < X_p/h$, where $X_p/h \cong 1.5$,
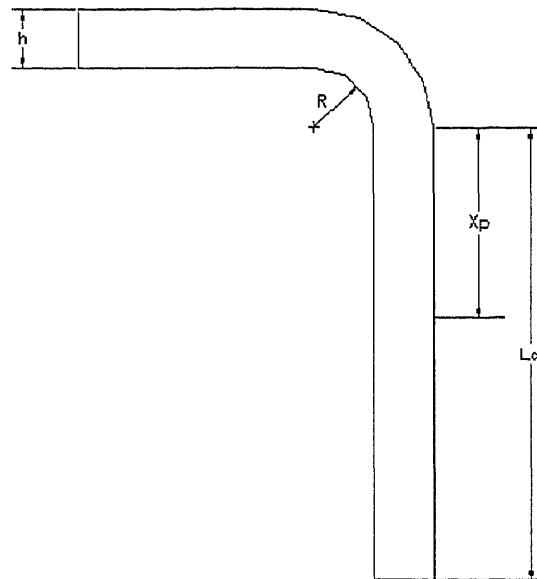
Figure 2.1.1
Bend Model Map of Downstream Pressure Differences

L_d is the outlet length, h is the duct height, and X_p is the distance into the downstream

tangent to which pressure differences at a cross-section extend, it can be shown that in this

range the pressure distribution within the bend is dependent on L_d/h, (see figure 2.2.1) in

addition, the loss coefficients in this range of values of L_d/h are very sensitive to variations

in L_d/h. The pressure gradients and the changes in pressure gradient due to changes of

downstream conditions were largest in the sharper bends; the magnitude of these effects

diminishes as R/h increases (where R is the bend radius), so that the influence of L_d/h on

the pressure distribution becomes small at about $R/h \geq 3.45$. There is a direct

correspondence between the severity of these adverse pressure gradients and the related

loss coefficients [5].

Other empirical observations have been noted for elbow or pipe bend loss. Experiments by Benedict [1] found, at a Reynolds number of about 2200, that about 50 pipe diameters of length downstream of an elbow are required before the elbow loss is fully realized in a piping system. Also, it is difficult to measure the pressures accurately near the vicinity of the elbow. Therefore, it is usually practiced to sample pressures at a number of points around the pipe and along the inlet and exit pipes of the elbow under study, and to establish from these the normal slope of the viscous pipe loss, and ultimately the elbow loss alone. With a computational model, the pressure distribution can be realized at many points without physical means, leaving the pressure distribution undisturbed. It should also be realized that when fittings or other piping loss elements are placed close to each other, such elements influence those downstream in an undetermined manner. Thus, predictions of pressure loss for elements placed in series cannot be too reliable, and that only tests conducted under nearly identical setups can yield meaningful results in such cases. A computational model can be created to simulate each loss element in a forthright and diligent manner to study pressure contours and reduce time on such physical models.

Hawthorne [7] discovered that results between theoretical and experimental analysis varied considerably. To correlate theoretical and experimental duct flows, approximations have been formed account for the non-linearity found in physical experimentation. Hawthorne cited several aspects in which flow approximation fails. First, the theory does not predict the distortion of the Bernoulli surfaces (constant lines of energy where Bernoulli's theory is valid), that is found in practice. It is, however, possible

to make a second-order calculation that predicts the distortion fairly satisfactorily in simple bends but not so successfully near the end-wall regions of cascades. Second, owing to the distortion of the Bernoulli surfaces by the secondary flow the conclusion that the secondary vorticity and velocities grow somewhat linearly with bend angle is limited to bend angles not exceeding approximately $\sqrt{d}/R$ radians, where d is the diameter or width of the duct and R is the bend radius. In fact for bends of prolonged curvature the secondary flow develops in an oscillatory fashion. The results of Hawthore's studies indicates that flow in bent pipes is extremely complicated and that the assumption made in handbooks that the bend losses are a simple function of bend angle or radius is likely to be inaccurate [7].

Previous empirical studies have developed loss coefficients for pipe bends with varying Reynolds number. For round pipes with 90° bends, loss coefficient relationships were recorded [6]. Flow analysis have been performed on elbow bends with a radius to height ratio (R/b) of 0.5, and also for R/b≅0 (representing an miter bend).
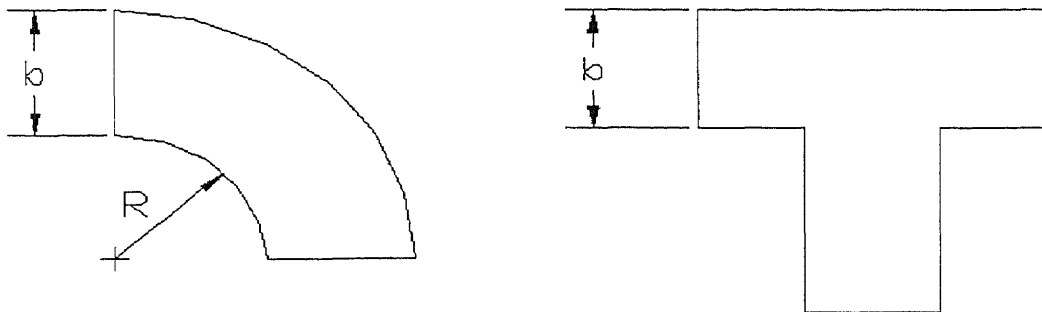
Figure 2.1.2
Mitered Bend versus Constant Radius Bend

The loss coefficients were higher for mitered bends than for smoother ones (R/b $\cong$ 0.5) at the same Reynolds number (ranging from 300 to 2000). For the smoother bends (R/b $\cong$ 0.5) the loss coefficients ranged from about 2 for a Reynolds number of approximately 2000 to an increasing value of approximately 2.7 for a lower Reynolds number of 300. Similarly, the R/b $\cong$ 0 bend had a loss coefficient of about 2.5 at a Reynolds number of 2000, and a loss value of about 3.7 at the 300 mark for Reynolds. The study was carried out further for lower Reynolds number involving the mitered bend (R/b $\cong$ 0) and the loss coefficients were found to decrease from the Reynolds point of 300 and approach a loss value minimum of 1.05 at a Reynolds number of 100. From the Reynolds number of 100 to a Reynolds number of approximately 0, the loss coefficient were found to increase slightly and peak at about 1.2. This relationship can easily be seen in Figure 1.3.1.

CHAPTER 3

BACKGROUND AND ANALYSIS

3.1 Uses and Capabilities

FIDAP is capable of analyzing a wide range of different problems. This range includes the following [4]:

Incompressible and compressible fluids.

Laminar and Turbulent flows.

Single-phase and two-phase flows.

Newtonian, non-Newtonian and visco-elastic fluids.

Flows in fully saturated porous media.

Flows with mass transport.

Steady-state and transient flows.

Forced convection problems.

Buoyancy-driven free convection problems.

Mixed convection problems.

Advection-diffusion problems (energy equation and/or species transport equations only).

Flows driven by body forces (gravitational, centrifugal, coriolis, electromagnetic).

Periodic, separating and recalculating flows.

Swirling flows.

Flows in rotating or translating frames of reference.

Flows with a free or moving surface, including moving contact points and lines.

Surface tension driven thermal flows. Flows driven by thermal surface tension gradients.

Solidification and melting, with latent heat release and mass transfer across phase-change boundaries. A decay model of the turbulent viscosity through the mushy zone is provided.

Mass transport due to homogenous and heterogeneous chemical reactions. Surface reactions and thermodiffusion effects are also included.

Diffuse gray and non-gray surface-to-surface radiation, including view factor calculations. Radiation interaction with participating medium.

Heat transfer in solid regions bounding the flow can be modeled; i.e., conjugate heat transfer problems.

Some typical areas of application of FIDAP are summarized below.

Electronics Industry - flow and thermal fields in cabinets and chassis or arrays of components and circuit boards, conjugate heat transfer problems, air flow in disk drives, clean room analysis.

Automotive Industry - flow distributions along external curved surfaces, lift and drag calculations, flow in ducts and manifolds, coolant flow around radiator blocks, radiator design, flow through pumps and valves, flow through filters, climate control in passenger compartments, catalytic converters, shock absorbers.

Metal forming Industry - continuous casting, extrusion, convection in tundishes, solidification in castings, phase change.

HVAC Industry - heat exchangers, regenerators, room ventilation flows, analysis of heating and air-conditioning systems, spray cooling.

Plastics Industry - analysis of injection molding runner systems; extrusion, sheet, coathanger, spiral, profile dies; blow molding dies.

Food and Beverage Industry - flow and temperature distributions in containers, ovens, food processing equipment.

Materials Processing Industries - semiconductor crystal growth, flows of molten glass, furnace design, microgravity processing in space.

Chemical Industries - flow, heat and mass transfer in chemical reactors, exothermic and endothermic reactions, chemical mixing, separation processes, drying, evaporation and condensation.

Biomedical Industries - blood flow in natural and artificial organs, flows in biomedical devices, tubes with and without constrictions, extrusion processes in product manufacture, modeling of cleansing processes, sprays and atomizers.

Environmental Studies - flow distributions around buildings, atmospheric thermal plumes, solar ponds.

Aerospace/Defense Industries - flow around submerged bodies, defense electronics, variable gravity effects, cabin ventilation, flows in fuel lines and tanks.

Nuclear Industry - flow and thermal distributions of coolants.

Thin Film Technology - coating flows of polymeric fluids, slot coaters, roll coaters, chemical vapor deposition, optical fiber coating.

Printing Industry - modeling of ink jets.

Crystal Growth - single crystal production from a melt.

Lubrication - film flows.

Machinery/Appliances - flow around impellers and propellers and in water turbines.

Instrumentation and Control - flow and thermal fields around sensing devices, vortex shedding, flows and pressure distributions in valves and control devices, choked flows in nozzles and valves.

PRE-PROCESSING	PROCESSING	POST-PROCESSING

FI-GEN

GRAPHICAL USER INTERFACE
ALLOWS GEOMETRICAL INPUT
VIA FIDAP EDITOR

FI-BC

GRAPHICAL USER INTERFACE
INPUT BC'S & IC'S VIA EDITOR
FORMATION OF BC GROUPS

FIMESH

CREATION OF MESH LOOPS
AND SURFACES

FIPREP

SIMULATION CONTROL
FLUID AND MEDIA
PROPERTIS SPECIFIED

FICONV

CONVERTS OTHER GEOMETRICAL
FILES INTO FIDAP, ACCEPTS
BC'S & IC'S AS WELL AS
OTHER FLUID PROPERTIES

FIDAP
MAIN
PROGRAM
MODULE

GUI

PLOTS VECTORS, CONTOURS,
NUMERICAL LISTINGS AND
MESH GENERATION GRAPHICS

FISOLV

FEM SOLVER OF UNKNOWN
VARIABLES

PATRAN, I-DEAS, OR FIDAP 6.0
FILES, ETC. INPUT FILES
OTHER FLUID PROPERTIES

Figure 3.2.1
FIDAP Structure Chart

3.2 FIDAP Structure

The FIDAP structure is a single integrated environment for the simulation of fluid flow analysis. The program consists of modules designed to perform all aspects of the model generation, problem setup, post-processing and solution phases of a flow problem. There are three general areas within the FIDAP program structure: pre-processing or problem description, processing or basic number crunching, and post-processing or analysis of results. FIDAP contains seven program modules which are used in the fluid flow analyses process: FIPREP, FIMESH, FI-GEN, FI-BC, FICONV, FISOLV, and FIPOST. Figure 3.2.1 on the following page displays a flow chart which depicts how FIDAP performs analysis.

3.2.1 Pre-Processing

The program FIDAP contains five modules which may be used for data generation in the pre-processing stage. FIPREP is used for simulation control as well as fluid property entry. The modules FI-GEN and FIMESH are used for mesh generation.. Primarily, FI-BC is used for boundary and initial condition applications. And finally, FICONV is used for file manipulation and conversion tasks. It should be noted that FICONV may be used in place of FI-GEN or FIMESH for creating FIDAP compatible mesh data by converting file information created in some other finite element programs. Such file conversions may be from PATRAN Neutral files, I-DEAS Universal files, or the FIDAP version 6.0 Neutral files. The FICONV can translate node and element information as well as boundary and initial conditions data from these external sources.

The primary step in computational analysis is proper modeling of the system into the graphical environment. In FIDAP, a model may be created within the program or it may be imported from a previously existing file. Some problems may need to be modified or converted before proper generation of the model can take place through the graphical user interface. The FICONV command is the FIDAP command used to invoke the FICONV conversion utility module. The FICONV module is used for file conversion. This utility integrates one or more input files. The FICONV module also performs adjustments on existing model files. Often, when a series of simulations are performed with FIDAP in which a parameter is being changed for each subsequent simulation, (e.g., the density, effectively increasing the Reynolds number), a point is reached where the solution process no longer converges and a mesh refinement is required. However, as the nodal points of the new, refined mesh no longer coincide with those of the old mesh, the last converged solution can no longer be used as an initial guess to the next simulation with a higher parameter value. In this situation, FICONV interpolates the solution from the last solution mesh onto a mesh of different density and creates a new restart results database that incorporates the old solution onto the new mesh.

The FIDAP module also allows internal graphical generation of the fluid model. The FI-GEN command is used to invoke the FI-GEN mesh generator. The FI-GEN module accepts geometrical graphical input to create a visual display of the desired model and is designed to show all points, curves, and surfaces that are desired by the user. However, only nodes lying on the mesh edges are displayed. After the model is graphically

displayed, it may be plotted, printed, or edited. The FIMESH program module is then used to map the model in integer or logical space. Logical space can have up to three dimensions in the FIDAP environment, represented by the indices I, J, and K. The maximum value for each logical index must be specified by the user. In two dimensions a logical space may be thought of in terms of a piece of ordinary, equally spaced graph paper on which the vertices formed by the lines are the possible locations of keypoints. The logical space representation of the flow domain is a topological map of your finite element mesh and is used to establish two things: mesh density and definition of nodes which will receive boundary conditions. It is important that a logical model be properly defined, or FIDAP will fail to recognize the accompanying geometrical coordinates.

The second step in pre-processing involves specifying initial and boundary conditions for the model. Initial conditions specify the starting state of the fluid for a transient simulation or a first guess for the non-linear solution iterations. Convergence of a solution strongly depends on the initial guess. In order to have a well defined problem, boundary conditions are required on all boundaries of the computational domain. Boundary conditions may consist of specified nodal values or specified fluxes across elemental sides for each active degree of freedom. It should be noted that only one type of these boundary conditions may be specified at any given boundary. For FIDAP, the default boundary condition at any unspecified boundary is zero flux for that degree of freedom. The module FIPREP is used for the specification of initial and boundary conditions for any FIDAP problem. In FIDAP, initial and boundary conditions can be applied in a number of different ways. At the lowest level, the required condition can be applied directly to the

node. Because this approach requires knowledge of the node numbers, as well as constant updating of the node numbers for any mesh modification, it is considered the least desirable. The FIDAP program allows for the creation of entities or element groups, and then conditions may be applied to the collection of element groups. There are three distinct advantages to referencing entities for the specification of initial and boundary conditions. First, it allows the identification of an entire region of the boundary to which to apply the condition. Second, the label used for identification is independent of any group or node number which allows mesh modifications to be made without affecting the previous definition. Lastly, boundary conditions maybe applied in a more favorable type of intuitive manner to physically identifiable portions of the computational domain. The FI-BC interactive module is used to define the boundary and initial conditions. This interface allows for activation of various commands which specify conditions. The FI-BC module is designed to significantly reduce the amount of time required to specify the initial and boundary conditions necessary for a FIDAP analysis. In essence FI-BC is an interactive graphical interface to the commands available in FIPREP.

3.2.2 Processing

The processing part of FIDAP requires no user interaction and is performed by the FISOLV program module. This module performs the cumbersome algebraic matrix manipulations. The FIDAP program notifies the user weather a solution was converged upon at the end of this stage. If a solution was converged upon, the user can begin displaying the results with FIPOST. If convergence is not reached, the user is advised to

change parameters within the solution method (by relaxing or upwinding settings), and then rerunning the solution. Convergence for the fully coupled solvers, which include Successive Substitution, Newton-Raphson Method, Modified-Newton and Quasi-Newton Methods is based on two criteria being satisfied simultaneously. The first criterion is a measure of the change in the solution from one iteration to the next. The second is a measure of how well the current solution satisfies the system of equations being solved.

3.2.3 Post-Processing

Lastly, FIDAP displays results of basic solution data via the FIPOST module. This module is a graphical post-processor that plots solution data as well as additional derived quantities. The FIPOST program module is used to post process the correctly defined fluid model. The FIPOST module requires two files for successful operation: a model database file and a corresponding results database file that was created by the FISOLV execution.

CHAPTER 4

METHOD OF SOLUTION

4.1 Governing Equations

The beginning of any fluid motion analysis originates with the use of the Navier-Stokes equations. These equations are valid for both laminar and turbulent flows. The solution of problems in incompressible fluid dynamics for which temperature changes are insignificant can be obtained by considering the equations of continuity and momentum alone. The Navier-Stokes equations are non-linear partial differential equations, and analytical solutions of these equations can be obtained for laminar flows. However, when turbulence is involved an analytical solution is usually impossible.

The Equation of Continuity: The equation of continuity expresses the principle of conservation of matter. For the rectangular Cartesian coordinate system, with coordinates x, y, z, measured relative to a stationary frame of reference, and corresponding velocity components u, v, w the continuity equation is

$$\partial\rho/\partial t + \partial(\rho u)/\partial x + \partial(\rho v)/\partial y + \partial(\rho w)/\partial z = 0 \qquad (4.1.1)$$

$\rho \equiv$ density of fluid

$t \equiv$ time

This is the general form of the equation of continuity, applicable to the non-steady flow of compressible fluid. Using the operator

$$D/Dt = \partial/\partial t + u\partial/\partial x + v\partial/\partial y + w\partial/\partial z \qquad (4.1.2)$$

where D/Dt is known as the material time, Eulerian, or substantive derivative, the continuity equation can be rewritten, through the expansion of the above equation, in the following form

$$1/\rho \; D\rho/Dt + \partial u/\partial x + \partial v/\partial y + \partial w/\partial z = 0 \qquad (4.1.3)$$

In steady motion the density at a fixed point is independent of time and the continuity equation for a compressible fluid is then

$$\partial(\rho u)/\partial x + \partial(\rho v)/\partial y + \partial(\rho w)/\partial z = 0 \qquad (4.1.4)$$

In incompressible flow the density, ρ, is constant and the continuity equation in both steady and unsteady flow is

$$\partial u/\partial x + \partial v/\partial y + \partial w/\partial z = 0 \qquad (4.1.5)$$

The Momentum Equations: The momentum equations are derived by applying Newton's second law, which states that the rate of change of momentum of a body is equal to the

sum of the applied forces, to an elementary volume of fluid. The applied forces acting on the fluid element are of two basic types:

(a) Forces acting throughout the entire element (e.g. gravitational forces);

(b) Forces acting on the surface of the element (e.g. static pressure and friction)

The first type are known collectively as body forces and the second group are called surface forces. On applying Newton's second law to a fluid element, centered at x, y, z, with parallel edges, the coordinate axes there results in

$$\rho Du/Dt = \rho X + \partial\sigma_{xx}/\partial x + \partial\tau_{xy}/\partial y + \partial\tau_{xz}/\partial z, \qquad (4.1.6a)$$

$$\rho Dv/Dt = \rho Y + \partial\tau_{yx}/\partial x + \partial\sigma_{yy}/\partial y + \partial\sigma_{yz}/\partial z, \qquad (4.1.6b)$$

$$\rho Dw/Dt = \rho Z + \partial\tau_{zx}/\partial x + \partial\sigma_{zy}/\partial y + \partial\sigma_{zz}/\partial z, \qquad (4.1.6c)$$

where the left-hand side of each equation is the rate of change of momentum, the first term on the right-hand side is the component body force, and the remaining terms, representing the components of the stress tensor, are the contributions of the surface forces. It should be noted that the first subscript denotes the axis to which the face of the element is perpendicular; the second suffix indicates the direction to which the stress is parallel. The shear stress terms satisfy the relations

$$\tau_{xy} = \tau_{yx}$$

$$\tau_{xz} = \tau_{zx} \qquad (4.1.7)$$

$$\tau_{yz} = \tau_{zy}$$

With the following assumptions: (i) that there is a linear relationship between the stress components and rates of deformation, and (ii) that the fluid is isotropic, that its properties are the same in all directions, the stress tensor components can take on a new form related to the static pressure, dynamic viscosity, and bulk viscosity. With these assumptions, for compressible viscous fluid flow, the three components of the momentum equation in rectangular Cartesian coordinates is

$$\rho Du/Dt = \rho X - \partial p/\partial x + \partial/\partial x[\mu(2\partial u/\partial x - 2/3(\partial u/\partial x + \partial v/\partial y + \partial w/\partial z))] +$$

$$\partial/\partial y[\mu(\partial u/\partial y + \partial v/\partial x)] + \partial/\partial z[\mu(\partial w/\partial x + \partial u/\partial z)] \qquad (4.1.8a)$$

$$\rho Dv/Dt = \rho Y - \partial p/\partial y + \partial/\partial x[\mu(2\partial v/\partial y - 2/3(\partial u/\partial x + \partial v/\partial y + \partial w/\partial z))] +$$

$$\partial/\partial z[\mu(\partial v/\partial z + \partial w/\partial z)] + \partial/\partial x[\mu(\partial u/\partial y + \partial v/\partial x)] \qquad (4.1.8b)$$

$$\rho Dw/Dt = \rho Z - \partial p/\partial z + \partial/\partial z[\mu(2\partial w/\partial z - 2/3(\partial u/\partial x + \partial v/\partial y + \partial w/\partial z))] +$$

$$\partial/\partial x[\mu(\partial w/\partial x + \partial u/\partial z)] + \partial/\partial y[\mu(\partial v/\partial z + \partial w/\partial y)] \qquad (4.1.8c)$$

These three equations, together with the continuity equation, are known collectively as the Navier-Stokes equations. For incompressible flow under conditions of small temperature variations the viscosity as well as the density may be assumed constant. The momentum equations take the simplified form

$$\rho Du/Dt = \rho X - \partial p/Dx + \mu(\partial^2 u/\partial x^2 + \partial^2 u/\partial y^2 + \partial^2 u/\partial z^2), \qquad (4.1.9a)$$

$$\rho Dv/Dt = \rho Y - \partial p/Dy + \mu(\partial^2 v/\partial x^2 + \partial^2 v/\partial y^2 + \partial^2 v/\partial z^2), \qquad (4.1.9b)$$

$$\rho Dw/Dt = \rho Z - \partial p/Dz + \mu(\partial^2 w/\partial x^2 + \partial^2 w/\partial y^2 + \partial^2 w/\partial z^2), \qquad (4.1.9c)$$

The analytical determination of the field flow in any general configuration rests on the solution of the above equations subject to the appropriate boundary and initial conditions. For the flow of a viscous fluid the condition of no-slip must be satisfied; that is, at a solid surface both the normal and tangential components of velocity must be zero [11].

4.2 FEM Approach

The above equations are solved through a finite element method via the computer package FIDAP. The domain that the equations govern is subdivided into elements. These elements are assembled through interconnection at a finite number of points on each element. This assembly provides a model of the continuum region of intersect [13].

Using a Eulerian description of the fluid motion for the field equations, the elements are taken to be fixed in space. Each element contains within itself functions which interpolate the dependent variables u_i and p based on values which are determined at the nodal points. These functions are of compatible order to the dependent functions. The velocity, pressure and temperature fields within each element are approximated by,

$$u_i(x,t) = \varphi^T U_i(t) \qquad (4.2.1)$$

$$p(x,t) = \psi^T P(t) \qquad (4.2.2)$$

where U_i and P are column vectors of element nodal point unknowns and φ and ψ are column vectors of the interpolation functions. Substituting these interpolation functions into the field equations as well as boundary condition yields a set of equations of the form:

$$\text{Momentum:} \quad f_1(\varphi, \psi, U_i, P) = R_1 \qquad (4.2.3)$$

$$\text{Continuity:} \quad f_2(\varphi, U_i) = R_2 \qquad (4.2.4)$$

where R_i is the residual resulting from the use of those approximation equations. The Galerkin method of weighted residuals seeks to reduce the error (residual) R_i to zero. This is achieved by making:

$$\int_{\Omega E} (f_1 \cdot \varphi)\, d\Omega = \int_{\Omega E} (R_1 \cdot \varphi)\, d\Omega = 0 \qquad (4.2.5)$$

$$\oint_{\Omega_E} (f_2 \cdot \psi) \, d\Omega = \oint_{\Omega_E} (R_2 \cdot \psi) \, d\Omega = 0 \qquad (4.2.6)$$

where Ω_E is the element domain. The application of the Galerkin procedure to the field equations results in a system of algebraic equations of the form:

$$[K] \, [\Phi] = [F] \qquad (4.2.7)$$

where [K] is the stiffness matrix, [Φ] is the column vector of unknowns and [F] is the source term which includes the effects of body forces and boundary conditions.

A nine nodal quadrilateral element has been used for computations. In terms of the normalized or natural coordinates of the element (i.e., r and s), the velocity approximations are found using biquadratic interpolation functions, given by:

$$\varphi = \begin{bmatrix} 1/4 \, rs \, (\, 1\text{-}r \,)(\, 1\text{-}s \,) \\ -1/4 \, rs \, (\, 1\text{+}r \,)(\, 1\text{-}s \,) \\ 1/4 \, rs \, (\, 1\text{+}r \,)(\, 1\text{+}s \,) \\ -1/4 \, rs \, (\, 1\text{-}r \,)(\, 1\text{+}s \,) \\ -1/2 \, s \, (\, 1\text{-}s \,)(\, 1\text{-}r^2 \,) \\ 1/2 \, r \, (\, 1\text{+}r \,)(\, 1\text{-}s^2 \,) \\ 1/2 \, s \, (\, 1\text{+}s \,)(\, 1\text{-}r^2 \,) \\ -1/2 \, r \, (\, 1\text{-}r \,)(\, 1\text{-}s^2 \,) \\ (\, 1\text{-}r^2 \,)(\, 1\text{-}s^2 \,) \end{bmatrix} \qquad (4.2.8)$$

The pressure approximations used with the element bilinear. The pressure values for the bilinear approximations are located at the four points of a 2X2 Gaussian integration. Its interpolation functions are given by,

$$\psi = \begin{bmatrix} 1/4\,(\,g\text{-}r\,)\,(\,g\text{-}s\,)\,/\,g^2 \\ 1/4\,(\,g\text{-}r\,)\,(\,g\text{-}s\,)\,/\,g^2 \\ 1/4\,(\,g\text{-}r\,)\,(\,g\text{-}s\,)\,/\,g^2 \\ 1/4\,(\,g\text{-}r\,)\,(\,g\text{-}s\,)\,/\,g^2 \end{bmatrix} \qquad (4.2.9)$$

$$g = 2\sqrt{\tfrac{1}{3}} \qquad (4.2.10)$$

It is necessary to provide appropriate boundary conditions for u and v on the boundary of the computational domain. At the channel wall U and V are taken to be zero (see figure 4.2.1). The inlet velocity is prescribed as parabolic and traveling strictly in the x-direction. On the top and bottom wall, rigid, no-slip conditions are applied, hence velocities are prescribed zero. For the outlet profile boundary, the fully-developed parabolic velocity profile is applied in the x-axial direction.
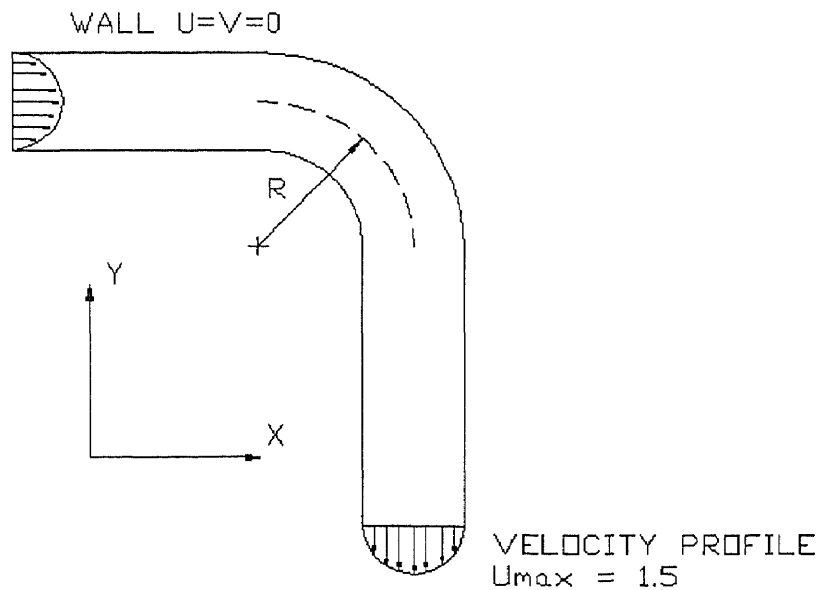
Figure 4.2.1
Boundary Conditions and Velocity Profile

For the numerical solution, a segregated implicit algorithm is used on the set of discretized equations resulting from the application of the Galerkin finite element method onto the field equations. The discretized implicit equations associated with each primary flow variable are assembled into smaller sub-matrices. Mixed velocity-pressure formulation is applied. An approximation is used initially and then the pressure is obtained from the solution of the Poisson type pressure matrix using the latest available values of the field variables. A criteria is established which terminates the iteration process for equation solution. This relative error of the solution vector u_i at the i_{th} iteration converges on the following criteria:

$$| \Delta u_i | / | u_i | < \varepsilon_u \qquad (4.2.11)$$

$$\Delta u_i = u_i - u_{i-1} \qquad (4.2.12)$$

where ε_u denotes a given tolerance, and $| \quad |$ denotes an appropriate norm. The second convergence criterion is based on the residual vector to check the tendency of errors as u_i tends to u. It is

$$| R(u_i) | / | R_o | < \varepsilon_f \qquad (4.2.13)$$

where R_o is a reference vector, usually taken to be $R(u_o)$. These two criteria provide an effective overall convergence criterion for solutions. Based on these equation, boundary

conditions, and the principles for solution, some flow computation programs have been built upon the FIDAP package. [14]

4.3 Determination of Loss Coefficient

In calculating pressure loss through a bend, two components may be considered with which to determine the loss value. One component is the pressure drop existing in the absence of the bend and the other is the pressure drop due to the bend. The pressure drop that would have existed in the absence of the bend is defined as the pressure loss in a straight duct of equivalent length. The pressure loss or excess pressure loss due to the bend itself is determined by subtracting the pressure loss in a straight duct of equivalent length from the total pressure loss of the duct section. The pressure loss due to the bend can then be used to calculate a loss coefficient, K. The quantity K is a dimensionless coefficient which may be used to account for partial pressure losses in any duct flow. This quantity may be determined from a basic relationship, the Darcy Equation:

$$\Delta p = 0.5 \, K \, \rho V^2 \tag{4.3.1}$$

$\Delta p \equiv$ pressure drop $\{N/m^2\}$

$K \equiv$ coefficient relating to pressure drop $\{dimensionless\}$

$\rho \equiv$ fluid density $\{kg/m^3\}$

$V \equiv$ fluid velocity $\{m/s\}$

The most common pipe loss component is that due to friction within the pipe. This loss is characterized by the friction factor, f. The variables involved are the pipe length, L, the pipe diameter, D, fluid viscosity, μ, density, ρ and flow velocity, V. When losses in a duct are being considered, other than a circular pipe, a hydraulic diameter is used instead of the circular diameter, D. The hydraulic or equivalent diameter, D_h, is

$$D_h = 4 \, A_c \, / \, A_p \qquad\qquad (4.3.2)$$

$A_c \equiv$ cross-sectional area $\{m^2\}$

$A_p \equiv$ wetted perimeter $\{m\}$

By using the friction factor, duct length, and hydraulic diameter, the following dimensionless loss coefficient may be found due to friction:

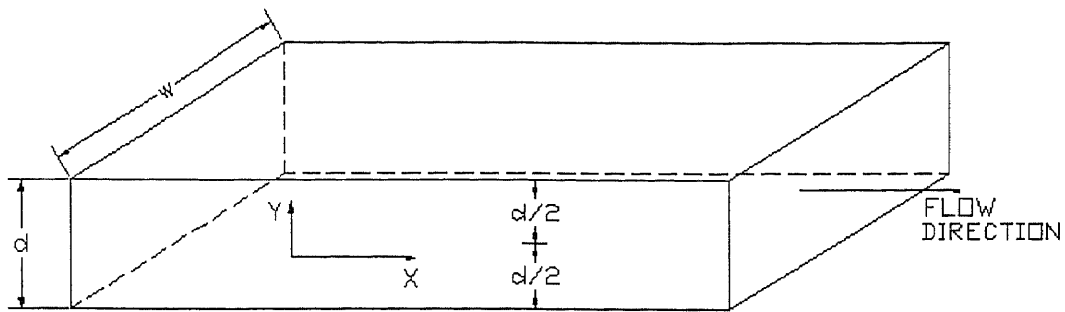$$K_f = f \, (L/D_h) \qquad\qquad (4.3.3)$$

$K_f \equiv$ coefficient of pressure loss due to friction $\{$dimensionless$\}$

$L \equiv$ length of duct in consideration $\{m\}$

$D \equiv$ diameter of duct or pipe in consideration $\{m\}$

$f \equiv$ friction factor

Figure 4.3.1
Flow Through a Rectangular Channel

We can derive the friction factor by beginning with a rectangular channel in three dimensions. Figure 4.3.1 represents a rectangular channel with width, w, and depth, d. Assume the width is much greater than the depth, so that the flow is two-dimensional. Take the velocity, V, in the x-direction, as a function of y only, while taking the pressure as a function of x but not of y. The momentum equation for a control volume located within the channel will yield:

$$\mu \ (dV/dy) = y \ (dp/dx) \qquad (4.3.4)$$

If we integrate the above, with V = 0 at y = ±d/2, to obtain

$$V = 0.5 \ \mu \ (dp/dx) \ (y^2 - d^2/4) \qquad (4.3.5)$$

We can determine the mean velocity, V_{mean}, by taking it's definition

$$V_{mean} = 1/d \int V \, dy \qquad (4.3.6)$$

After integration, this yields a mean velocity equal to:

$$V_{mean} = - (dp/dx) \, (d^2/12\mu) \qquad (4.3.7)$$

For the cross section of figure 4.3.1, the hydraulic diameter is given by

$$D_h = 4dw \, / \, (2d + 2w) \qquad (4.3.8)$$

For $d \ll w$, the hydraulic diameter reduces to

$$D_h = 2d \qquad (4.3.9)$$

By taking the friction factor definition, in terms of pressure gradient, mean velocity, and hydraulic diameter:

$$f = - (dp/dx)D_h \, / \, (0.5\rho \, V^2_{mean}) \qquad (4.3.10)$$

By solving equation 4.3.7 for (dp/dx) in terms of V_{mean}, Then substituting that expression along with equation 4.3.9, we obtain the friction factor in terms of Reynolds Number:

$$f = 96/Re_{Dh} \qquad (4.3.11)$$

Where $Re_{Dh} = \rho\, V_{mean}\, D_h\, /\, \mu$

In our model, the loss coefficient due to friction will be calculated using this relation for f. This loss coefficient will be used in the Darcy relation to determine the straight bend pressure loss. This will be deducted from the total pressure loss in the bend.

$$\Delta p_{bend} = \Delta p_{total} - \Delta p_{straight} \qquad (4.3.12)$$

The quantity, Δp_{total}, will be determined by FIDAP. The pressure loss due to the straight bend equivalent will be defined as follows:

$$\Delta p_{straight} = 0.5\, K_f\, \rho\, V^2_{mean} \qquad (4.3.13)$$

It should be noted that the total straight length of the pipe is determined by adding the entrance length and the exit length required for the flow to regain a fully developed state.

The excess pressure is used to determine a pressure loss coefficient for the bend, K_b:

$$K_b = 2 \, \Delta p_{bend} \, / \, \rho \, V^2_{\ mean} \qquad\qquad (4.3.14)$$

Where K_b is the loss coefficient due solely to the bend. Using these governing equations we may proceed into the analysis of the two-dimensional channel bend using the FIDAP package.

CHAPTER 5

METHODOLOGY, RESULTS, AND DISCUSSION

5.1 Method of Analysis within FIDAP

For repetitive modeling situations, such as in this analysis, a file which modeled the 90°

bend was created to analyze different flow velocities (a listing of this file can be found in

the appendix). The problem examined water at ambient conditions (atmospheric pressure

and 70°F) flowing through a two-dimensional channel with a 90° bend of constant radius.

The density, viscosity, and maximum velocity were specified in the input file.

Density = 0.998 g / cm^3

Viscosity = 1.002 x 10^{-2} g / cm-s

Duct Width = 1 cm

Duct Bend Radius = 1.5 cm

The input velocity was represented by the following parabolic equation:


$$V = 4 \, V_{max} \, (y - y^2) \qquad\qquad (5.1.1)$$

Where V and V_{max} are in cm/s and y is measured from the bottom wall in cm for $0 \leq y \leq 1$.

The file was read in each time by FIDAP and then solved. FIDAP was used to analyze

eighteen different Reynolds Numbers for each particular 90° bend model. Pressure and

velocity nodal values were determined throughout the channel. Reynolds numbers from 50 to 1800 were analyzed by FIDAP.

After model analysis by FIDAP, a convergence of solution report would state if the unknown quantities were valid according to the parameters set. If the solution had converged within the number of specified iterations, then the results were considered valid and used in the determination of the bend loss coefficient. As the Reynolds number increased and conditions headed towards turbulence, a solution became harder to converge upon. When convergence did not occur, solution parameters had to be tweaked. Methods of tweaking included the following: change of solution method, increased relative error allowance, and increased number of solution iterations (file restarts).

The channel model was defined by elements which consisted of nodal points. FIDAP output files provided specific values for velocity and pressure at all nodal points. These values were used to determine the pressure loss due to the channel bend. A sample calculation is provided in detail in the appendix for an input velocity maximum of 1.503 cm/s. The velocity and pressure distributions for this particular input velocity are contained in the appendix (Figures 5.1.2 through 5.1.33). Figure 5.1.1 graphically shows the location of the lines within the bend from where the velocity and pressure distributions were taken. The actual values taken from FIDAP output files are listed in the appendix as well (Table 5.1.2). The x-direction and y-direction values were used to determine the velocity profile within the bend.
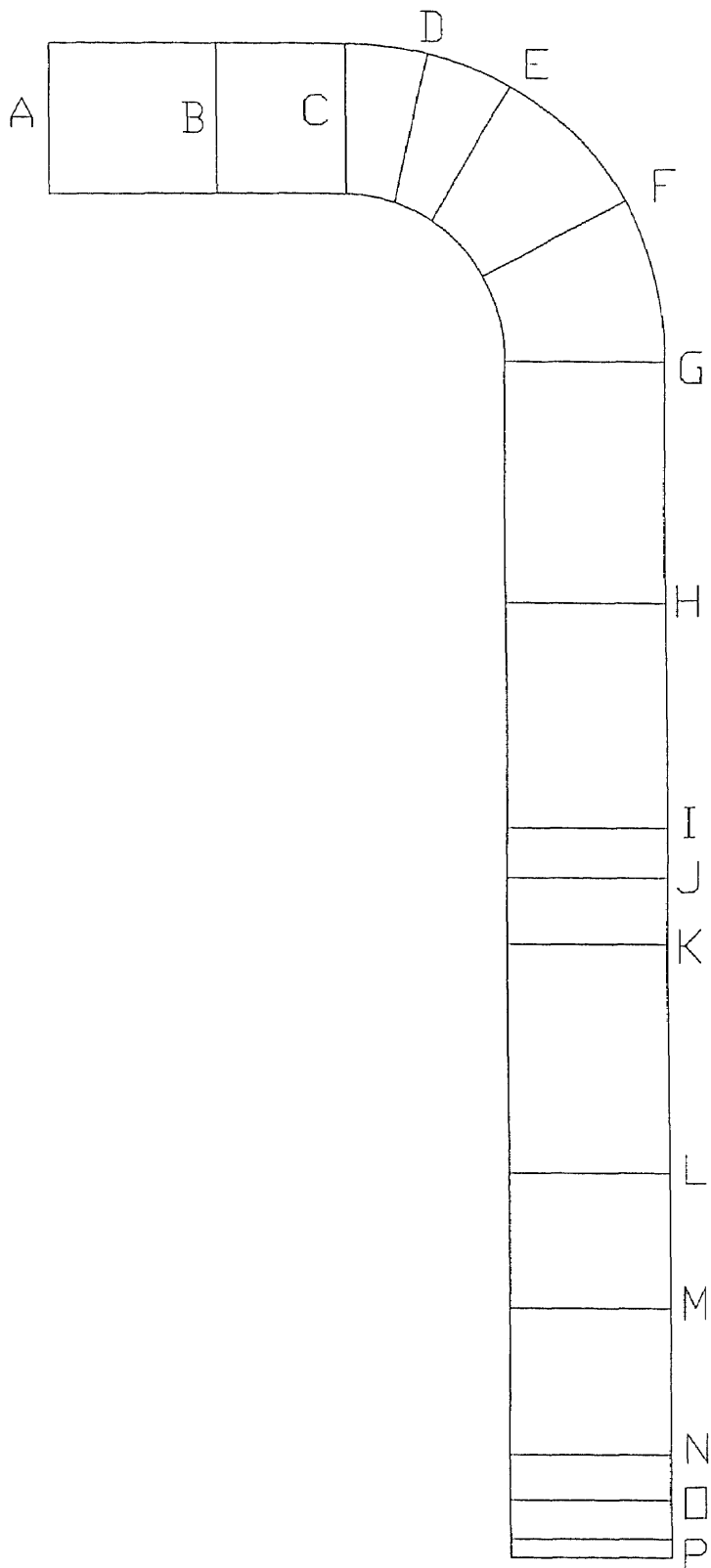
Figure 5.1.1
Graphical Lines for Pressure and Velocity Values

Table 5.1.1
Pressure and Velocity Distributions for Specified Lines within Channel Bend

FIGURE 5.1.1 LETTER	VELOCITY PROFILE FIGURE	PRESSURE DISTRIBUTION FIGURE	X-VELOCITY DISTRIBUTION FIGURE	Y-VELOCITY DISTRIBUTION FIGURE
A	5.1.2	5.1.18	5.1.34	5.1.50
B	5.1.3	5.1.19	5.1.35	5.1.51
C	5.1.4	5.1.20	5.1.36	5.1.52
D	5.1.5	5.1.21	5.1.37	5.1.53
E	5.1.6	5.1.22	5.1.38	5.1.54
F	5.1.7	5.1.23	5.1.39	5.1.55
G	5.1.8	5.1.24	5.1.40	5.1.56
H	5.1.9	5.1.25	5.1.41	5.1.57
I	5.1.10	5.1.26	5.1.42	5.1.58
J	5.1.11	5.1.27	5.1.43	5.1.59
K	5.1.12	5.1.28	5.1.44	5.1.60
L	5.1.13	5.1.29	5.1.45	5.1.61
M	5.1.14	5.1.30	5.1.46	5.1.62
N	5.1.15	5.1.31	5.1.47	5.1.63
O	5.1.16	5.1.32	5.1.48	5.1.64
P	5.1.17	5.1.33	5.1.49	5.1.65

5.2 Results

Initially, All eighteen Reynolds Numbers were analyzed for the 90° channel bend with an inner bend radius to duct width ratio equal to 1.5. All numbers found to complete each calculation, as is performed in the sample calculation, are compiled and listed in the appendix (Tables 5.2.1.a and 5.2.2.a). The pressure loss coefficient, K_b, for the bend was found for each Reynolds Number and graphed on Figure 5.2.1. Table 5.2.1 summarizes the pressure values determined, as well as each pressure loss coefficient determined.

A second analysis was performed to determine the effect of decreasing the bend

radius to duct width ratio on pressure loss. The FIDAP model was changed so that the

bend radius was 2 cm and the duct width was 2 cm. This gave a bend radius to duct width

ratio of 1.0. The same Reynolds Numbers were run on FIDAP and the velocity and

pressure profiles were determined. Table 5.2.2 lists values of pressure and the pressure

loss coefficients determined. Figure 5.2.2 is a plot of the Pressure loss coefficients, K_b,

versus Reynolds Number.

Table 5.2.1
Solution Results for 90° Channel Bend with a Bend Radius to Duct Width Ratio of 1.5

VELOCITY MAX (cm/s)	REYNOLDS NUMBER	ΔP TOTAL	ΔP STRAIGHT LENGTH	ΔP BEND	K LOSS COEFFICIENT
0.376	50	1.872	1.829	0.043	1.367
0.752	100	3.803	3.658	0.145	1.158
1.128	150	5.720	5.487	0.233	0.826
1.503	200	7.655	7.311	0.344	0.687
1.879	250	9.524	9.140	0.384	0.491
2.255	300	11.471	10.968	0.502	0.445
3.006	400	15.443	14.621	0.822	0.410
3.758	500	19.385	18.279	1.106	0.353
4.509	600	23.420	21.932	1.488	0.330
5.261	700	27.539	25.590	1.949	0.317
6.012	800	31.615	29.243	2.373	0.296
6.764	900	35.688	32.900	2.788	0.275
7.515	1000	39.732	36.553	3.178	0.254
8.267	1100	43.845	40.211	3.634	0.240
9.018	1200	47.843	43.864	3.979	0.221
10.521	1400	56.277	51.175	5.102	0.208
12.024	1600	64.621	58.485	6.136	0.191
13.258	1800	73.435	65.801	7.634	0.188

Table 5.2.2
Solution Results For 90° Channel Bend with a Bend Radius to Duct Width Ratio of 1.0

| VELOCITY MAX (cm/s)	REYNOLDS NUMBER	ΔP TOTAL	ΔP STRAIGHT LENGTH	ΔP BEND	K LOSS COEFFICIENT
0.188	50	0.399	0.368	0.031	3.929
0.376	100	0.819	0.737	0.082	2.602
0.564	150	1.228	1.105	0.122	1.735
0.752	200	1.651	1.474	0.177	1.412
0.940	250	2.095	1.842	0.253	1.291
1.127	300	2.498	2.209	0.289	1.026
1.503	400	3.436	2.946	0.490	0.979
1.879	500	4.373	3.682	0.691	0.882
2.255	600	5.356	4.420	0.936	0.830
2.631	700	6.300	5.157	1.143	0.745
3.006	800	7.323	5.892	1.432	0.714
3.382	900	8.379	6.629	1.750	0.690
3.758	1000	9.441	7.366	2.075	0.663
4.134	1100	10.545	8.103	2.442	0.644
4.509	1200	11.597	8.838	2.759	0.612
5.261	1400	13.796	10.312	3.484	0.568
6.012	1600	16.032	11.784	4.249	0.530
6.764	1800	18.312	13.258	5.054	0.498
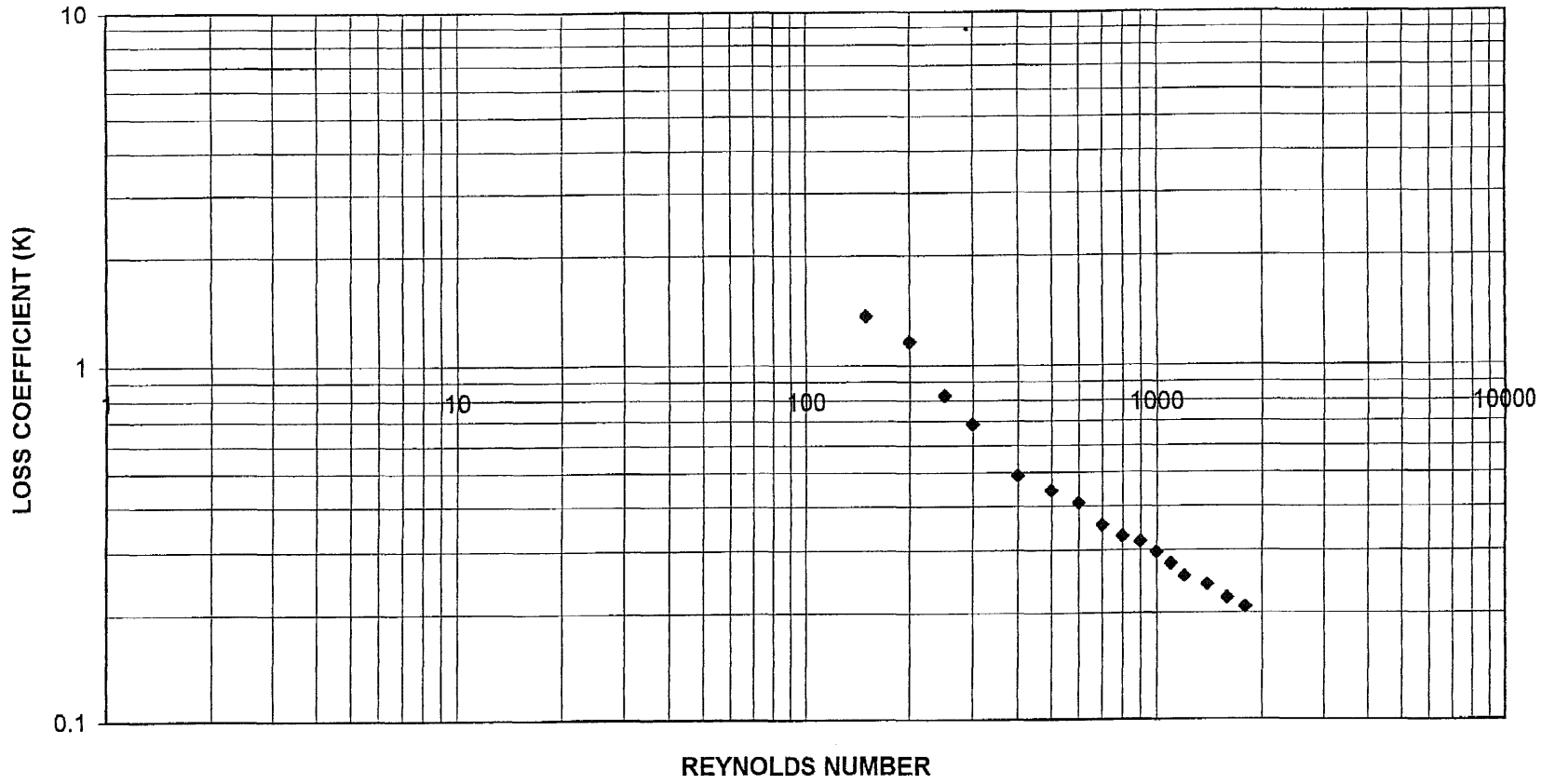
Figure 5.2.1
Pressure Loss Coefficient versus Reynolds Number for a Bend Radius to Duct Width Ratio of 1.5
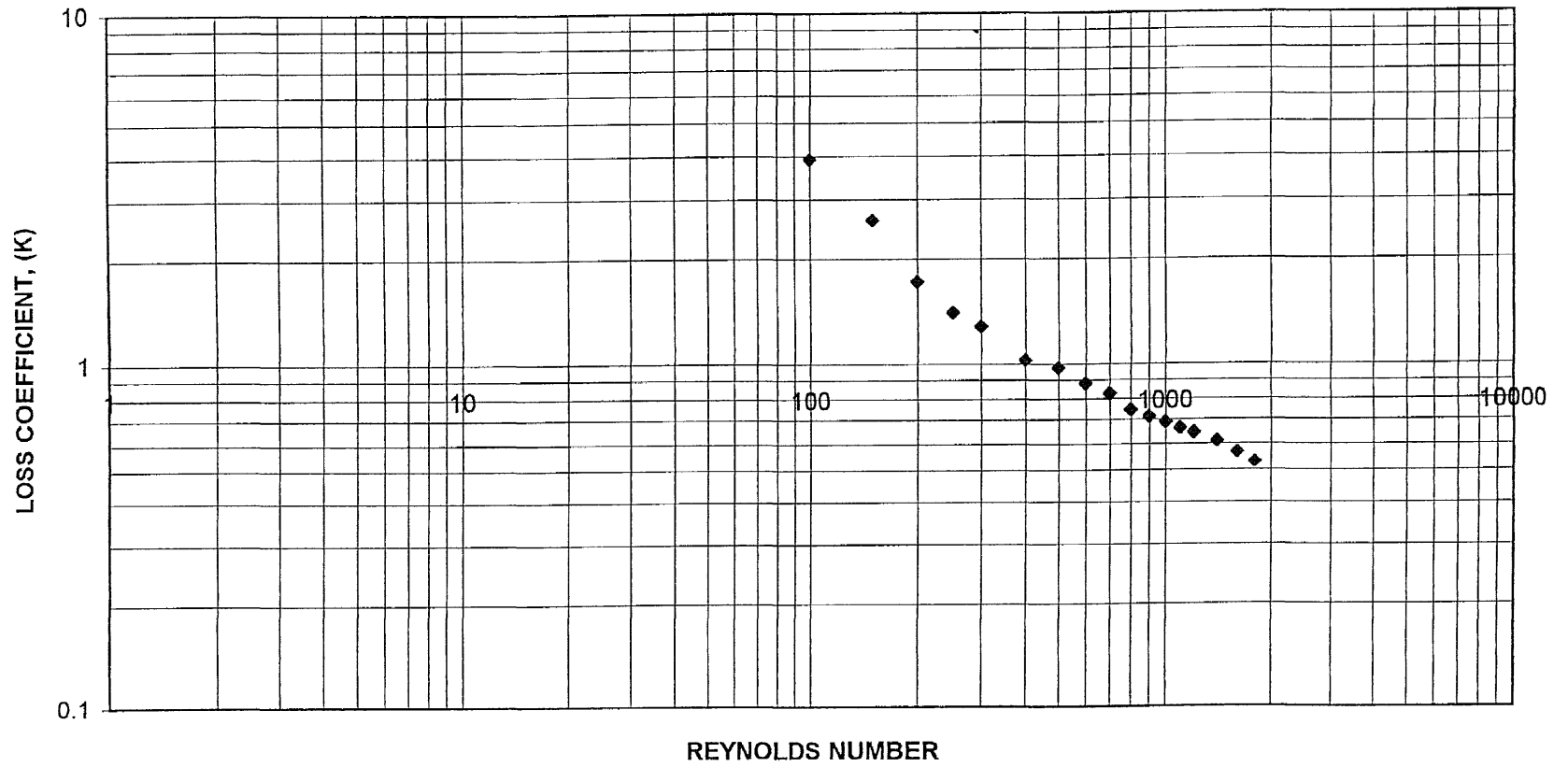
Figure 5.2.2

Pressure Loss Coefficient versus Reynolds Number for a Bend Radius to Duct Width Ratio of 1.0

5.3 Discussion

5.3.1 Computer Solution

The validity of these results is based on the assumption that the equations of continuity and momentum are applicable to this problem. The FIDAP package solved these equations through finite element analysis. By keeping the Reynolds Number low, turbulent modeling is avoided. Laminar flow is predictable and linear, and higher order terms in solutions are negligible. Therefore, this problem is simple to analyze and will lend itself to valid results.

There are distinctions between empirical analysis and the generated computer solution. Empirical study focuses on various positions within the model. In the case of this particular model, the pressure change would have been sampled from some point in the entrance of the bend and then along the downstream of the bend exit. The computer analysis determined values for numerous points within the model. Values for velocity and pressure could be determined for hundreds of points within the model. This would have been very difficult for an empirical study to accomplish.

5.3.2 Pressure Loss Coefficient Trends

Some important observations involving pressure and velocity can be seen within the model. Certain trends can be discussed with respect to changes in duct geometry. As R/D increases, pressure loss due to the bend decreases. Accordingly, if we held the duct diameter, D, constant and let the bend radius, R, approach infinity, the duct would approach a straight length. Therefore, the bend would be eliminated from the model and so would any pressure changes due to its presence. This would leave friction losses in a

straight duct as the sole cause for total pressure losses. By allowing the radius, R, to become infinite the duct length becomes infinitely long and therefore the pressure loss for the straight duct would become infinite. Figure 5.3.1 & 5.3.2 show the loss coefficient, K_b, decreasing as the ratio of R/D increases. From Tables 5.2.1 and 5.2.2, an example for a Reynolds Number of 50 shows a K_b value of 3.929 for an R/D of 1.0 as compared to a K_b value of 1.367 for an R/D of 1.5.

By further examining figure 5.3.1 we may compare the loss coefficients between both ducts as Reynolds Number increases. Table 5.3.1 depicts the percentage increase in pressure loss coefficient value between a bend radius to duct width ratio of 1.0 to a ratio of 1.5. The largest percentage increase value is at a Reynolds Number of 50. Then the percentage increase gap is lowered as Reynolds number increases and steadies out at a mean value of 148.42%. Most changes in loss percentages fall between values of 130% and 170%.
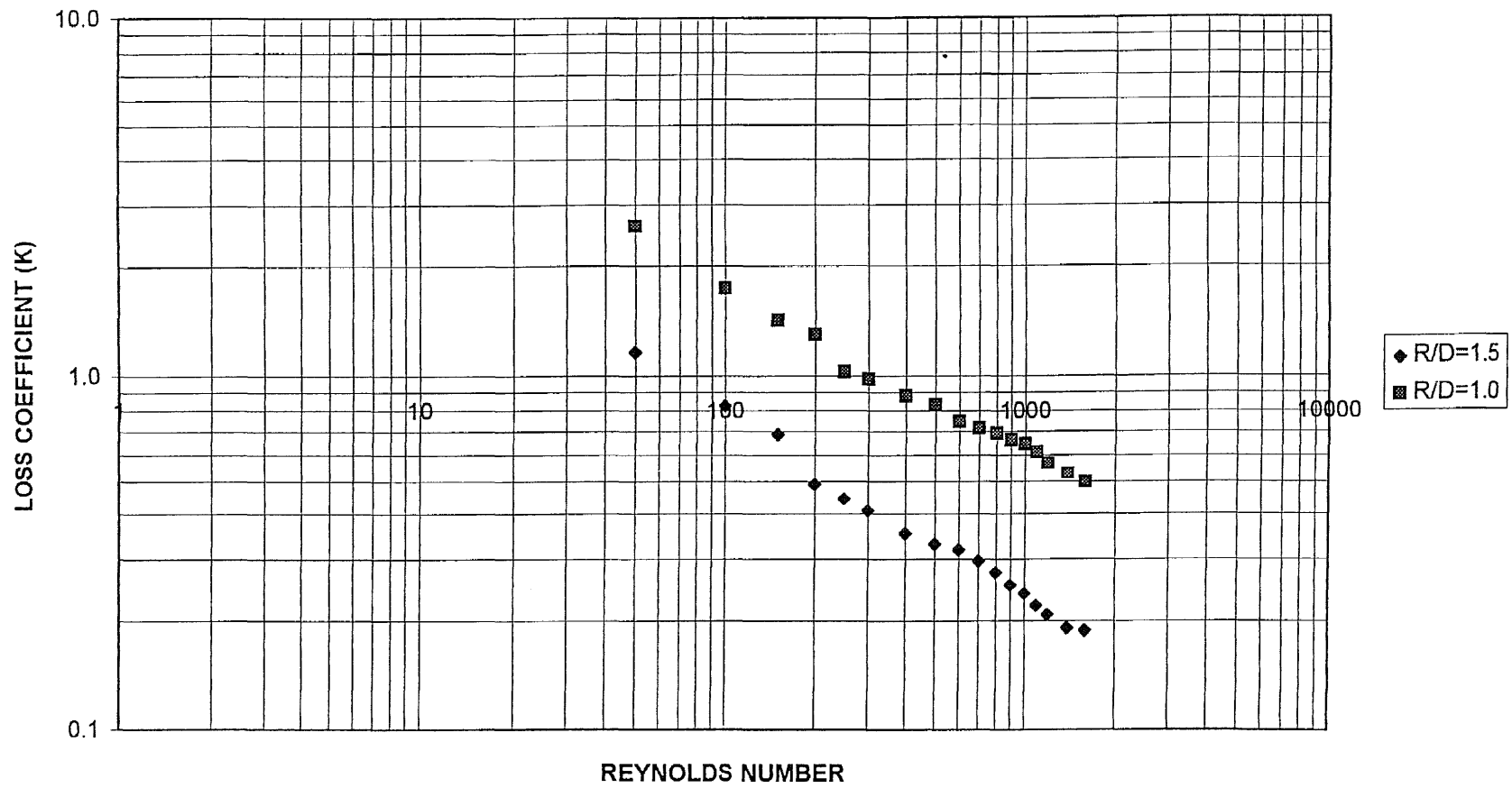
Figure 5.3.2.a
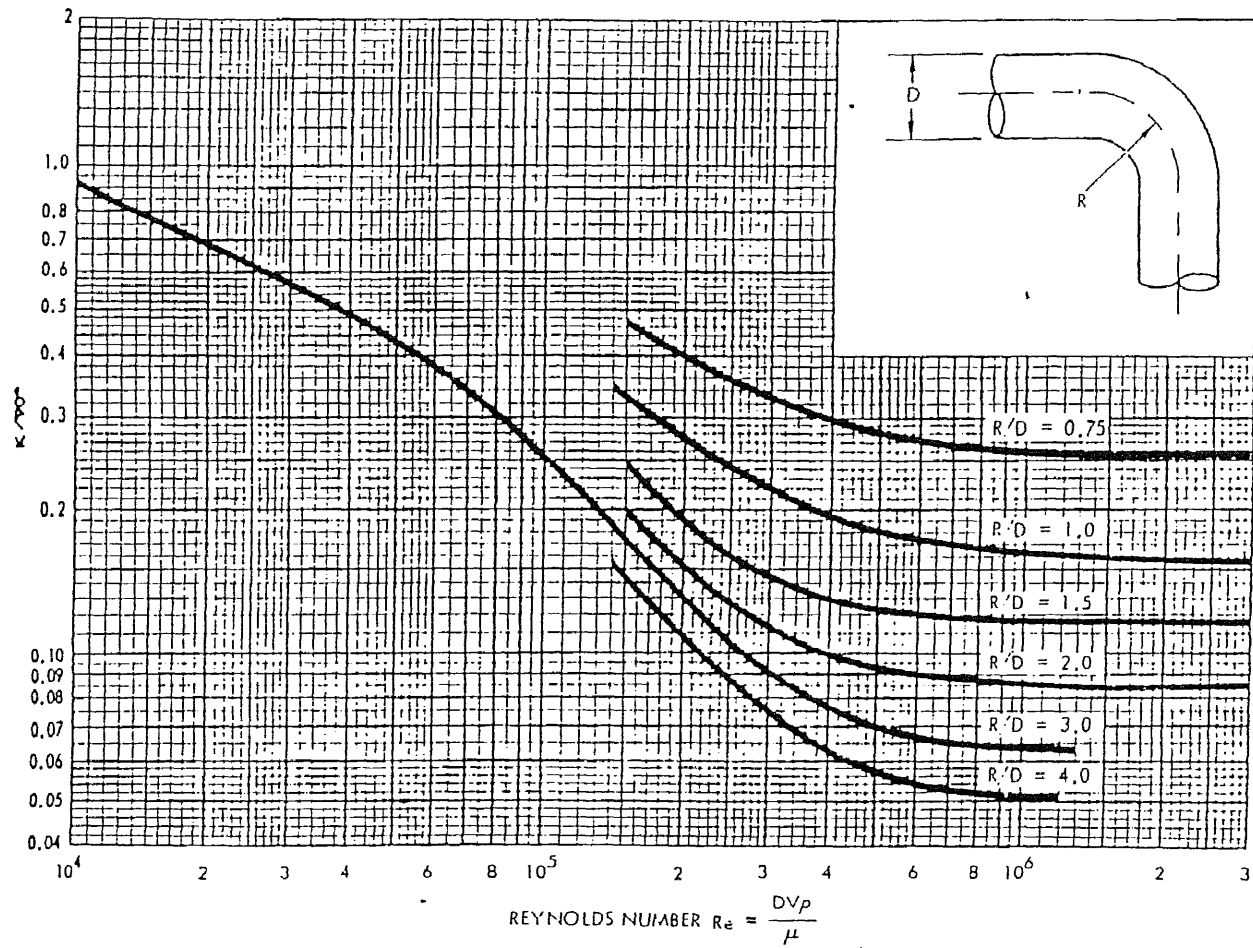**Pressure Loss Coefficient, Kb, versus Reynolds Number 90 Bends**

Figure 5.3.2.b
Resistance Coefficients K for 90° Bends

Table 5.3.2.a
Percentage Increase in Loss Coefficient Between R/D = 1.0 and R/D = 1.5 as
Reynolds Number Changes

REYNOLDS NUMBER	K R/D=1.0	K R/D=1.5	% INCREASE
50	3.929	1.367	187.34
100	2.602	1.158	124.69
150	1.735	0.826	110.07
200	1.412	0.687	105.44
250	1.291	0.491	163.32
300	1.026	0.445	130.44
400	0.979	0.410	138.64
500	0.882	0.353	149.84
600	0.830	0.330	151.50
700	0.745	0.317	134.51
800	0.714	0.296	141.33
900	0.690	0.275	151.15
1000	0.663	0.254	161.14
1100	0.644	0.240	168.75
1200	0.612	0.221	177.36
1400	0.568	0.208	173.07
1600	0.530	0.191	176.98
1800	0.498	0.188	164.83

By examining Figure 5.3.1 it can be observed that as Reynolds Number increases, effect on the pressure loss coefficient due to the bend decreases. Also, when Reynolds Number is below 1000, the effect of the bend is more dramatic on the pressure loss coefficient. For an R/D of 1.5 the value of K_b at a Reynolds Number of 50 is 1.367 while at a Reynolds Number of 1000 the value of K_b is only 0.254 (shown in Table 5.3.1). From Figure 5.3.1 it is seen that the absolute value of the slope of the downward curve in the Reynolds Number region of 50 to 1000 (about 3.469×10^{-3}) is larger than the absolute value of the slope of the Reynolds number region extending beyond 1000 (about 1.688×10^{-4}). This would indicate that as Reynolds Number increases the loss coefficient value would

become constant. Figure 5.3.1 graphically demonstrates this point and shows further similarities between loss coefficient curves for varying R/D ratios.

Figure 1.3.1 depicts an empirically determined curve for a 90° Ell (circular elbow, R/D=1.5) for K values for a Reynolds Number range of 300 to 2000. The value of K is 2.6 for a Reynolds Number of 300, and is 1.8 for a Reynolds Number of 1800. The curve behaves similarly to those of Figure 5.3.1. For a Reynolds Number of 300 Figure 5.2.1 gives a K_b of 0.455, and for a Reynolds Number of 1800 Figure 5.2.1 gives a K_b of 0.188. The magnitude of K from Figure 1.3.1 is greater than that of Figure 5.2.1 due to increased pressure losses in the three dimensional bend. The three dimensional bend has more surface area per unit length for fluid contact than the two-dimensional bend, and therefore the friction loss in the bend is greater.

5.3.3 Pressure and Velocity Distribution Trends within the Duct

Variations in the velocity and pressure distributions are observed as the water flows through the duct. As the fluid begins in the entrance of the duct, the velocity profile is a symmetrical, parabolic function. The parabolic profile of the velocity skews as it nears the bend. The skewing of the velocity profile becomes more pronounced as the fluid travels through the bend. The velocity profile eventually returns to the symmetrical, parabolic function, seen in the entrance region, at some point in the exit region. When the velocity profile is skewed, it's value increases towards the top wall and decreases near the bottom wall. Figure 5.3.3 defines the top and bottom walls of the model. Table 5.3.3 and Figure 5.3.4 relate velocity profiles to physical locations within the bend. From Table 5.1.2 the

centerline (by a notation of 0.5) nodal velocity values can be found for several profiles within the duct. As the fluid enters the bend the centerline value is 1.503 cm/s. The velocity centerline values changes respectively: 1.498 cm/s, 1.420 cm/s, 1.445 cm/s, 1.479 cm/s, 1.522 cm/s, and 1.503 cm/s as the fluid travels through and exits the bend. The largest velocity nodal value observed within the bend is 1.571 cm/s and develops early in the entrance of the fluid into the bend.

TOP WALL
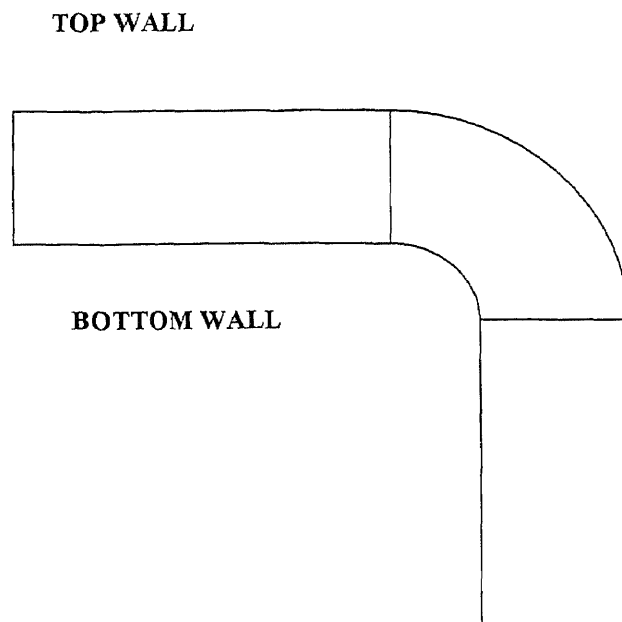
BOTTOM WALL

Figure 5.3.3.a
Top and Bottom Wall Definition for Channel Bend Model

The pressure distribution varies as the fluid flows through the bend. Figure 5.3.4 and Table 5.3.2 relate pressure distributions along perpendicular lines to the top and bottom wall defined in the channel. These pressure distributions are used to determine pressure gradient values that are perpendicular to flow (along lines traveling normal from the top wall to the bottom wall). The pressure gradient across lines within the entrance region is

approximately zero. As the fluid approaches and enters the bend, the magnitude of the pressure gradient increases. During the fluid's travel through the bend the pressure dramatically increases on the bottom wall region. At some point after exiting the bend, the pressure gradient reverses itself, and pressure becomes higher on the top wall region. After some distance into the exit of the duct, the fluid pressure gradient once again becomes zero across lines perpendicular to the top and bottom wall of the bend.

Values for pressure nodal values are found in Table 5.1.2, and the pressure gradients (perpendicular to flow) can be calculated for the specified profile lines. As the fluid enters the bend, the pressure gradient value is -0.2156 g/cm-s^2 (from top to bottom wall). Further gradient values are -0.9043 g/cm-s^2, -0.8476 g/cm-s^2, -0.7663 g/cm-s^2, -0.6078 g/cm-s^2, and 0.0012 g/cm-s^2 as the fluid continues through and exits the bend (Figures 5.1.20 to 5.1.25). Within the bend and along the bottom wall pressure values initially decrease (7.4592 g/cm-s^2, 6.8682 g/cm-s^2, 6.8406 g/cm-s^2, from Table 5.1.2) and then begins to increase (6.8579 g/cm-s^2, 6.9044 g/cm-s^2) for two nodes until it finally drops again (6.6343 g/cm-s^2) and continues to fall all the along the exit length. Along the top wall the pressure values increase as the fluid enters the bend (7.6748 g/cm-s^2, 7.7725 g/cm-s^2) then drops as it continues through and exits the bend (7.6882 g/cm-s^2, 7.6242 g/cm-s^2, 7.5122 g/cm-s^2, 6.6331 g/cm-s^2). As the Reynolds Number increases the magnitude of the pressure gradient values within the bend also increase.

Pressure gradients and velocity profiles demonstrate a converse relationship as they change throughout the bend of the channel. The velocity profiles are symmetrical when the pressure gradient values are zero. The most skewed velocity profile (Figure

5.1.5) is found at the greatest magnitude pressure gradient value within the bend (-.9043 g/cm-s^2, Figure 5.1.21). As the velocity profile returns to symmetry (Figures 5.1.6 to 5.1.8) the corresponding pressure gradient values return to zero (Figures 5.1.21 to 5.1.23). This converse relationship is also seen when the velocity profile skews slightly towards the bottom wall (Figure 5.1.9) after exiting the bend and the pressure gradient value becomes positive (.0012 g/cm-s^2, Figure 5.1.24).

Table 5.3.3.a
Pressure Differential Across Perpendicular Lines between the Top and Bottom Walls of the Channel Bend

FIGURE 5.3.4 LETTER	PRESSURE DISTRIBUTION FIGURE	PRESSURE DIFFERENTIAL FROM TOP TO BOTTOM WALL
A	5.1.18	0
B	5.1.19	0
C	5.1.20	NEGATIVE
D	5.1.21	NEGATIVE
E	5.1.22	NEGATIVE
F	5.1.23	NEGATIVE
G	5.1.24	NEGATIVE
H	5.1.25	POSITIVE
I,J,KLM,N,O,P	5.1.27 - 5.1.33	0

Table 5.3.3.b
Velocity Profiles Across Perpendicular Lines between the Top and Bottom Walls of the Channel Bend

FIGURE 5.3.4 LETTER	VELOCITY PROFILE FIGURE	VELOCITY PROFILE TYPE (SKEW or SYMM.)
A	5.1.2	SYMMETRICAL
B	5.1.3	SYMMETRICAL
C	5.1.4	SKEW
D	5.1.5	SKEW
E	5.1.6	SKEW
F	5.1.7	SKEW
G	5.1.8	SKEW
H	5.1.9	SYMMETRICAL
I,J,K,L,M,N,O,P	5.1.10 - 5.1.17	SYMMETRICAL
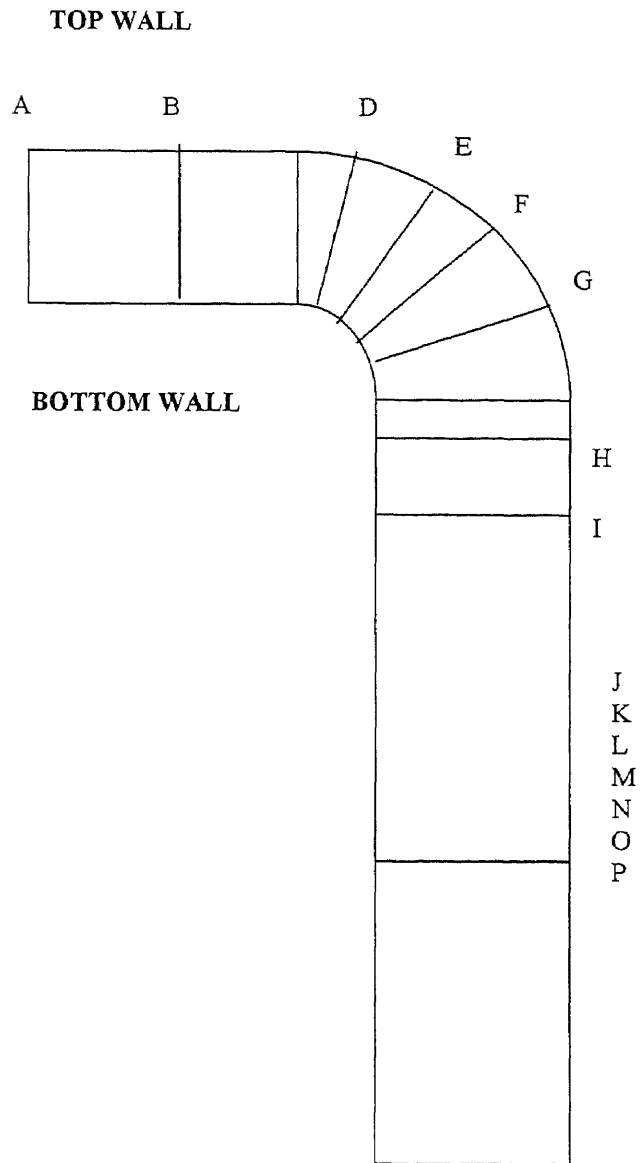
Figure 5.3.3.b
Pressure and Velocity Profiles Across Perpendicular Lines Between the Top and
Bottom Walls of the Channel Bend

5.4 Conclusions

Pressure loss coefficients were determined for laminar two dimensional incompressible channel flow in a 90° bend using the FEM software package, FIDAP. Curves for loss coefficients were determined for ducts with a bend radius to duct width ratio of 1.5 and 1.0. Similarities between Figures 5.3.1 and Figure 5.3.2 validate the method and results generated by the use of FIDAP.

The pressure loss coefficient decreased with increasing Reynolds Number. Initial pressure loss coefficient values (Reynolds Number of 50) were high as compared to final pressure loss values (Reynolds Number of 1800) within the channel. For an R/D ratio of 1.5, at a Reynolds Number of 50, the pressure loss coefficient, K, was 1.367. When Reynolds Number was 1800 the value had decreased to 0.188. For an R/D ratio of 1.0, at a Reynolds Number of 50, K was 3.929, while dropping down to 0.498 for a Reynolds Number of 1800. Both dropping by a factor of about 7.5. The pressure loss coefficient dropped more significantly for Reynolds Number ranging from 50 to 1000 than in the range of 1000 to 1800. After 1000 the decrease in loss coefficient became smaller and indicated the possibility of reaching a constant. As the ratio of R/D decreased from 1.5 to 1.0 the value of the pressure loss coefficient for each Reynolds Number was increased by an approximate ratio of 2.5.

Within the channel bend itself the pressure demonstrated an inverse relationship with fluid velocity. As the fluid moved through the duct entrance, with the velocity remaining symmetrical and parabolic, the pressure gradient across perpendicular lines running from the top wall to the bottom wall was zero. Upon the fluid entering the bend, the pressure decreased along the top wall and increased along the bottom wall.

Simultaneously, the velocity increased towards the top wall and decreased along the bottom wall. As the fluid continued through the bend, the magnitude of the pressure gradient increased as pressure increased against the bottom wall, while the maximum velocity value moved toward the top wall. Near the exit of the bend the pressure increased on the top wall and decreased on the bottom wall, and the velocity maximum moved past the channel centerline toward the bottom wall. Shortly after that point, the velocity became symmetrical about the channel centerline and the pressure gradient returned to zero.

FIDAP Program for modeling of a two-dimensional, 90° channel bend with constant radius. duct radius to duct height ratio of 1.5.


```
FIMESH (2-D, IMAX=9, JMAX=5)
EXPI(DELTAS)
/1 2 3 4 5 6 7 8 9
/1 0 10 0 22 0 37 0 137
1 0 9 0 12 0 15 0 100
EXPJ(DELTAS)
/1 2 3 4 5
/1 0 9 0 17
1 0 8 0 8
/ HORIZONTAL AND VERTICAL MESH RATIO SPACING
$h=1
$v=1
/ DIMENSIONAL DEFINITION OF DUCT, CO-ORDINATE LAYOUT
POINT(SYSTEM=1)
/PT# I J K X Y Z
/      r
1 1 1 1 0.0 1.0 0
/        il  r
2 3 1 1 5.0 1.0 0.0
/        il.r  ol
4 9 1 1 6.0 -60.0 0.0
/        il.r.h  ol
5 9 5 1 7.0 -60.0 0.0
/        il  r.h
7 3 5 1 5.0 2.0 0.0
/          r.h
8 1 5 1 0.0 2.0 0.0
/          r.h/2
10 1 3 1 0.0 1.5 0.0
/        il.r.h/2 ol
13 9 3 1 6.5  -60.0 0.0
/          il  r.h/2
11 3 3 1 5.0  1.5 0.0
/CENTER OF ARC(S)
/          il
9 0 0 0 5.0 0.0 0.0
COORDINATE(SYSTEM=2,ROTATION,CYLINDRICAL)
```

```
9
POINT(SYSTEM=2)
/        r
3 7 1 1 1.0 0.0
/        r.h
6 7 5 1 2.0 0.0
/        r.h/2
12 7 3 1 1.5 0.0
/        r
14 5 1 1 1.0 45
/        r.h
15 5 5 1 2.0 45
/        r.h/2
16 5 3 1 1.5 45
/DEFINITION OF LINES FOR DUCT WALLS, ENTRANCE, EXIT, AND SPECIFIC
/SECTIONS
LINE
1 2
8 7
3 12 $h
12 6 $v
4 13 $h
13 5 $v
2 11 $h
11 7 $v
5 6
4 3
14 16 $h
16 15 $v
1 10 $h
10 8 $v
2 11 $h
11 7 $v
ARC
2 14 9 $h
14 3 9 $v
11 16 9 $h
16 12 9 $v
7 15 9 $h
15 6 9 $v
/MESH FORMATION INFORMATION
SURFACE
1 5
ELEMENTS(QUADRILATERAL,NODES=9,ENTITY="FLUID")
1 5
```

```
ELEMENTS(BOUNDARY,EDGE,FACE,ENTITY="WALL")
4 1
8 5
ELEMENTS(BOUNDARY,EDGE,FACE,ENTITY="OUTLET")
4 5
ELEMENTS(BOUNDARY,EDGE,FACE,ENTITY="INLET")
1 8
/ENTRANCE NOTATION OF INITIAL CONDITIONS
BCNODE(UX,CONSTANT)
8 5
4 1
BCNODE(UY,CONSTANT)
8 5
4 1
1 8
/VELOCITY INPUT
BCNODE(UX,PARABOLIC=0)
1 8 3.006
END
FIPREP
DATAPRINT(CONTROL)
EXECUTION(NEWJOB)
PRINTOUT(NONE)
PROBLEM(2D,INCOMPRESSIBLE,STEADY,NONLINEAR,NEWTONIAN,MOMEN
        TUM,ENERGY,FIXED,SINGLEPHASE)
RENUMBER(PROFILE)
ENTITY(FLUID,NAME="FLUID")
ENTITY(PLOT,NAME="WALL")
ENTITY(PLOT,NAME="OUTLET")
ENTITY(PLOT,NAME="INLET")
DENSITY(CONSTANT=0.998)
VISCOSITY(CONSTANT=.01002)
END
```

FIDAP Program for modeling of a two-dimensional, 90° channel bend with constant radius. Duct radius to duct height ratio to 1.0.

```
FIMESH (2-D, IMAX=9, JMAX=5)
EXPI(DELTAS)
/1 2 3 4 5 6 7 8 9
/1 0 10 0 22 0 37 0 137
1 0 9 0 12 0 15 0 100
EXPJ(DELTAS)
/1 2 3 4 5
/1 0 9 0 17
1 0 8 0 8
$h=1
$v=1
POINT(SYSTEM=1)
/PT# I J K X Y Z
/           r
1 1 1 1 0.0 1.0 0
/       il  r
2 3 1 1 5.0 1.0 0.0
/       il.r  ol
4 9 1 1 6.0 -100.0 0.0
/       il.r.h  ol
5 9 5 1 8.0 -100.0 0.0
/       il  r.h
7 3 5 1 5.0 3.0 0.0
/           r.h
8 1 5 1 0.0 3.0 0.0
/           r.h/2
10 1 3 1 0.0 2.5 0.0
/       il.r.h/2 ol
13 9 3 1 7.5  -100.0 0.0
/       il  r.h/2
11 3 3 1 5.0 2.5 0.0
/CENTER OF ARC(S)
/           il
9 0 0 0 5.0 0.0 0.0
COORDINATE(SYSTEM=2,ROTATION,CYLINDRICAL)
9
POINT(SYSTEM=2)
/       r
3 7 1 1 1.0 0.0
```

```
/       r.h
6 7 5 1 3.0 0.0
/       r.h/2
12 7 3 1 2.0 0.0
/       r
14 5 1 1 1.0 45
/       r.h
15 5 5 1 3.0 45
/       r.h/2
16 5 3 1 2.0 45
LINE
1 2
8 7
3 12 $h
12 6 $v
4 13 $h
13 5 $v
2 11 $h
11 7 $v
5 6
4 3
14 16 $h
16 15 $v
1 10 $h
10 8 $v
2 11 $h
11 7 $v
ARC
2 14 9 $h
14 3 9 $v
11 16 9 $h
16 12 9 $v
7 15 9 $h
15 6 9 $v
SURFACE
1 5
ELEMENTS(QUADRILATERAL,NODES=9,ENTITY="FLUID")
1 5
ELEMENTS(BOUNDARY,EDGE,FACE,ENTITY="WALL")
4 1
8 5
ELEMENTS(BOUNDARY,EDGE,FACE,ENTITY="OUTLET")
4 5
ELEMENTS(BOUNDARY,EDGE,FACE,ENTITY="INLET")
1 8
```

```
BCNODE(UX,CONSTANT)
8 5
4 1
BCNODE(UY,CONSTANT)
8 5
4 1
1 8
BCNODE(UX,PARABOLIC=0)
1 8 3.006
END
FIPREP
DATAPRINT(CONTROL)
EXECUTION(NEWJOB)
PRINTOUT(NONE)
PROBLEM(2D,INCOMPRESSIBLE,STEADY,NONLINEAR,NEWTONIAN,MOMEN
        TUM,ENERGY,FIXED,SINGLEPHASE)
RENUMBER(PROFILE)
ENTITY(FLUID,NAME="FLUID")
ENTITY(PLOT,NAME="WALL")
ENTITY(PLOT,NAME="OUTLET")
ENTITY(PLOT,NAME="INLET")
DENSITY(CONSTANT=0.998)
VISCOSITY(CONSTANT=0.01002)
END
```

APPENDIX B

SAMPLE CALCULATION OF PRESSURE LOSS COEFFICIENT

PROBLEM DEFINITION:

Water @70°F flowing through a two-dimensional duct containing the following properties:

$$\rho = 0.998 \text{ g/cm}^3$$
$$\mu = 1.002 \times 10^{-2} \text{ g/cm-s}$$
$$V_{max} = 1.503 \text{ cm/s}$$

The duct geometry for this particular problem has an inlet length of 5 cm, a 90° bend with a radius of 1.5 cm, and an exit length of 55.8 cm. The duct width or duct diameter is 1 cm. This calculation will determine a loss coefficient due to the pressure loss created by the bend within the duct.

The velocity equation is $V(y) = 4V_{max} (y - y^2)$.

Begin by determining the mean velocity within the duct.

$$V_{mean} = 1/D \int V \, dy$$

Integrate V(y) between the limits of the duct entrance:

$$V_{mean} = 1/D \int 4V_{max} (y - y^2) \, dy \text{ from y=0 to y=D}$$

$$V_{mean} = 4V_{max}/D \left[y^2/2 - y^3/3 \right] \Big|_{y=0 \text{ to } y=D}$$

$$\mathbf{V_{mean} = 2/3 \ V_{max}}$$

Determine the Reynolds Number using the following equation:

$$Re = (\rho \ V_{mean} \ D_h) / \mu$$

Where $D_h = 2D$

Substituting values stated in problem

$$\mathbf{Re \approx 200}$$

Using the definition of the friction factor, f, for a two-dimensional channel

$$\boldsymbol{f = 96 / Re}$$

Substituting values stated in problem

$f = 0.48$

Determine the equivalent straight duct length for flow to return to fully developed flow after exiting the bend.

SL_{FDF} = Entrance length + Exit length

Entrance length = 5 cm

Exit length = 55.8 cm

SL_{FDF} = 5 + 55.8 = 60.8 cm

The value for (L/D_h) can then be determined to find the coefficient of friction loss within the duct.

$K_f = f (L/D_h)$

$K_f = 14.592$

Pressure loss due to friction in the duct

$\Delta P_{SL} = 0.5 \, K_f \, \rho \, (V_{mean})^2$

Substituting values

$\Delta P_{SL} = 7.3105628 \text{ g/cm-s}^2$

Determine the pressure loss due to the bend

$\Delta P_{TOTAL} = \Delta P_{SL} + \Delta P_{BEND}$

rearranging above equation

$\Delta P_{BEND} = \Delta P_{TOTAL} - \Delta P_{SL}$

The total pressure loss is taken from the FIDAP solution. It is the determined by subtracting the pressure value found at the exit point of the bend from the pressure value found at the duct entrance. The average values for the entrance and exit lines are found in Table 5.2.1.a. The specific nodal values are located in Table 5.2.1.

$\Delta P_{TOTAL} = 8.1599224 - 0.50486836 = 7.655054 \text{ g/cm-s}^2$

Therefore

$\Delta P_{BEND} = 7.655054 - 7.3105628 = 0.344491$ g/cm-s^2

The loss coefficient for the bend is then determined by

$K_B = 2 \, \Delta P_{BEND} / \rho \, (V_{mean})^2$

Substituting values

$K_B = 0.687$

APPENDIX C

FIDAP GRAPHICAL AND NODAL OUTPUT
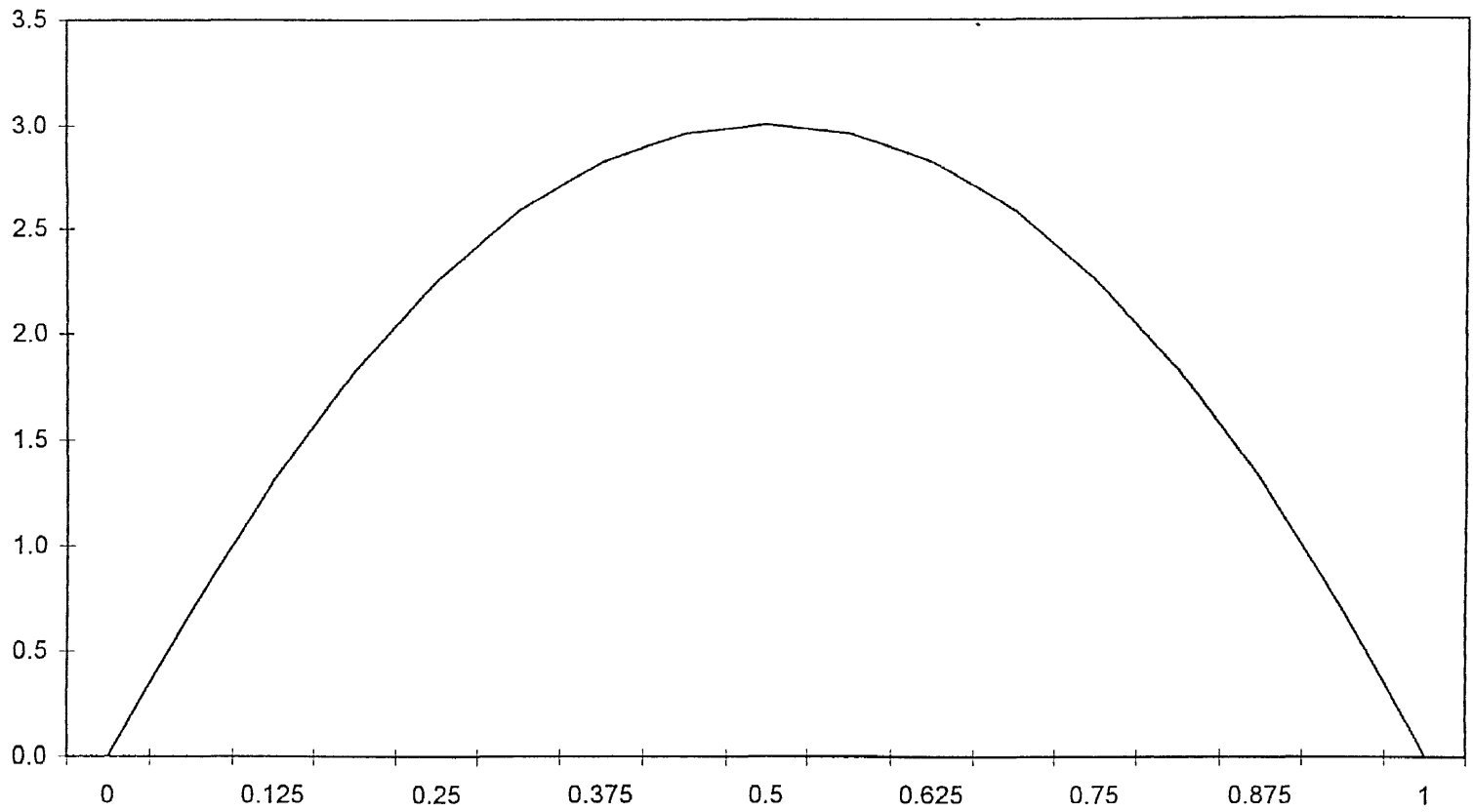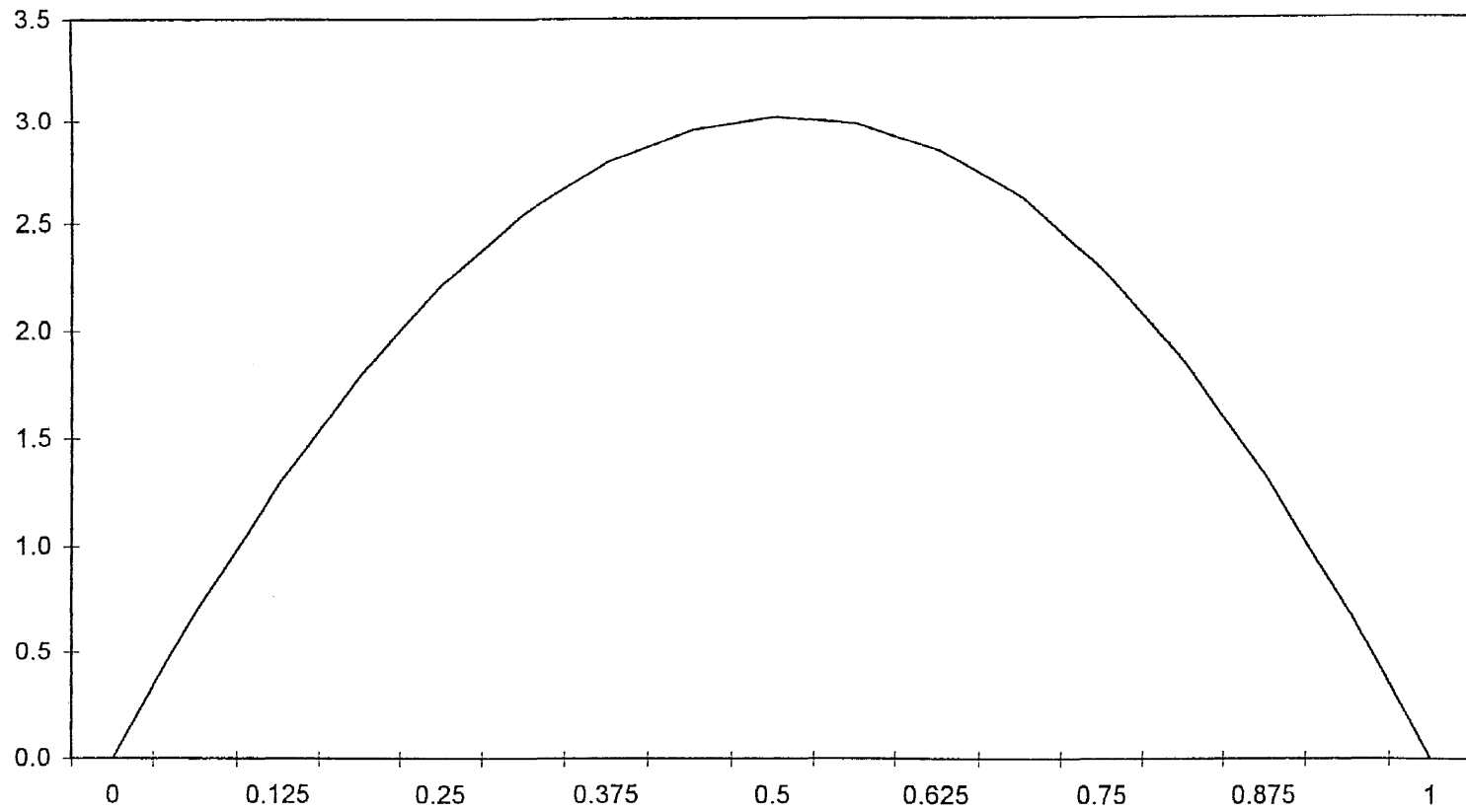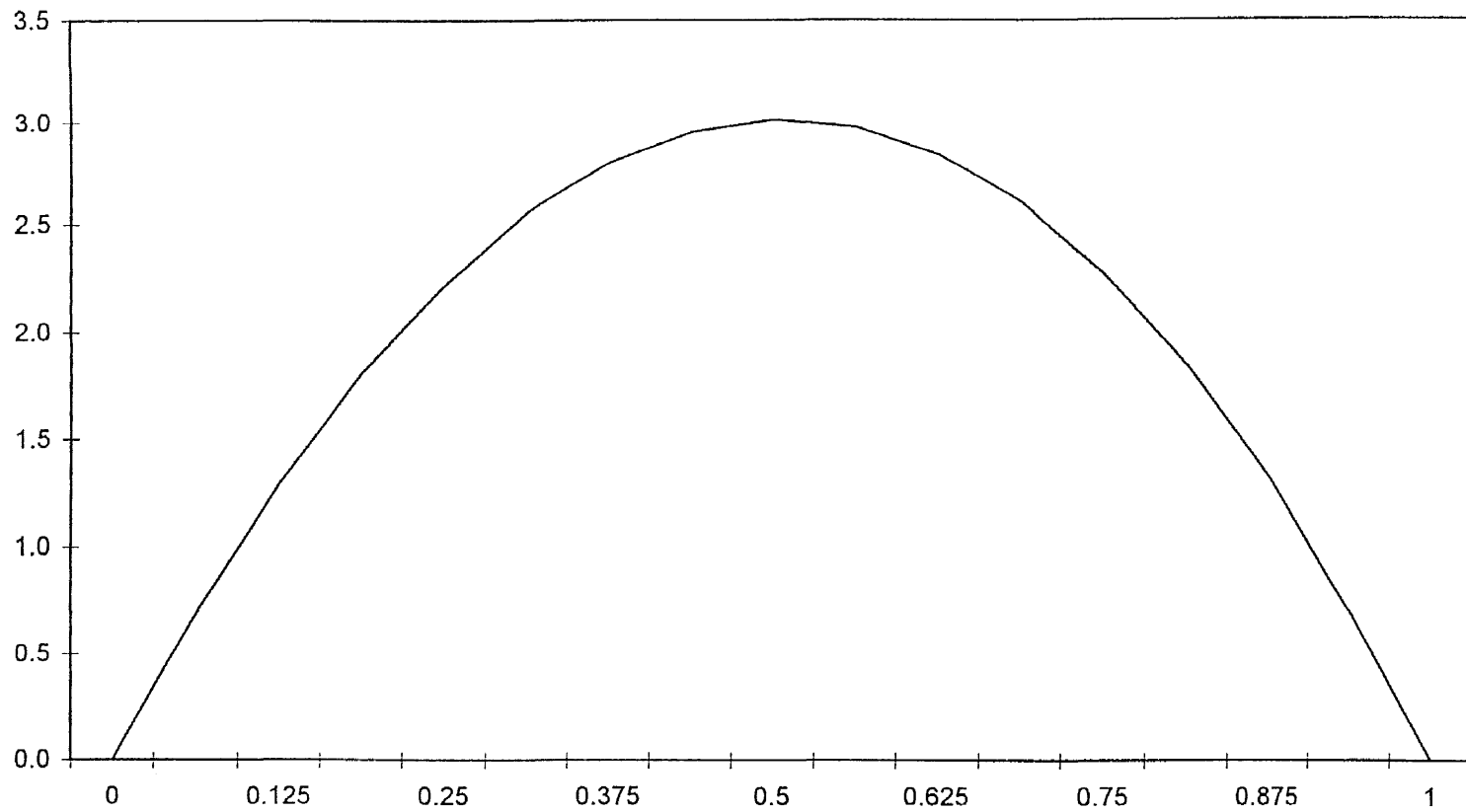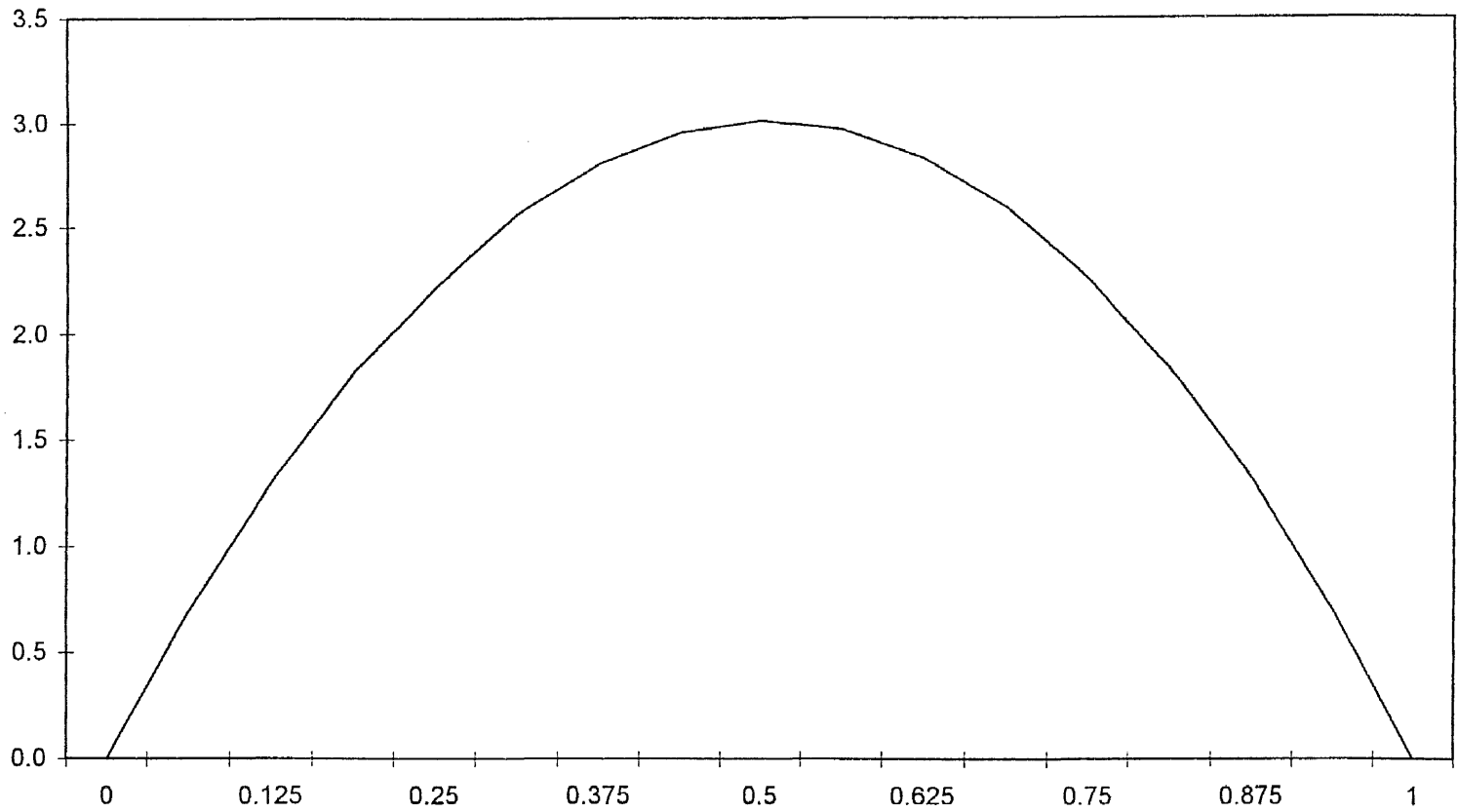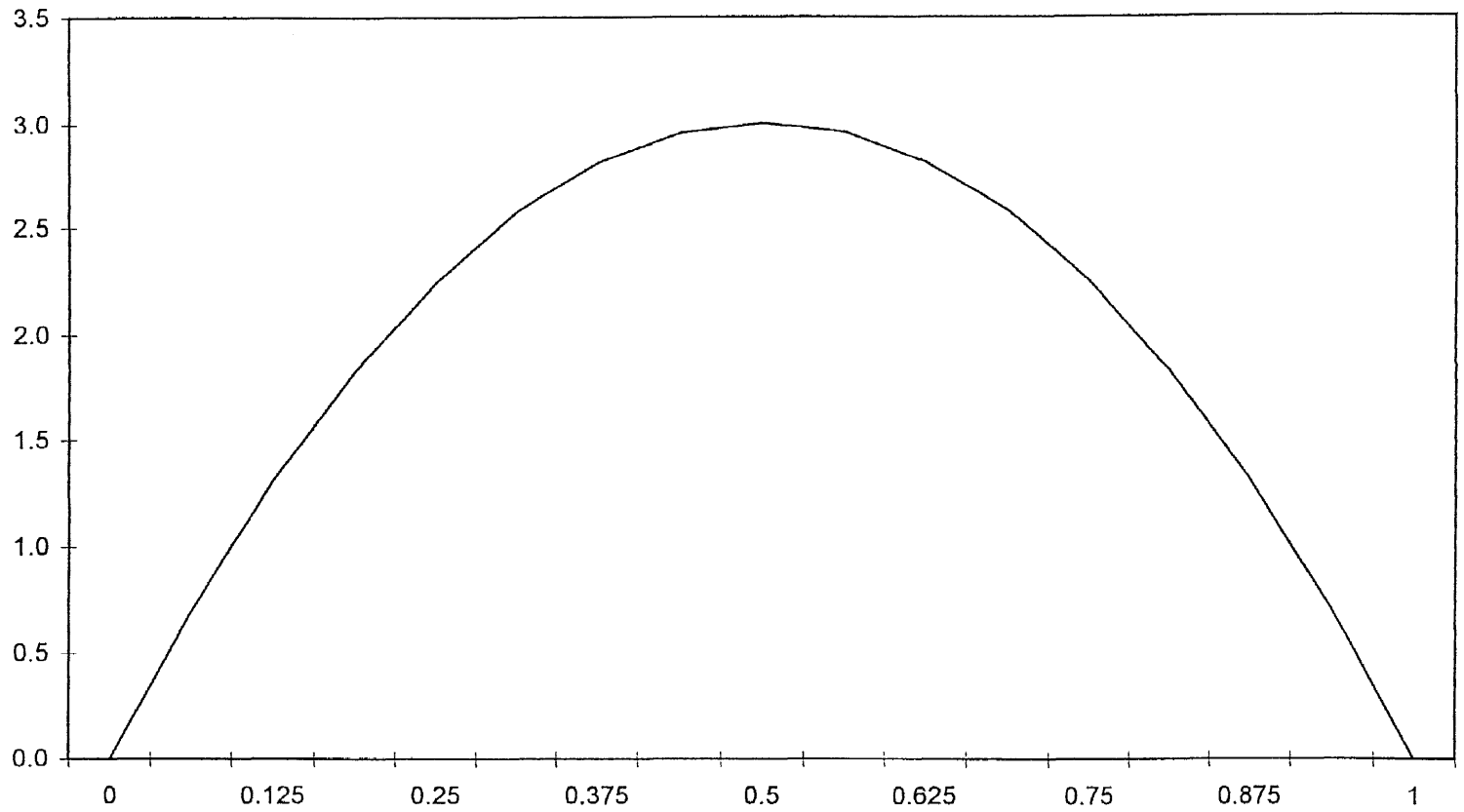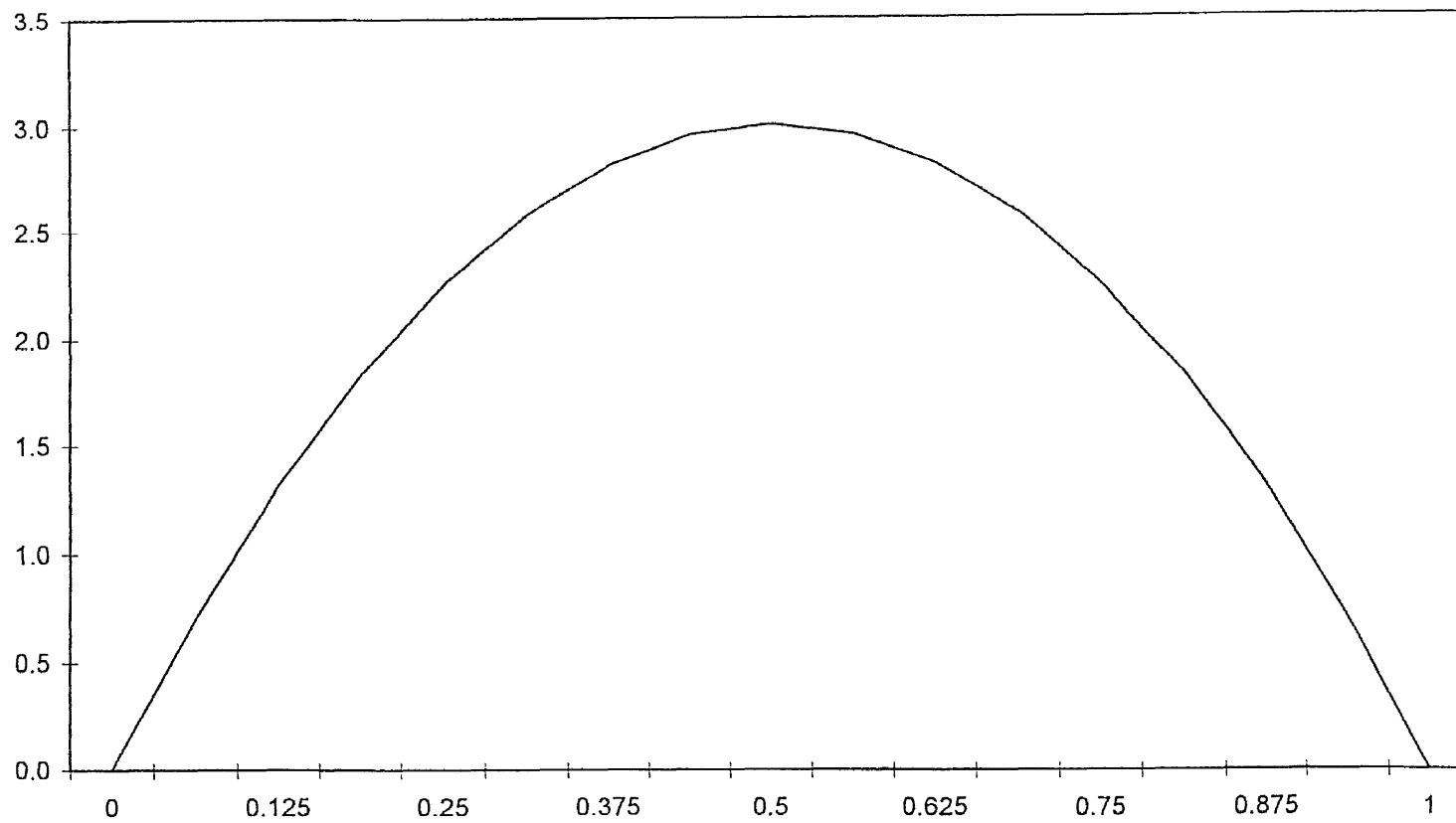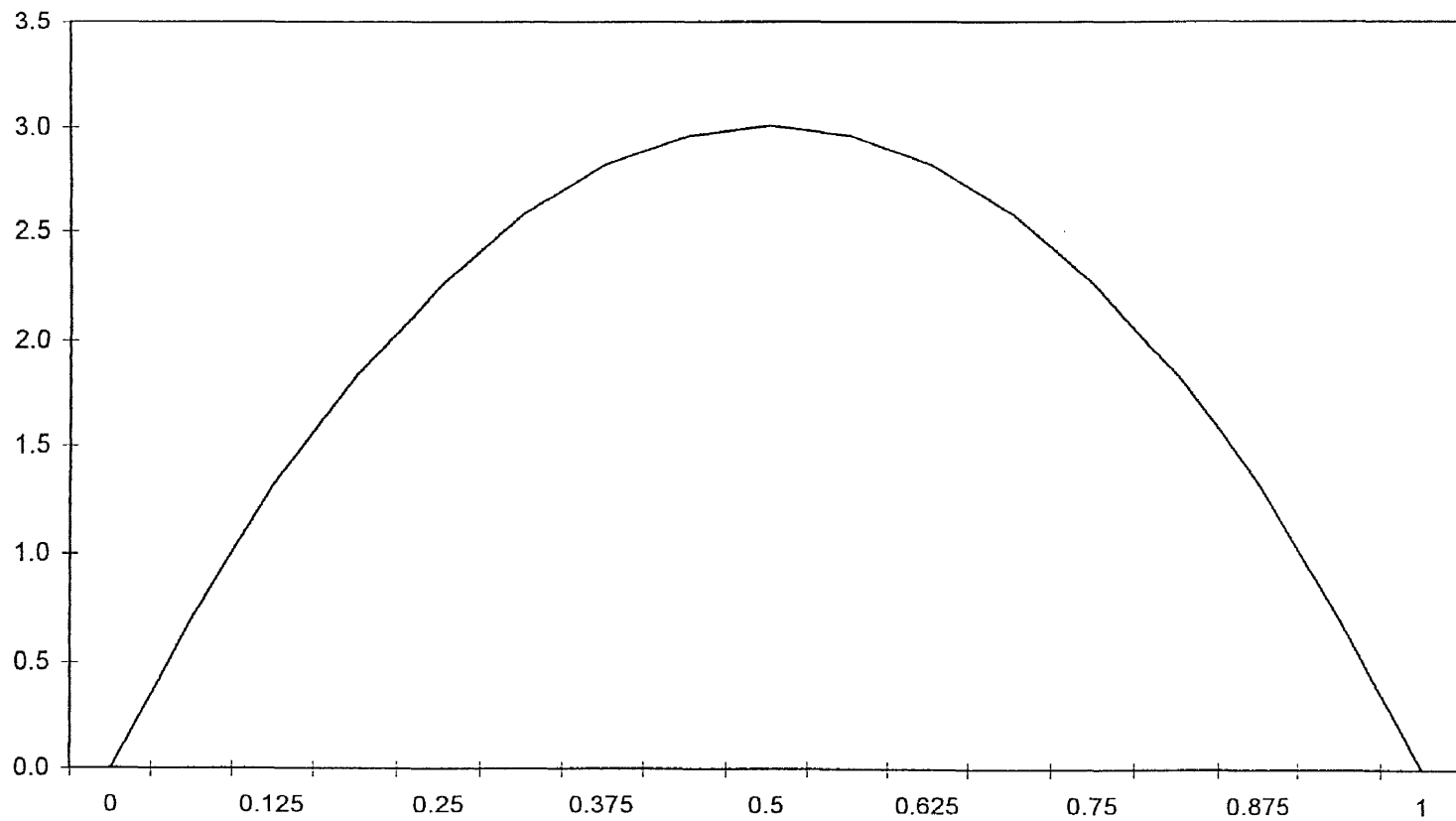
Figure 5.1.2
Velocity Distribution for Line 1 2193
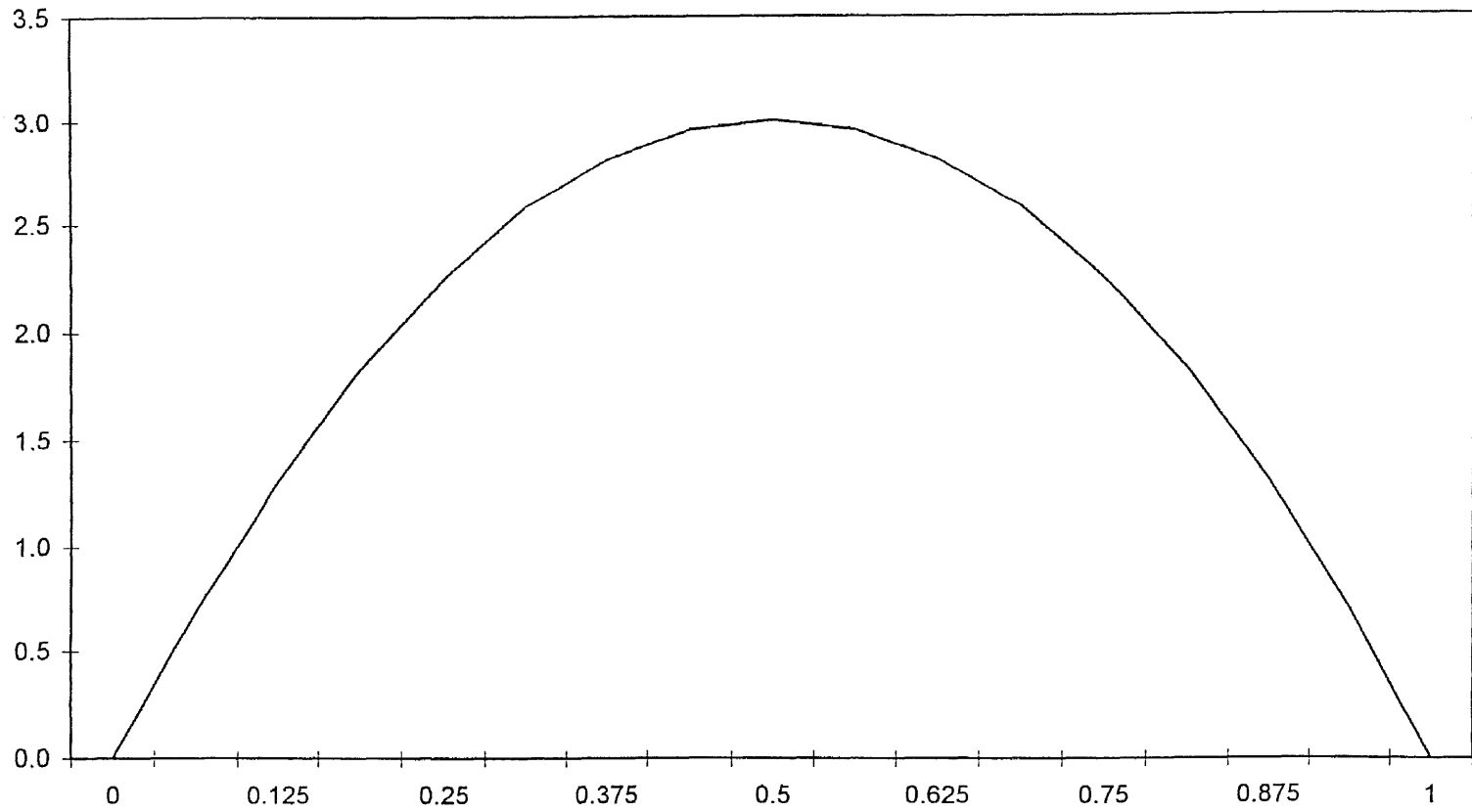
Figure 5.1.3
Velocity Distribution for Line 5 2197
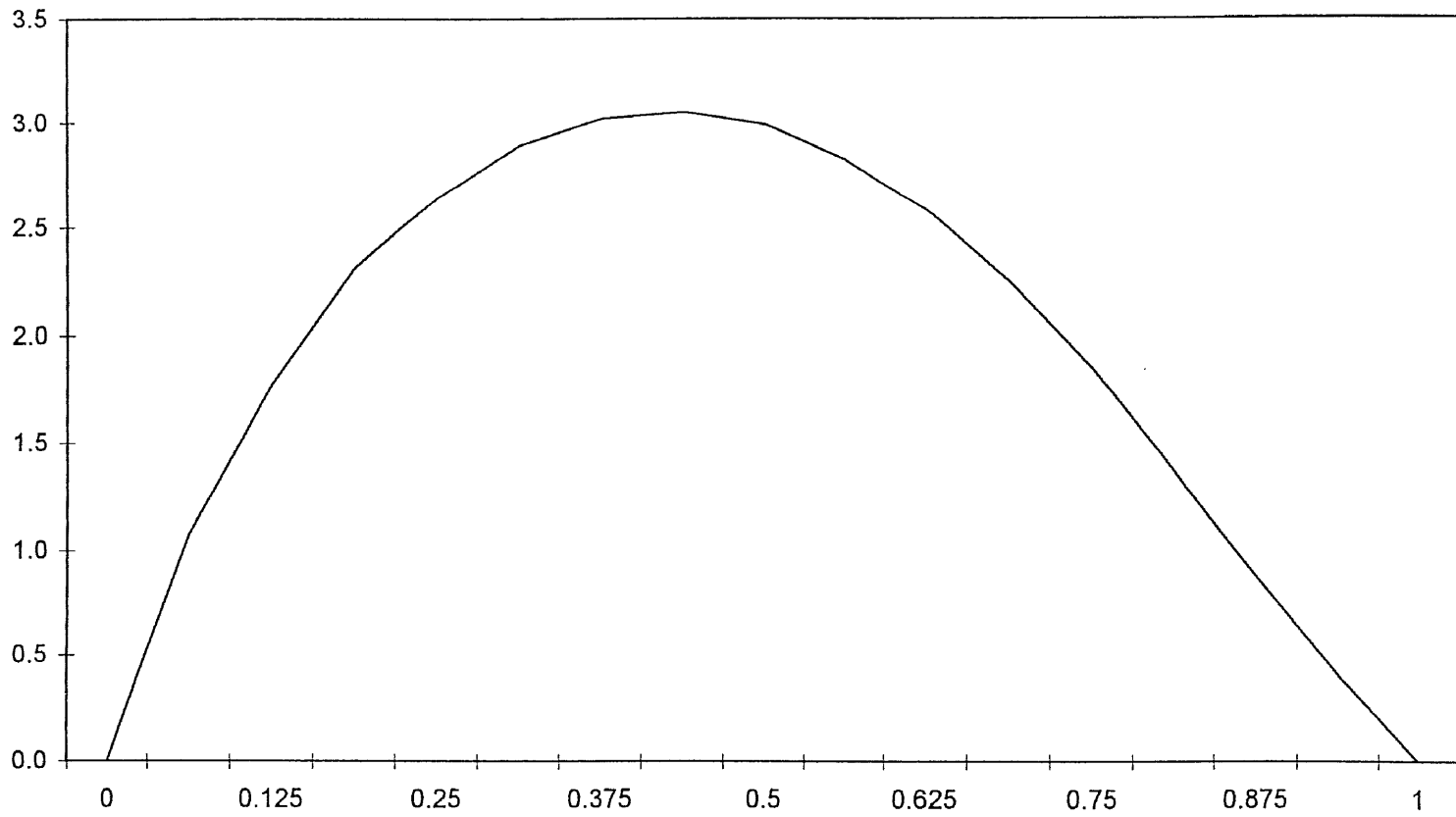
Figure 5.1.4
Velocity Distribution for Line 10 2202
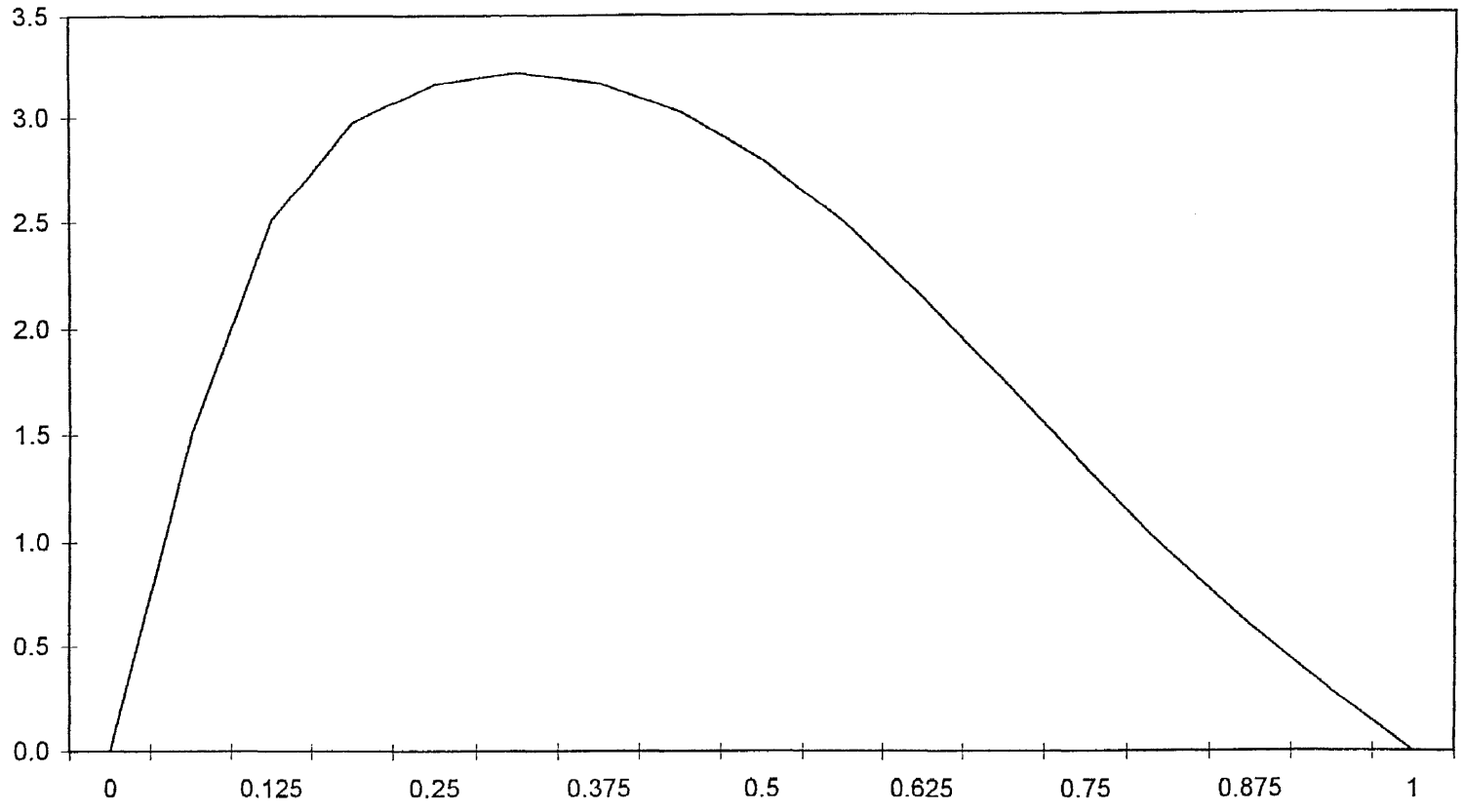
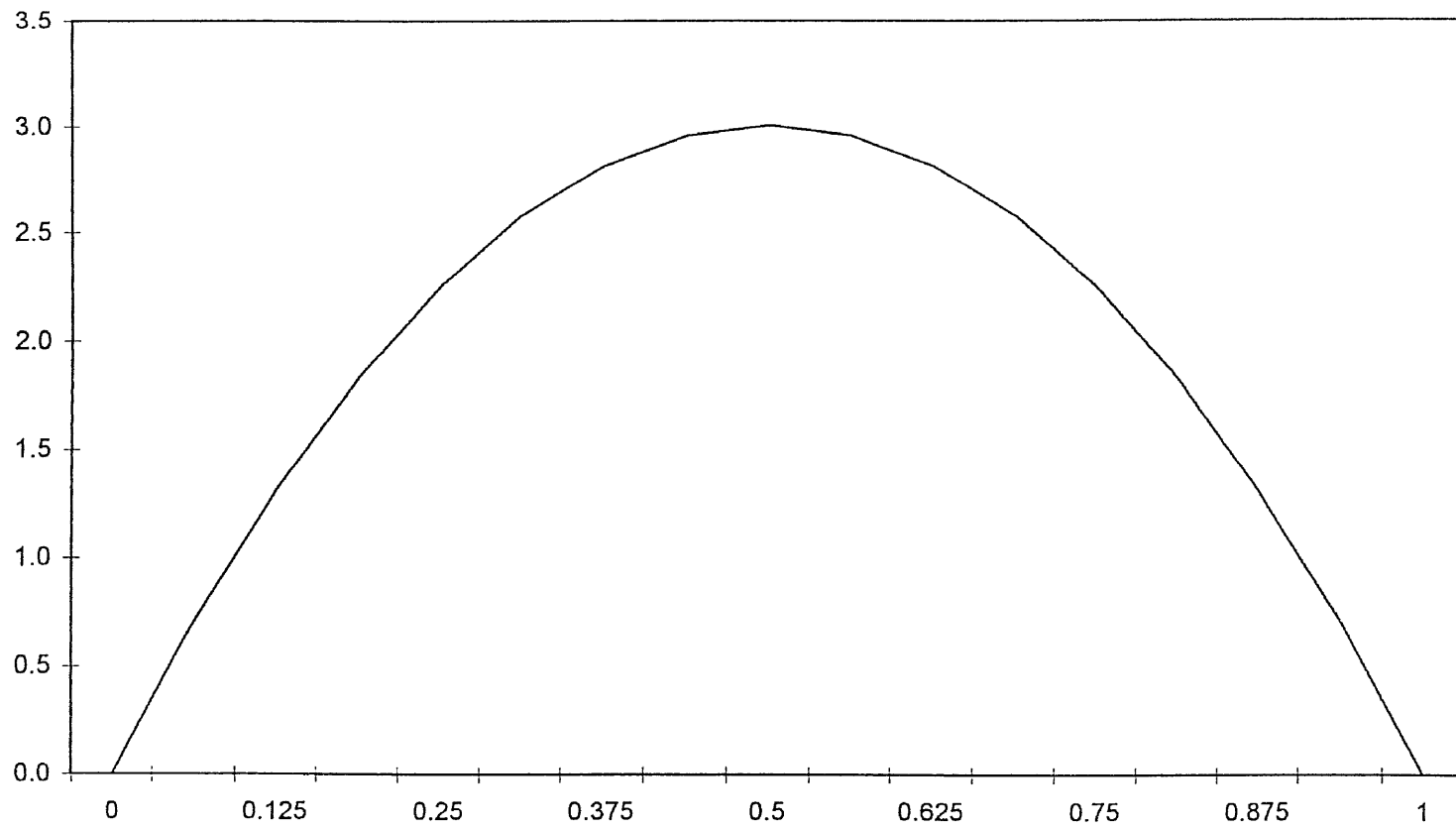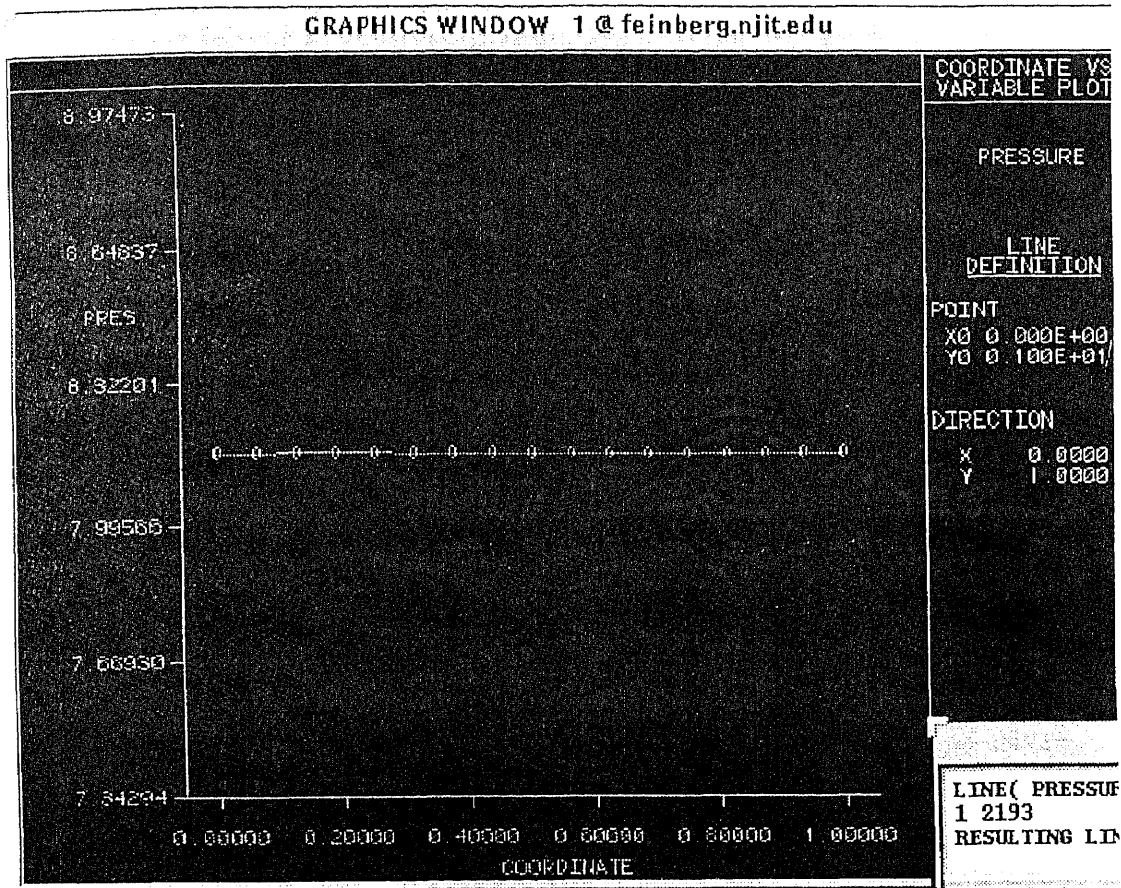**Figure 5.1.5**
Velocity Distribution for Line 20 2212
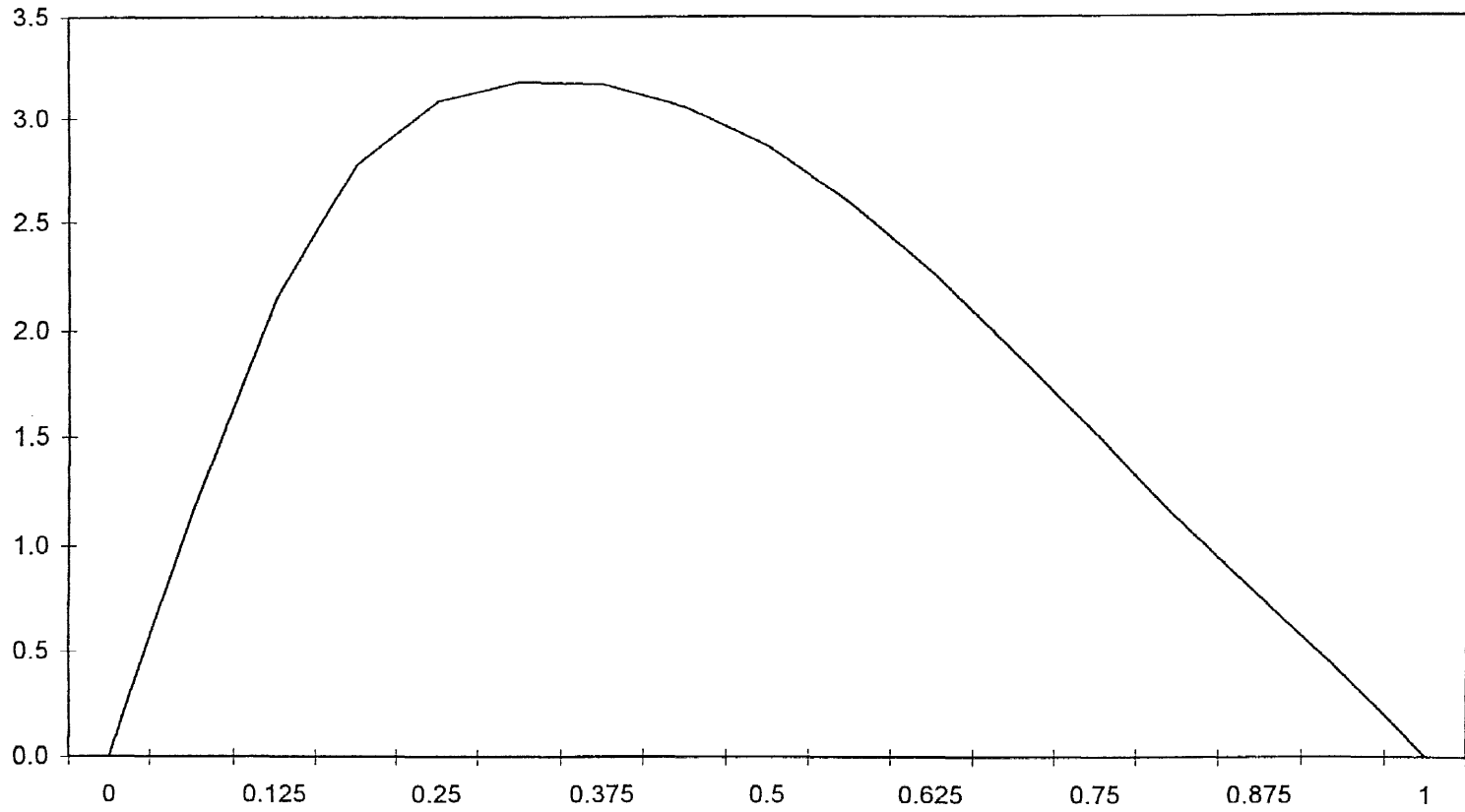
Figure 5.1.6
Velocity Distribution for Line 25 2217
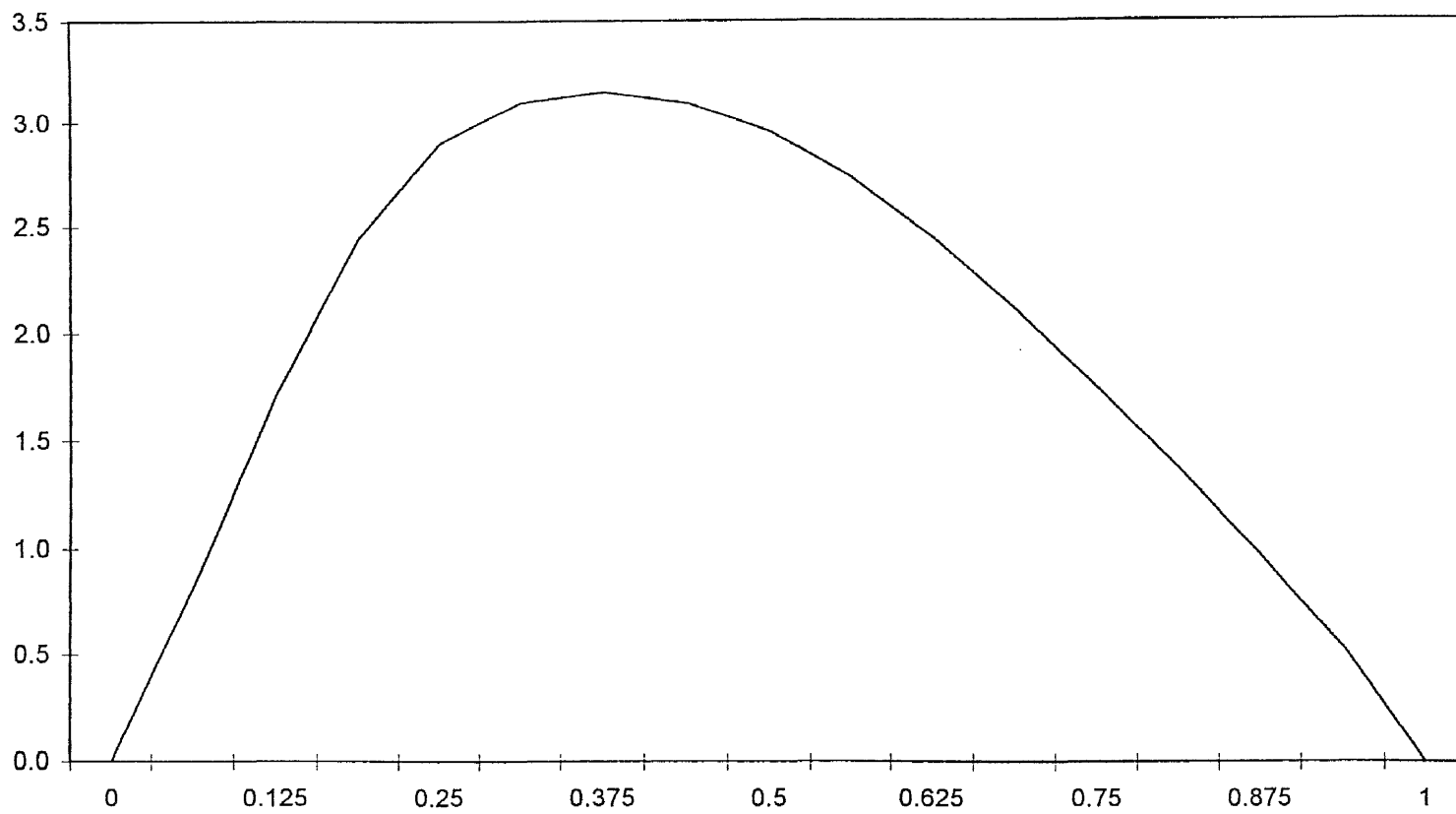
Figure 5.1.7
Velocity Distribution for Line 30 2222
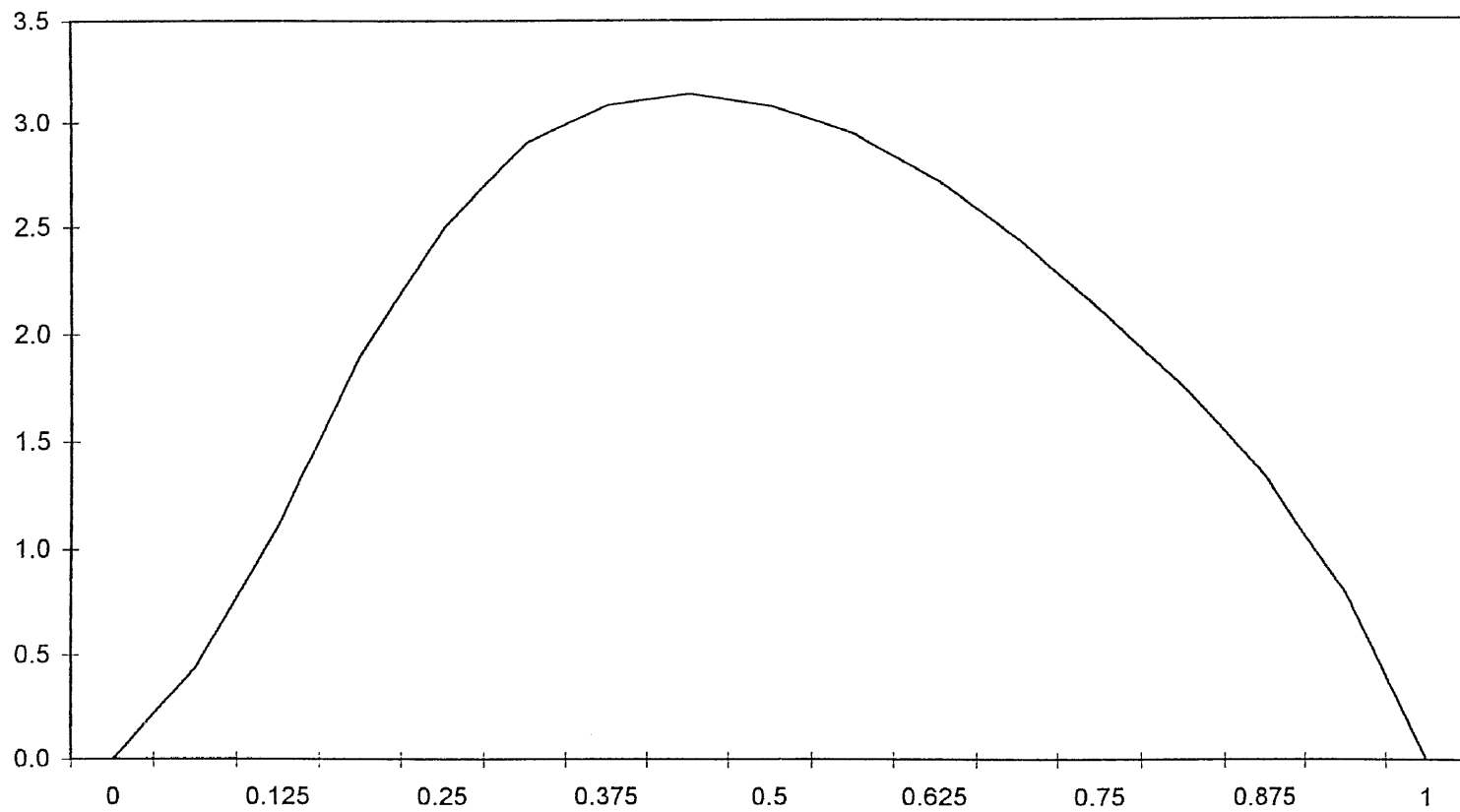
Figure 5.1.8
Velocity Distribution for Line 35 2227
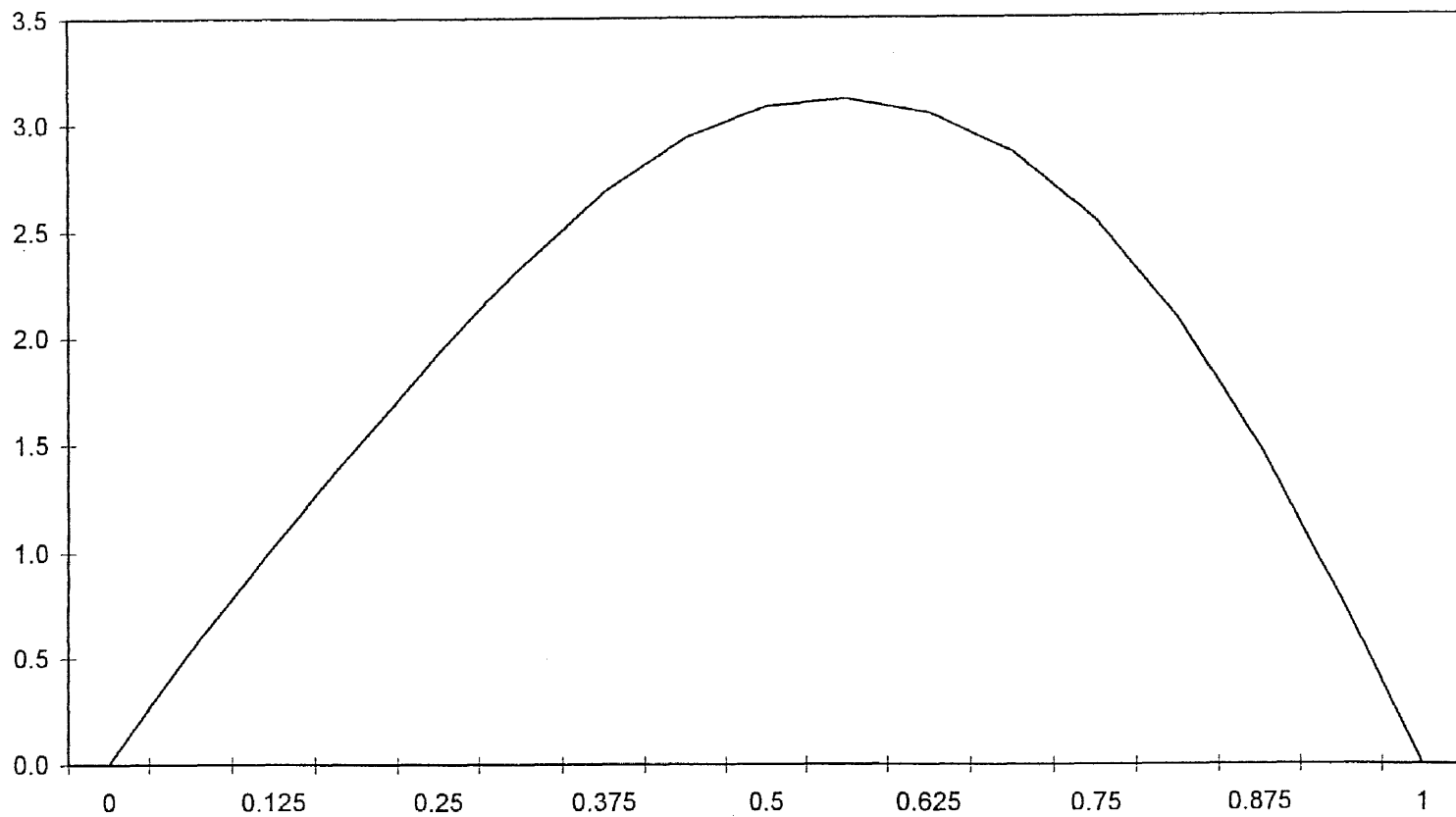
Figure 5.1.9
Velocity Distribution for Line 45 2237
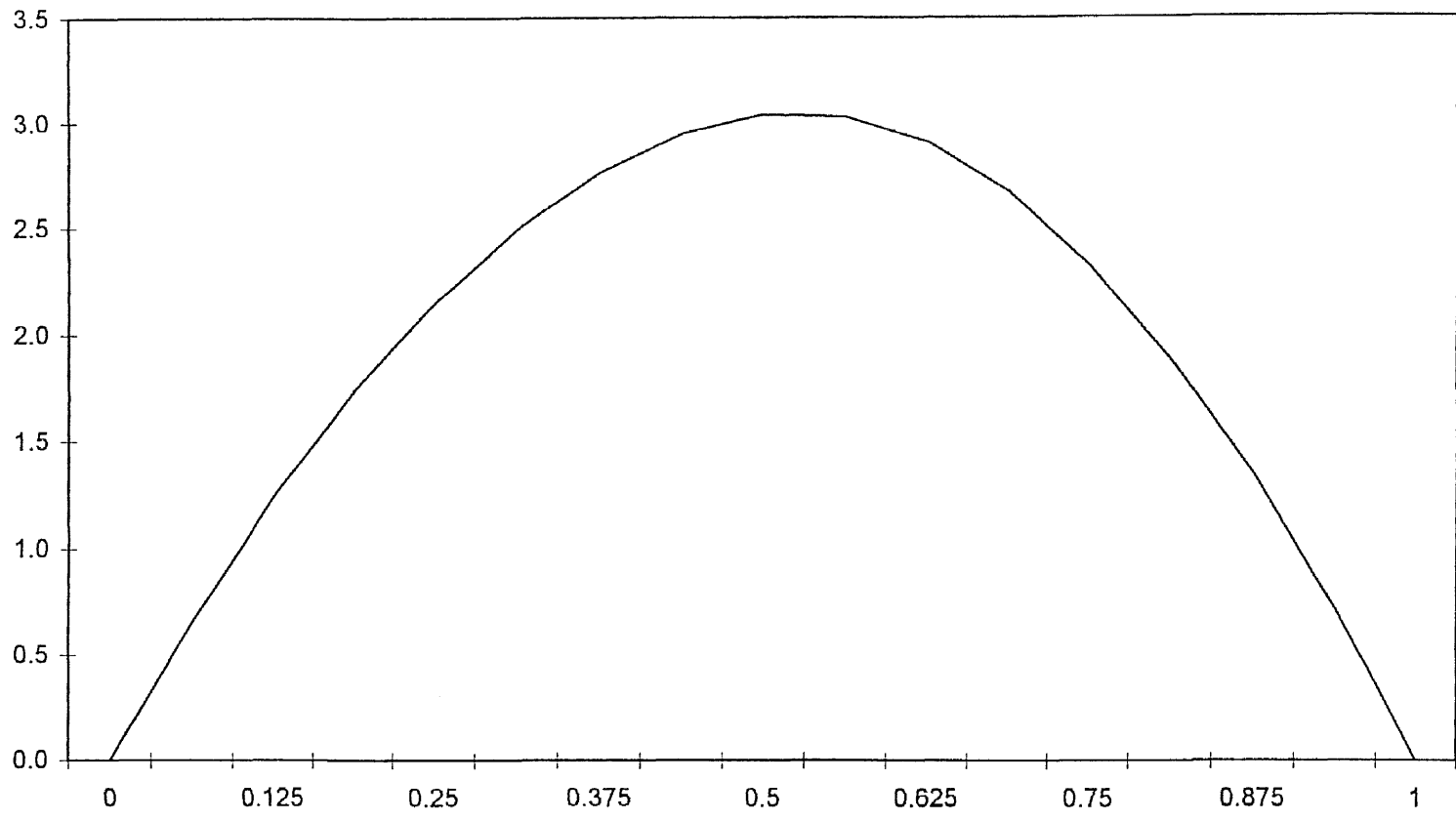
Figure 5.1.10
Velocity Distribution for Line 55 2247

Figure 5.1.11
Velocity Distribution for Line 65 2257

Figure 5.1.12
Velocity Distribution for Line 70 2262

Figure 5.1.13
Velocity Distribution for Line 75 2267

Figure 5.1.14
Velocity Distribution for Line 95 2287

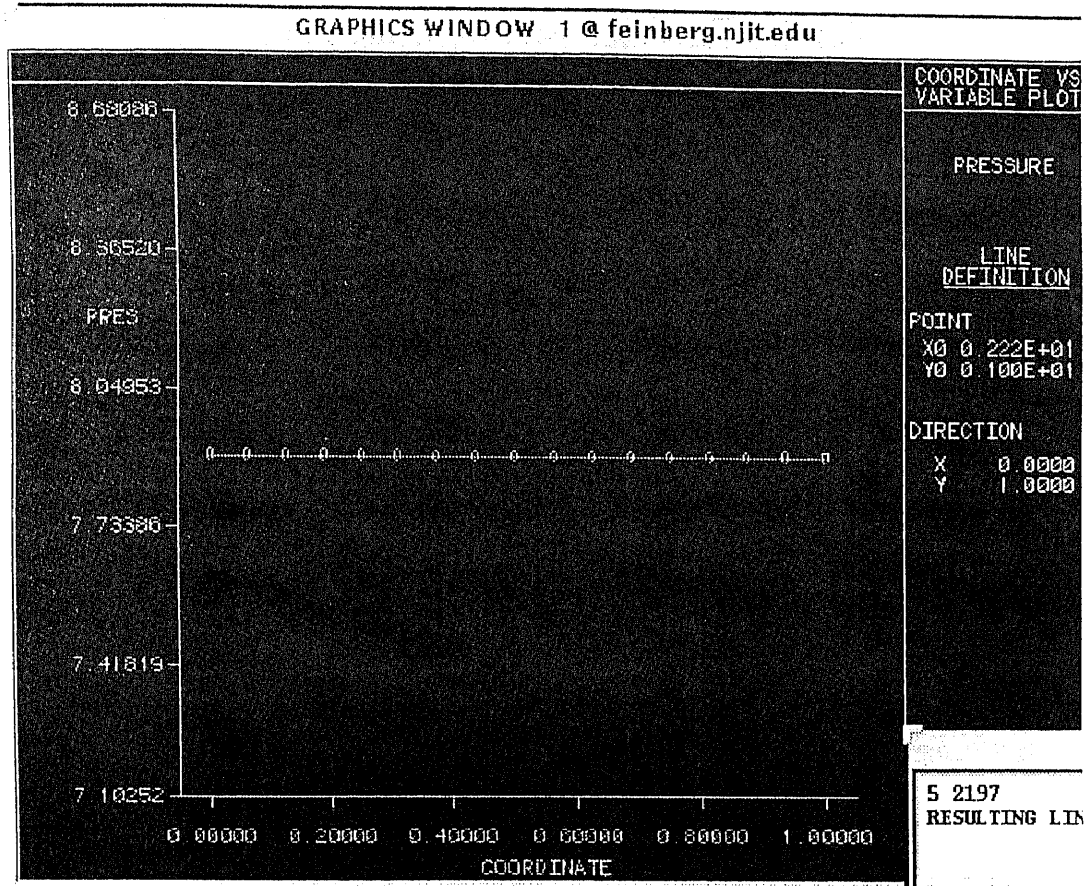**Figure 5.1.15**
Velocity Distribution for Line 110 2302

Figure 5.1.16
Velocity Distribution for Line 120 2312

Figure 5.1.17
Velocity Distribution for Line 130 2322

Figure 5.1.18
Pressure Distribution for Line 1 2193

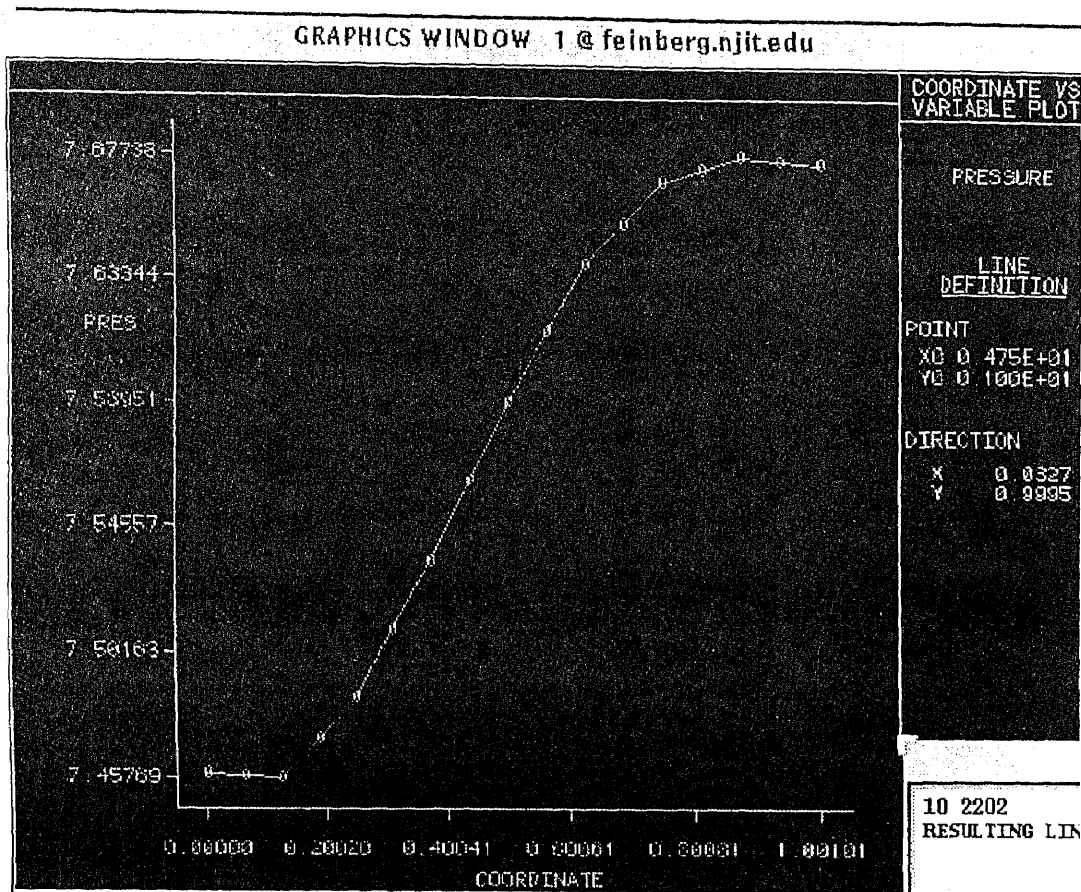**Figure 5.1.19**
Pressure Distribution for Line 5 2197

Figure 5.1.20
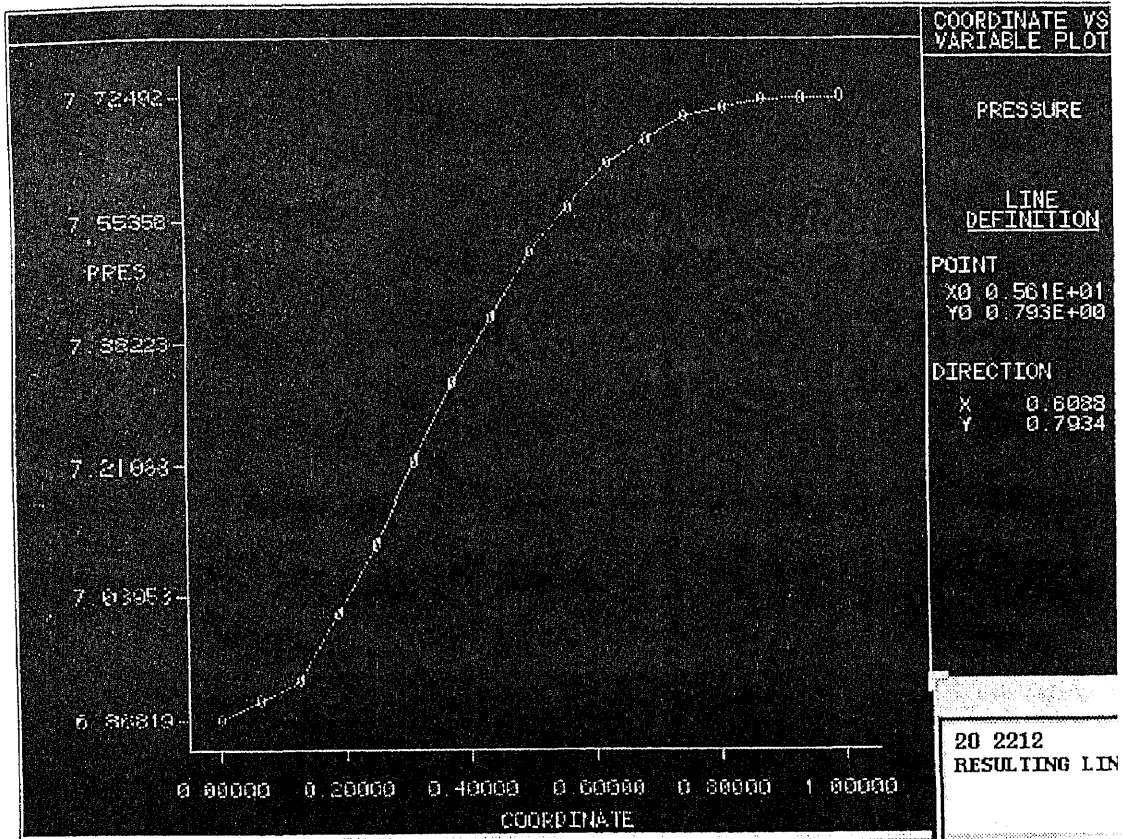**Pressure Distribution for Line 10 2202**

Figure 5.1.21
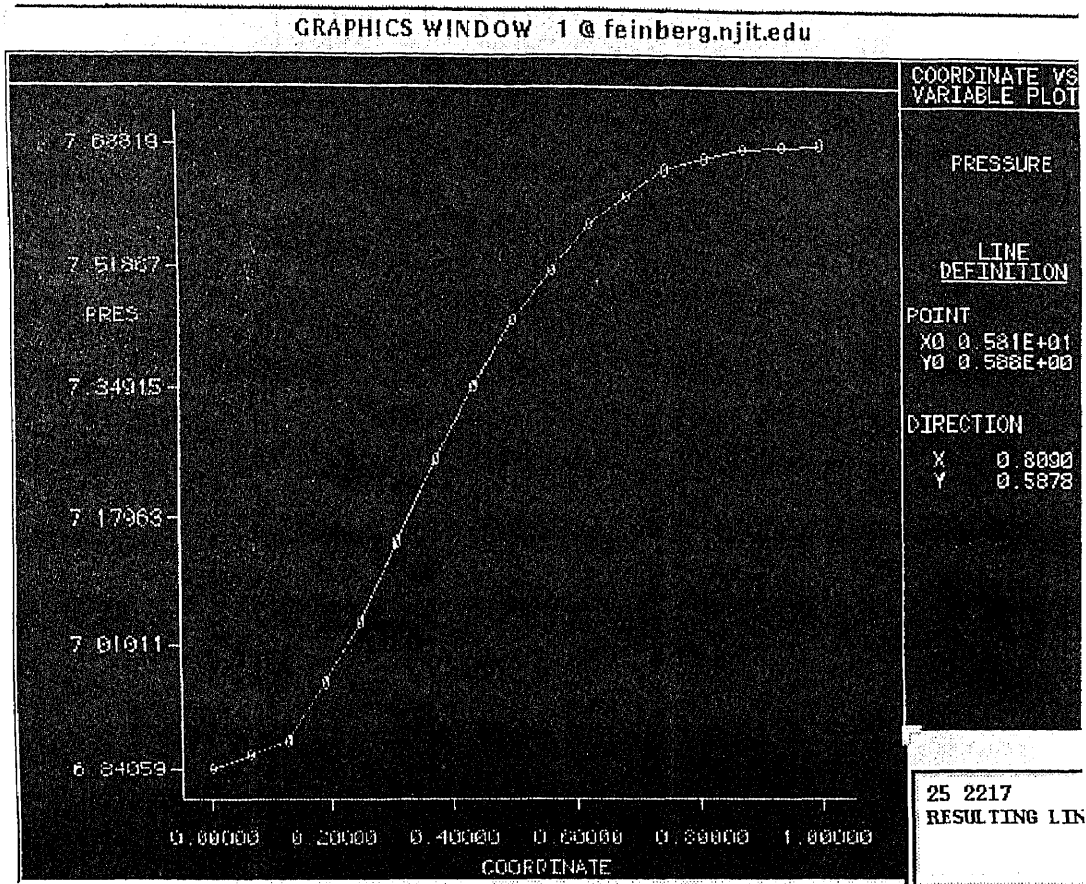Pressure Distribution for Line 20 2212

Figure 5.1.22
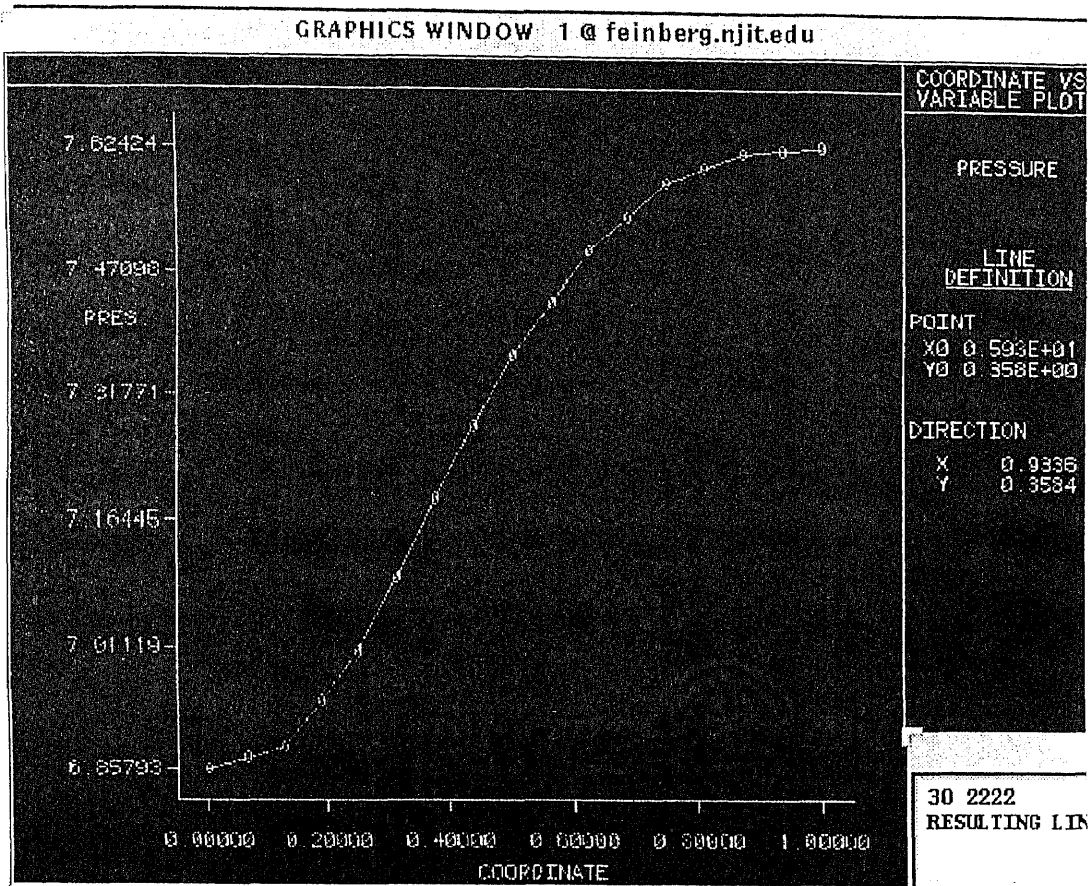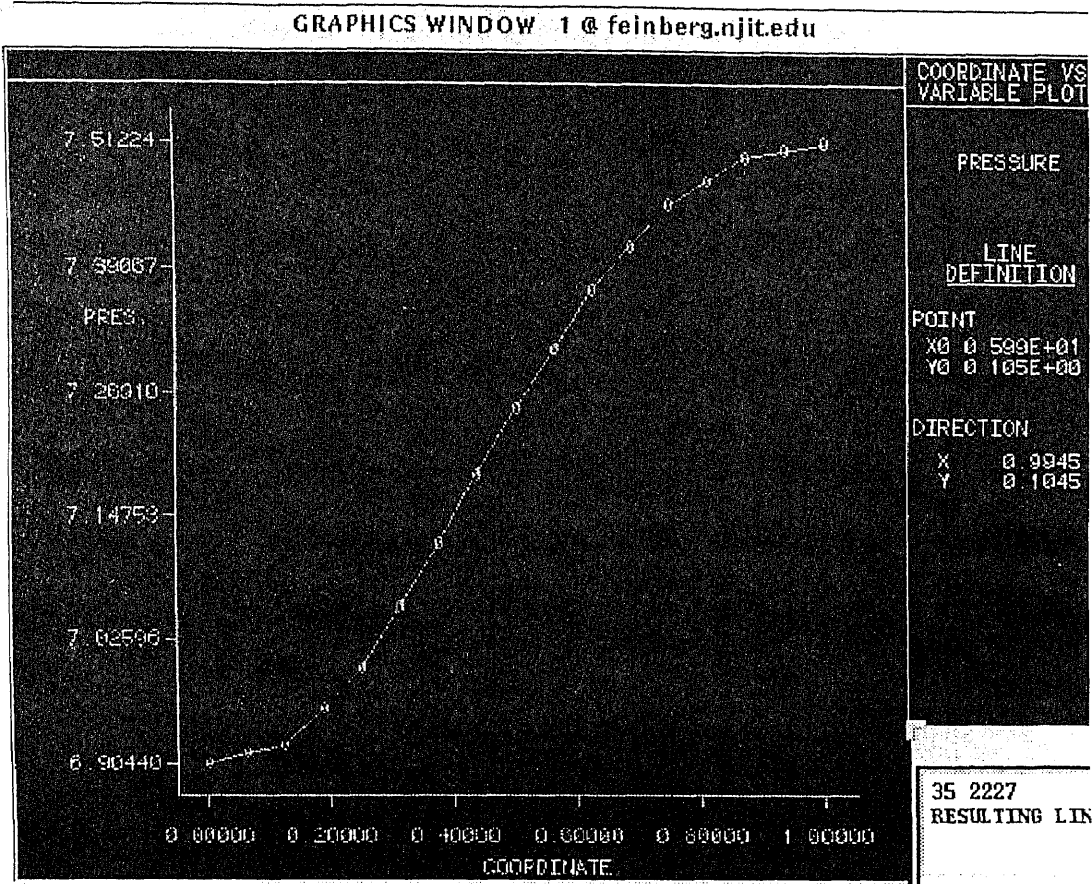**Pressure Distribution for Line 25 2217**

Figure 5.1.23
Pressure Distribution for Line 30 2222

Figure 5.1.24
Pressure Distribution for Line 35 2227

Figure 5.1.25
Pressure Distribution for Line 45 2237

90

**Figure 5.1.26
Pressure Distribution for Line 55 2247**

Figure 5.1.27
Pressure Distribution for Line 65 2257
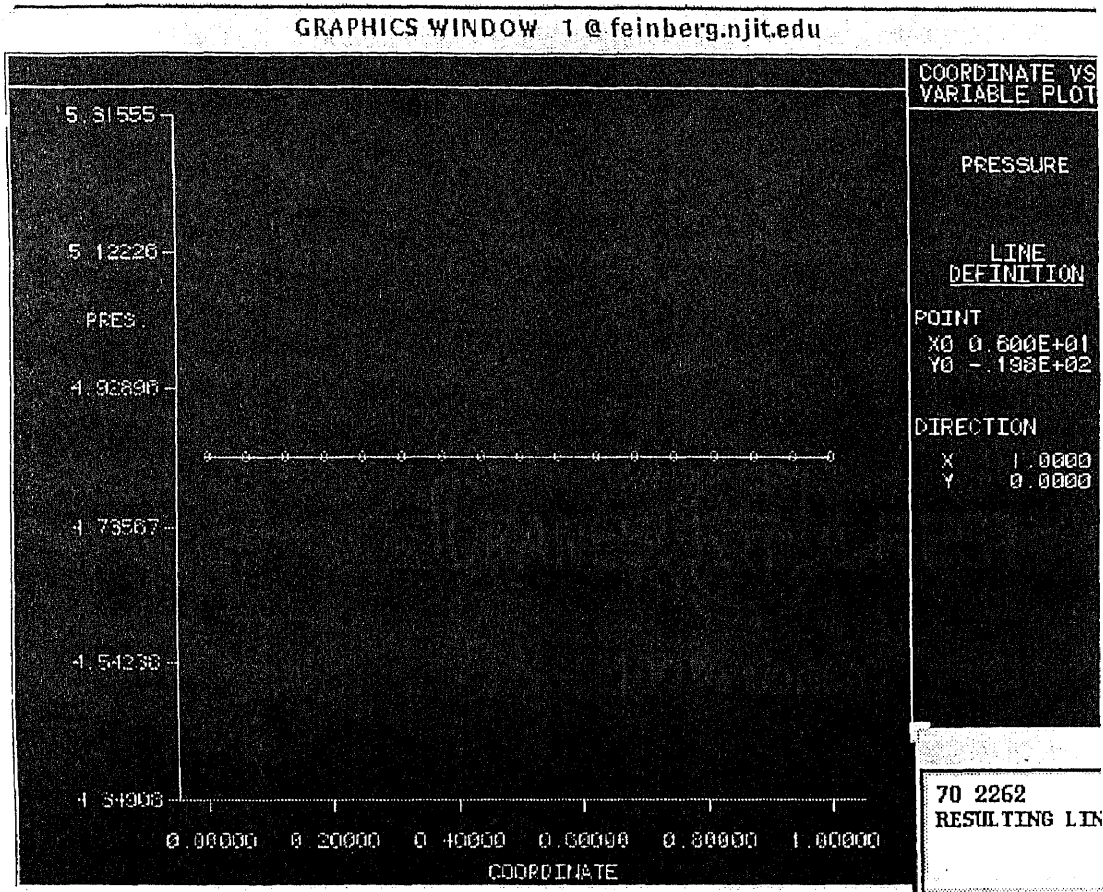
Figure 5.1.28
Pressure Distribution for Line 70 2262
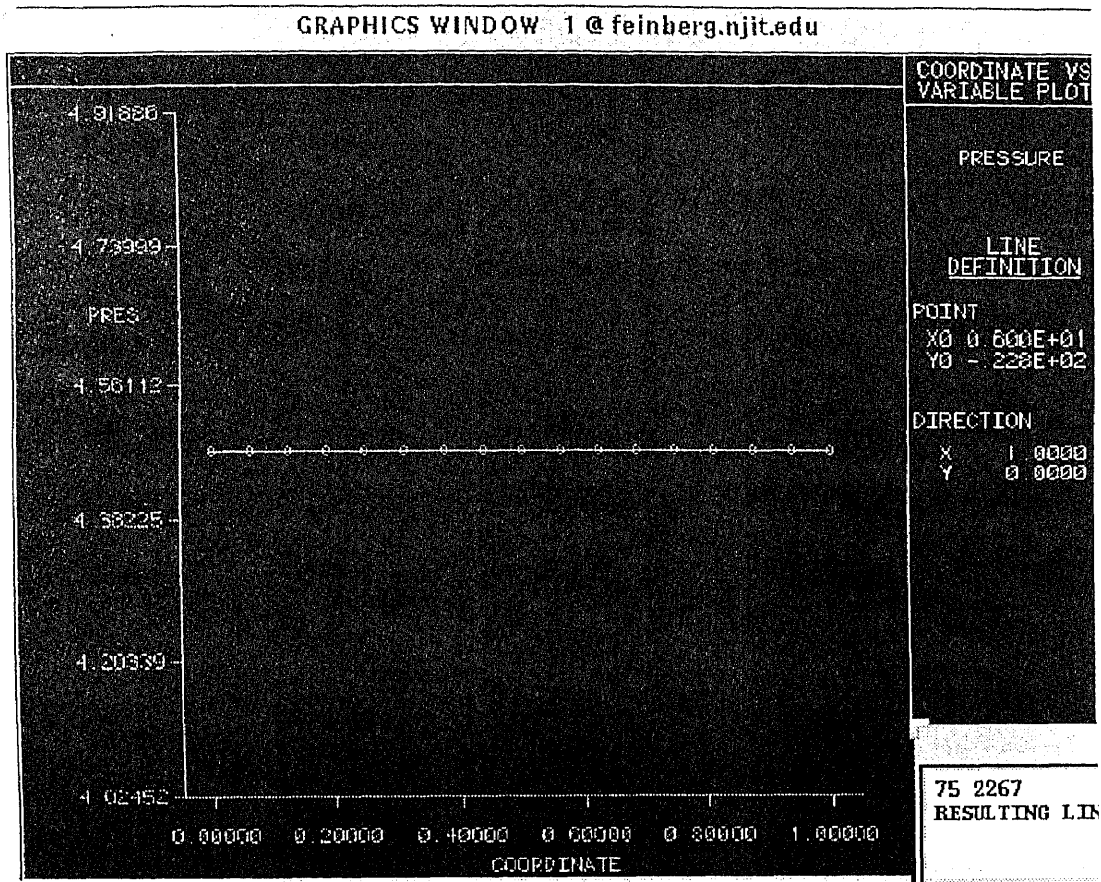
Figure 5.1.29
Pressure Distribution for Line 75 2267
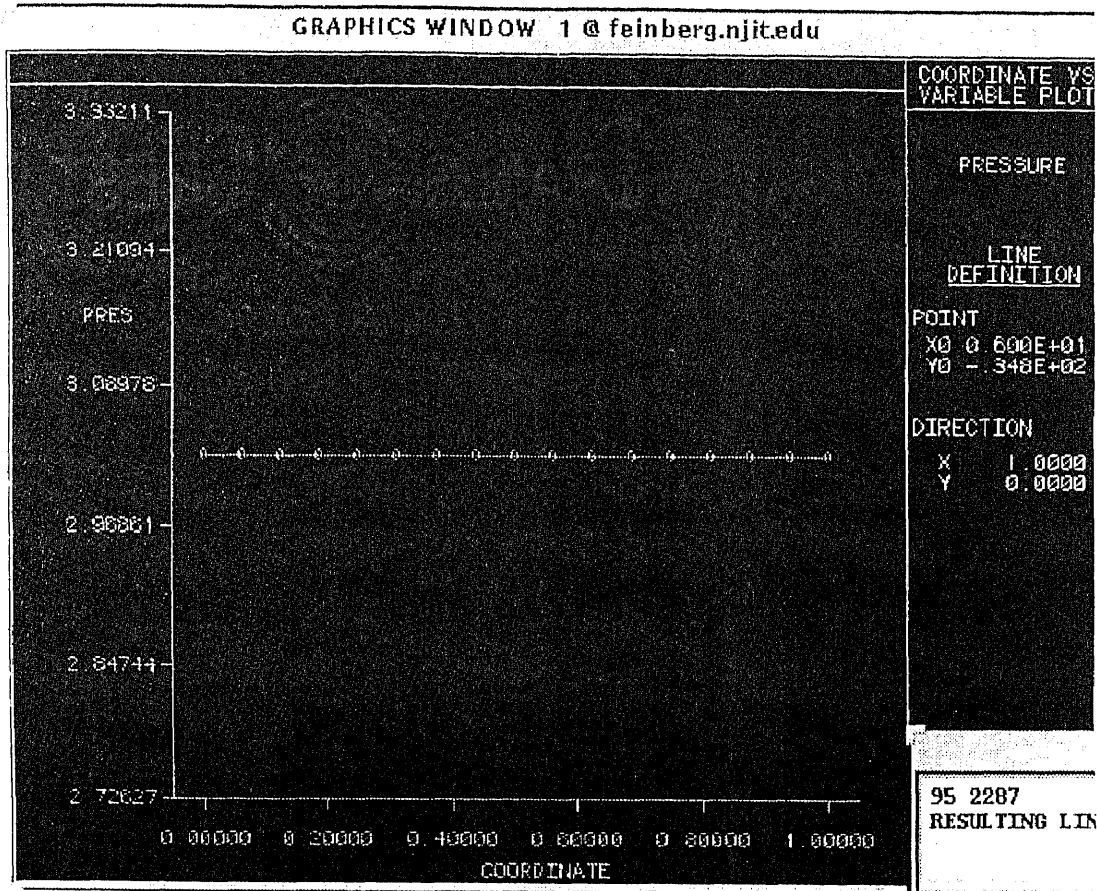
Figure 5.1.30
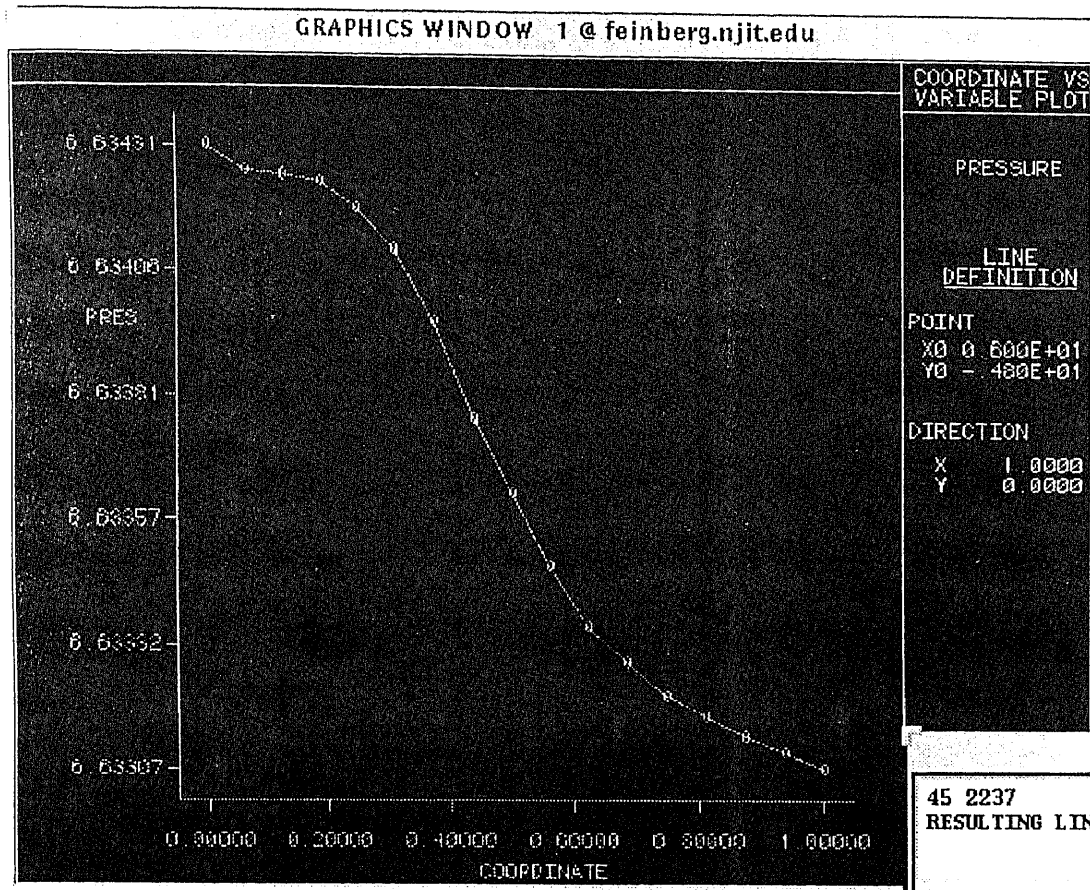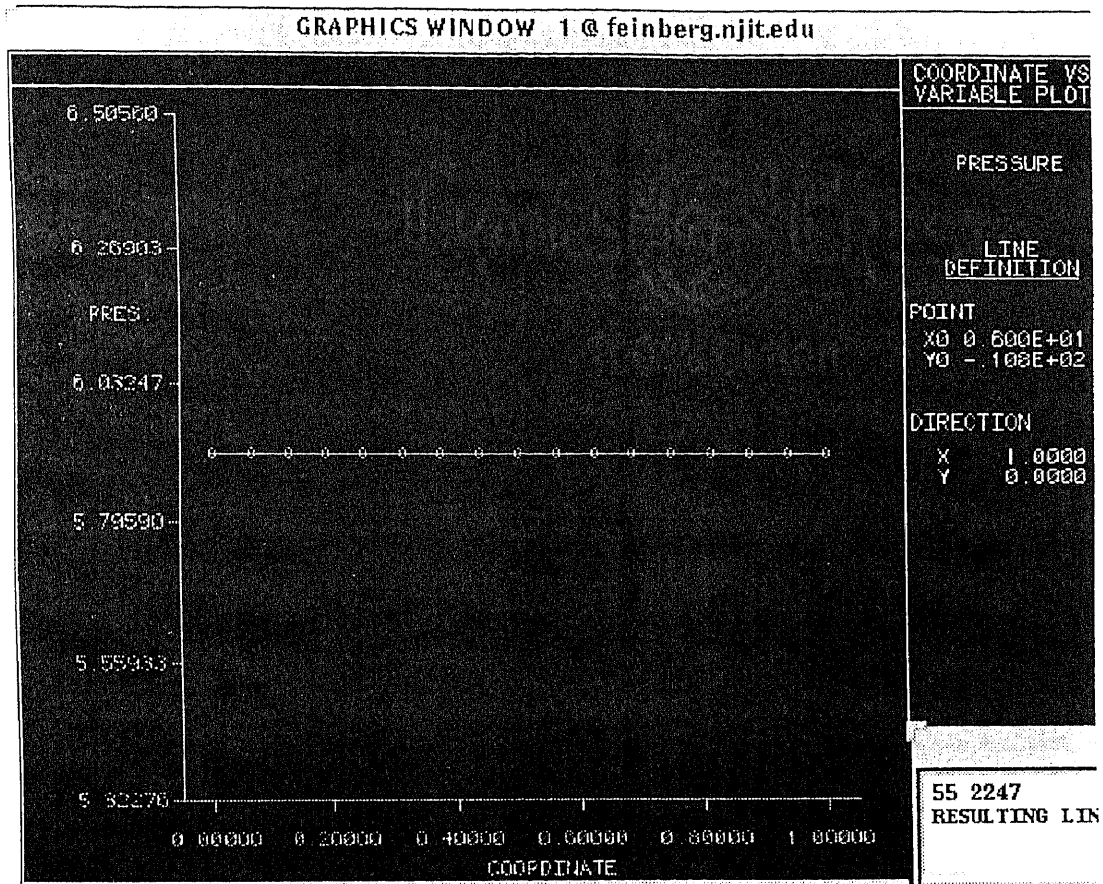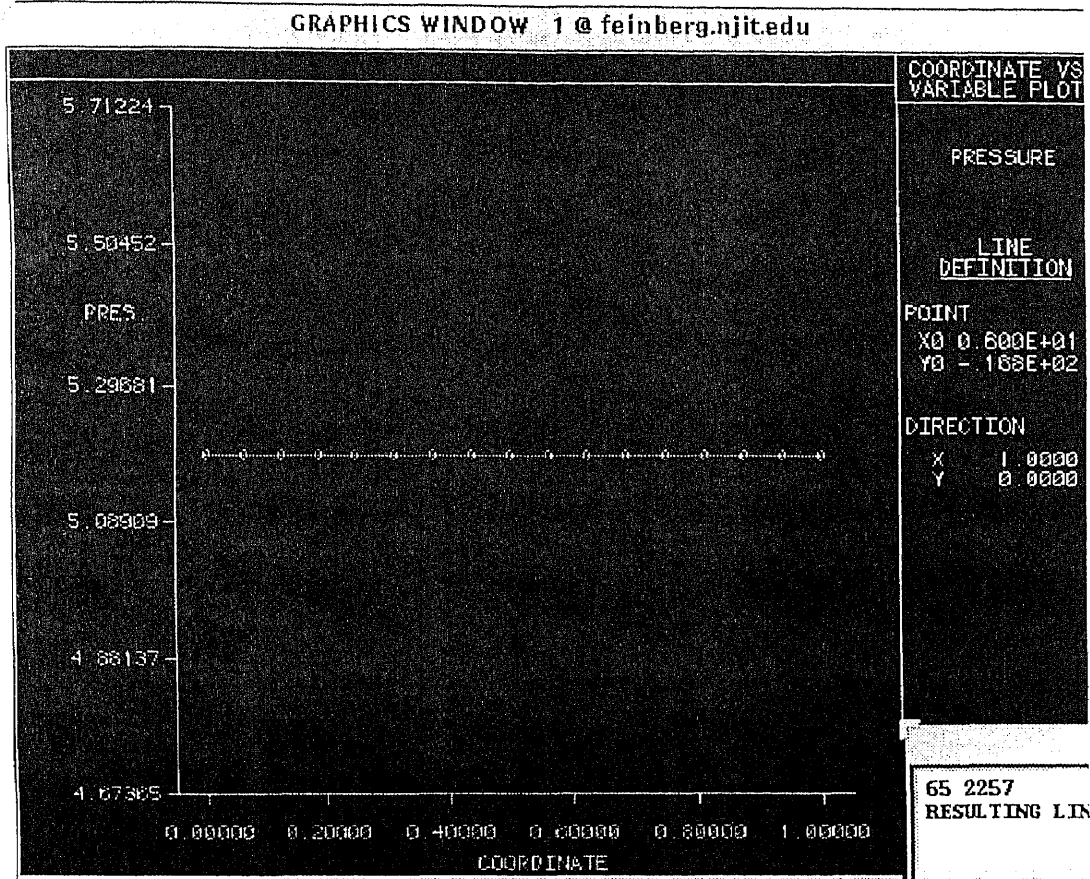**Pressure Distribution for Line 95 2287**
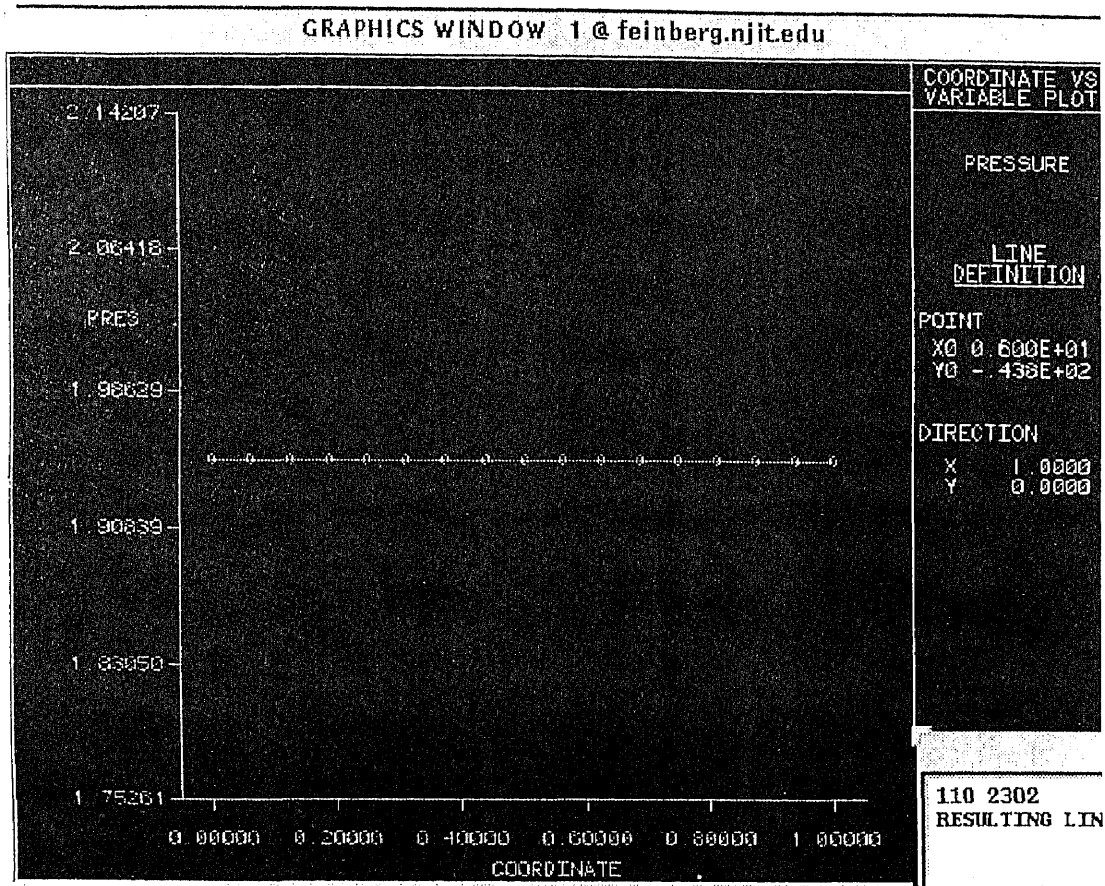
Figure 5.1.31
Pressure Distribution for Line 110 2302
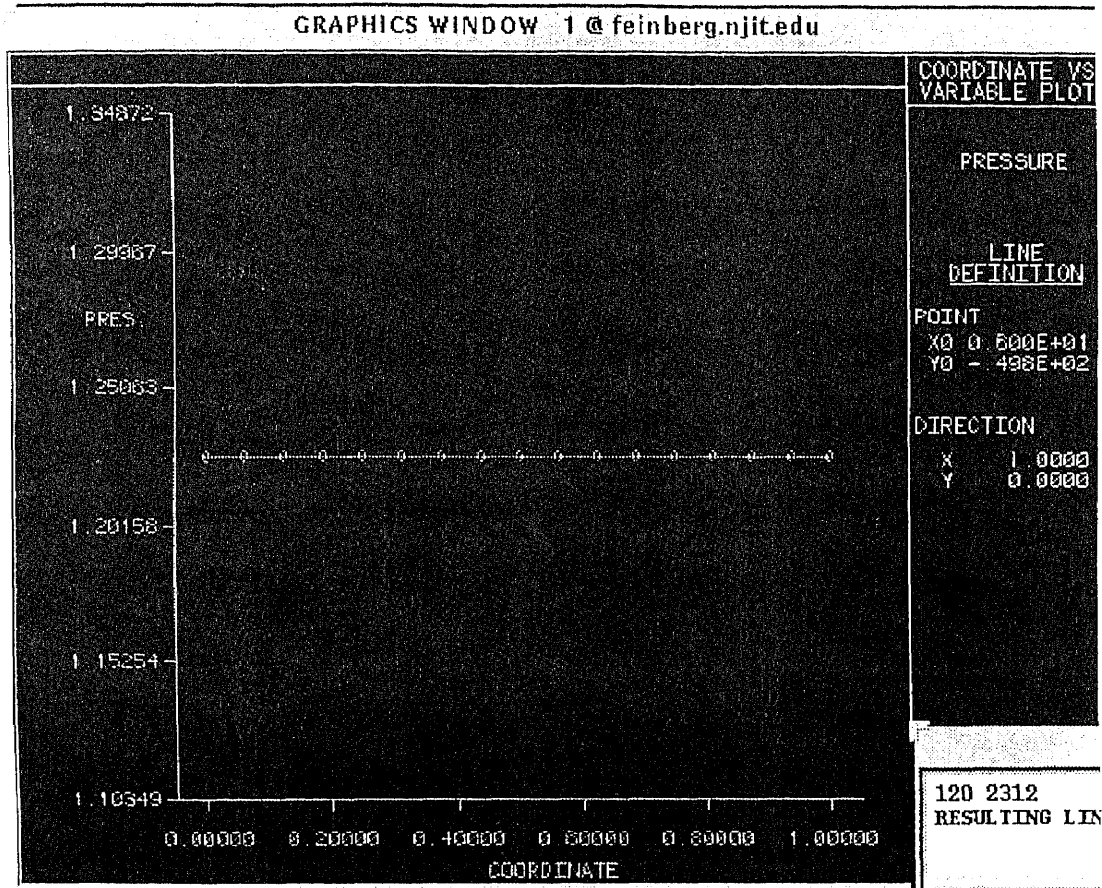
Figure 5.1.32
Pressure Distribution for Line 120 2312
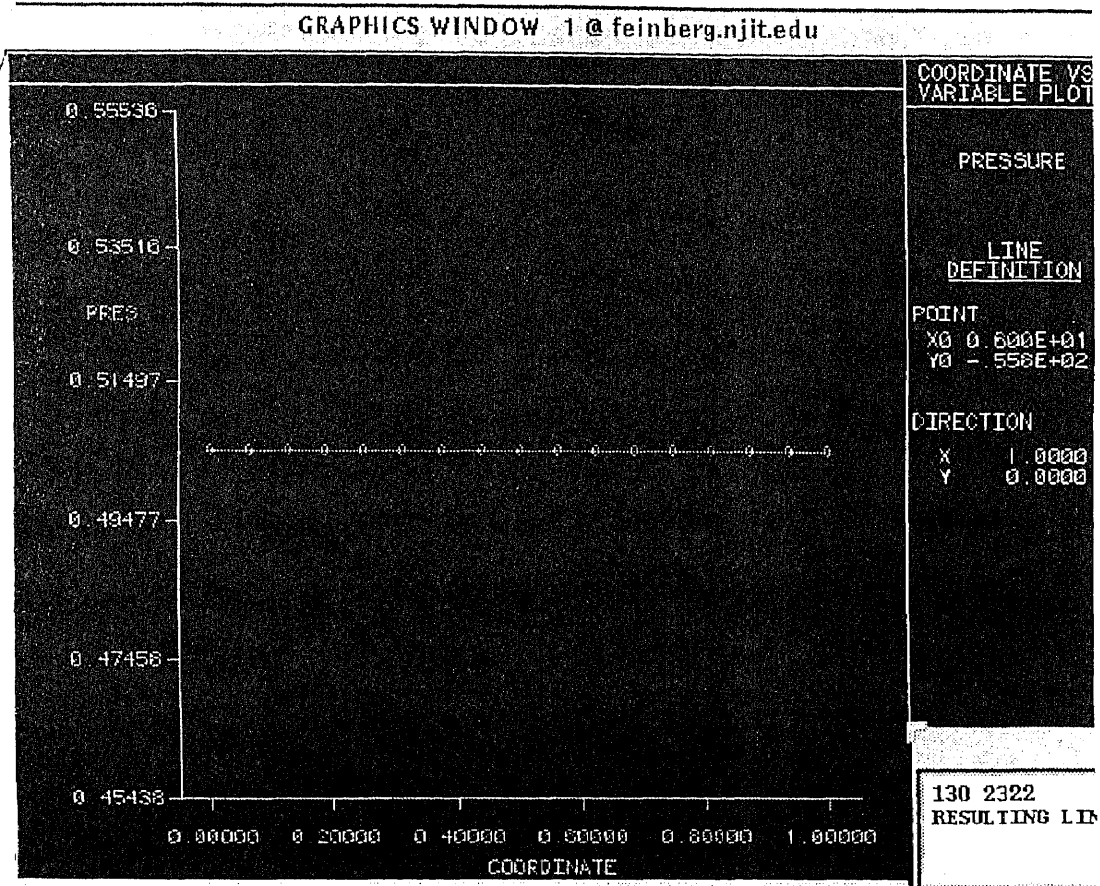
Figure 5.1.33
Pressure Distribution for Line 130 2322
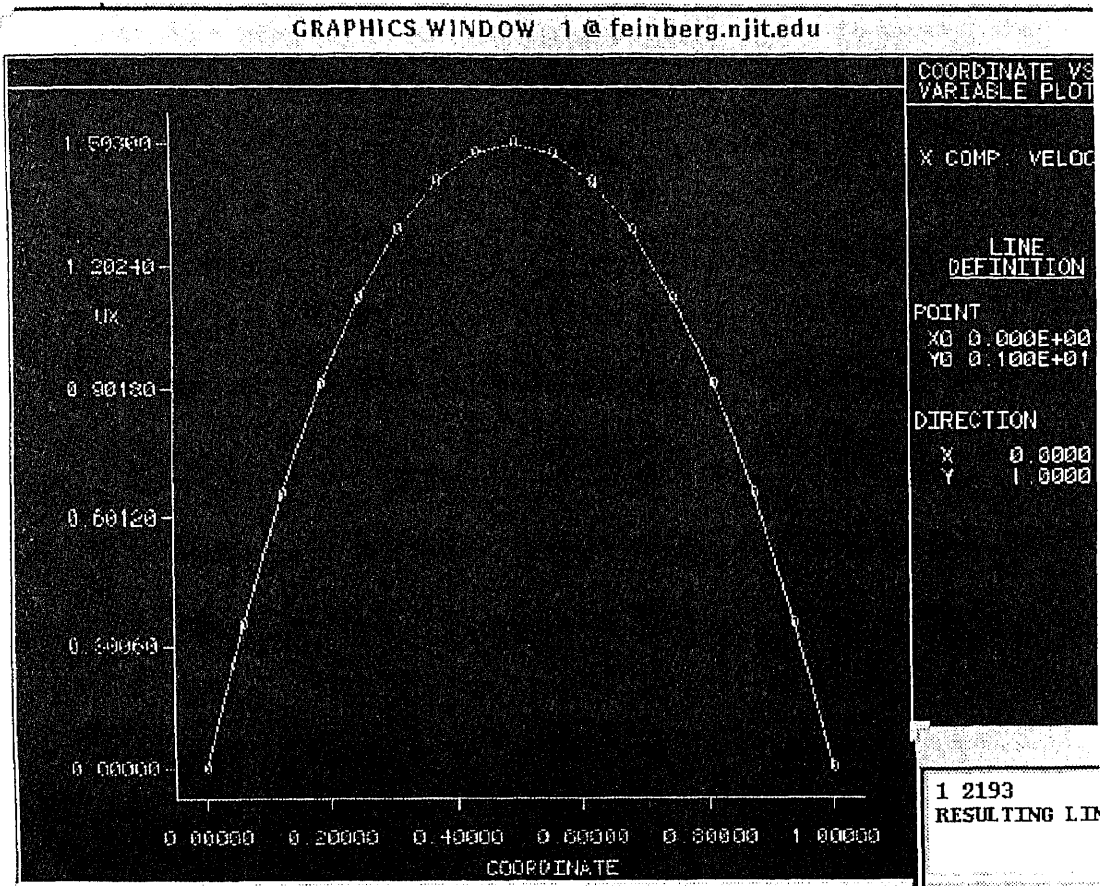
Figure 5.1.34
X-Component Velocity Distribution for Line 1 2193

Figure 5.1.35
X-Component Velocity Distribution for Line 5 2197

Figure 5.1.36
X-Component Velocity Distribution for Line 10 2202

Figure 5.1.37
X-Component Velocity Distribution for Line 20 2212

Figure 5.1.38
X-Component Velocity Distribution for Line 25 2217

Figure 5.1.39
X-Component Velocity Distribution for Line 30 2222

Figure 5.1.40
X-Component Velocity Distribution for Line 35 2227

Figure 5.1.41
X-Component Velocity Distribution for Line 45 2237

Figure 5.1.42
X-Component Velocity Distribution for Line 55 2247

Figure 5.1.43
X-Component Velocity Distribution for Line 65 2257

Figure 5.1.44
X-Component Velocity Distribution for Line 70 2262

Figure 5.1.45
X-Component Velocity Distribution for Line 75 2267

Figure 5.1.46
X-Component Velocity Distribution for Line 95 2287
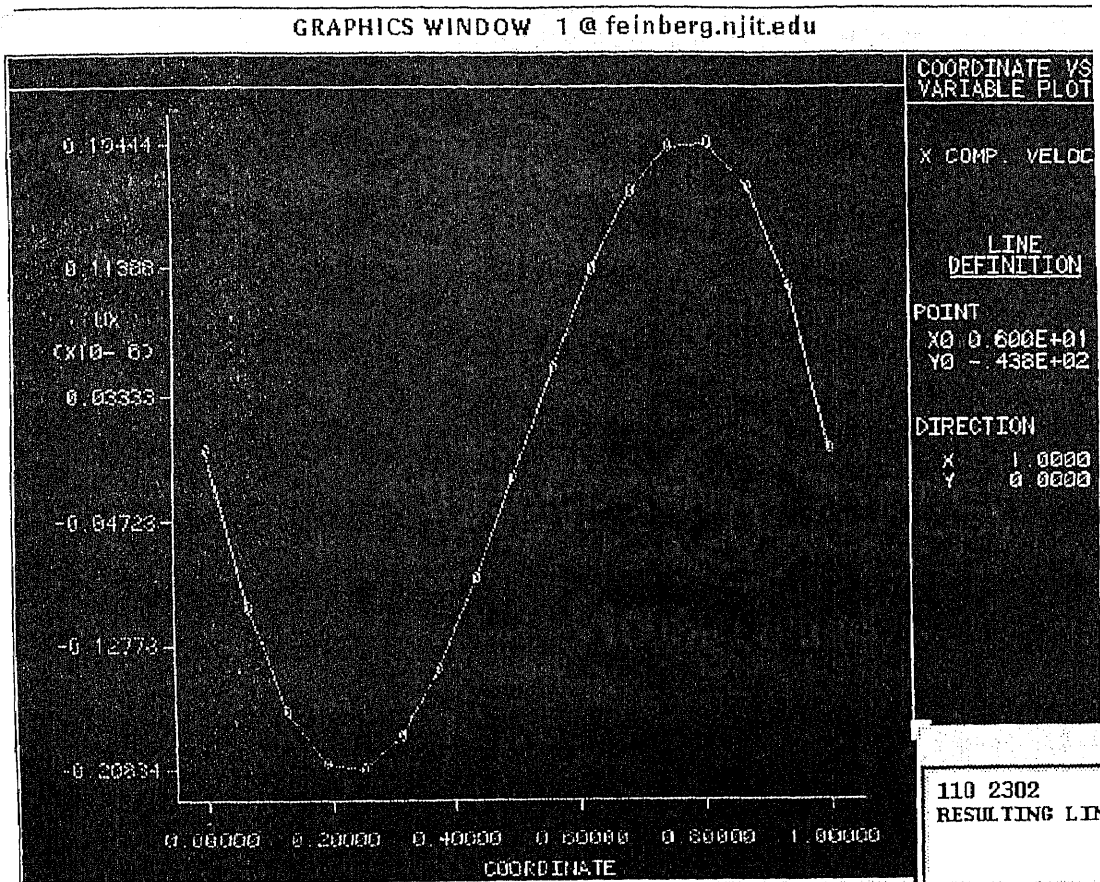
Figure 5.1.47
X-Component Velocity Distribution for Line 110 2302
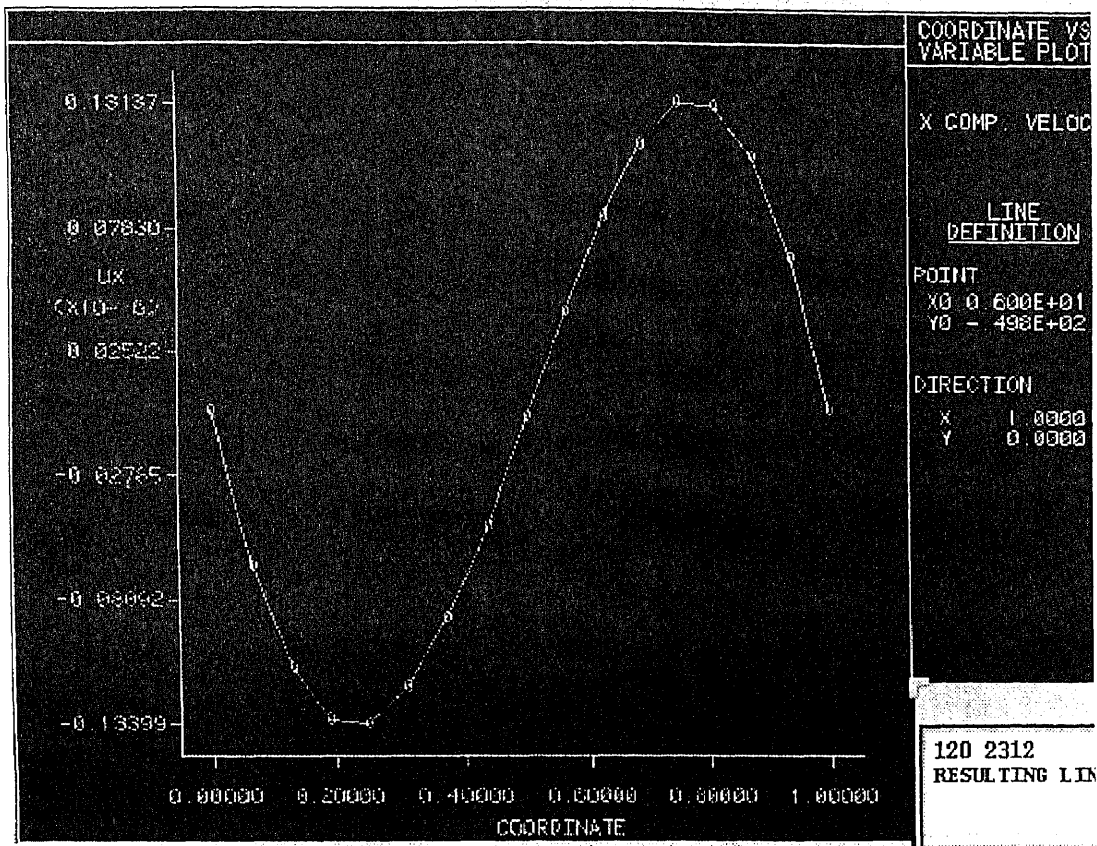
Figure 5.1.48
X-Component Velocity Distribution for Line 120 2312
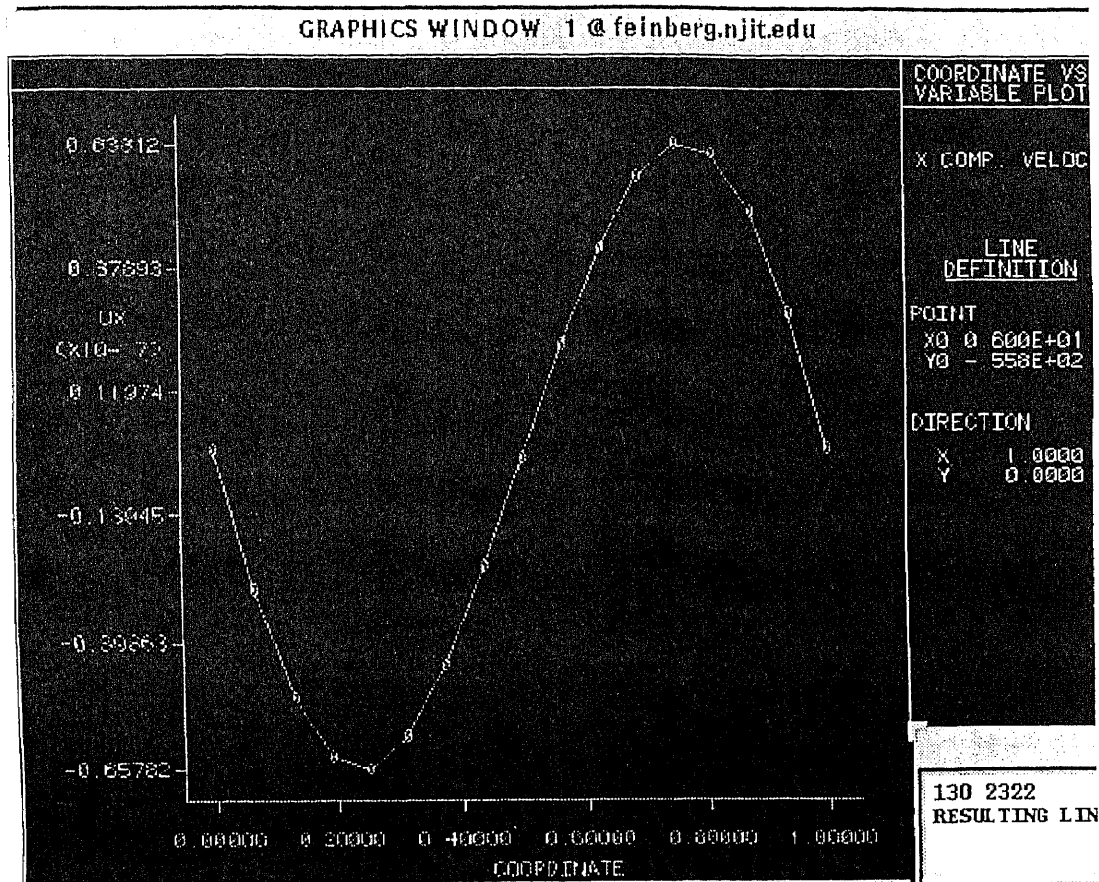
Figure 5.1.49
X-Component Velocity Distribution for Line 130 2322
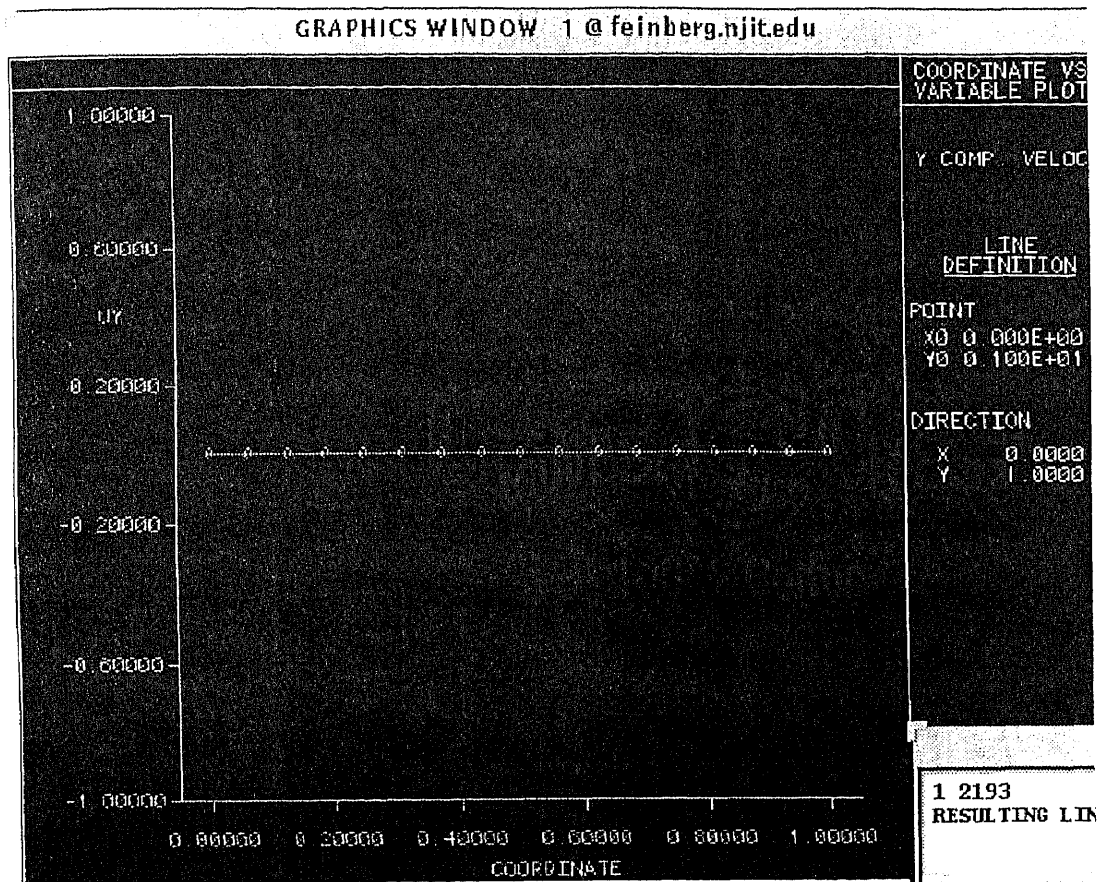
Figure 5.1.50
Y-Component Velocity Distribution for Line 1 2193
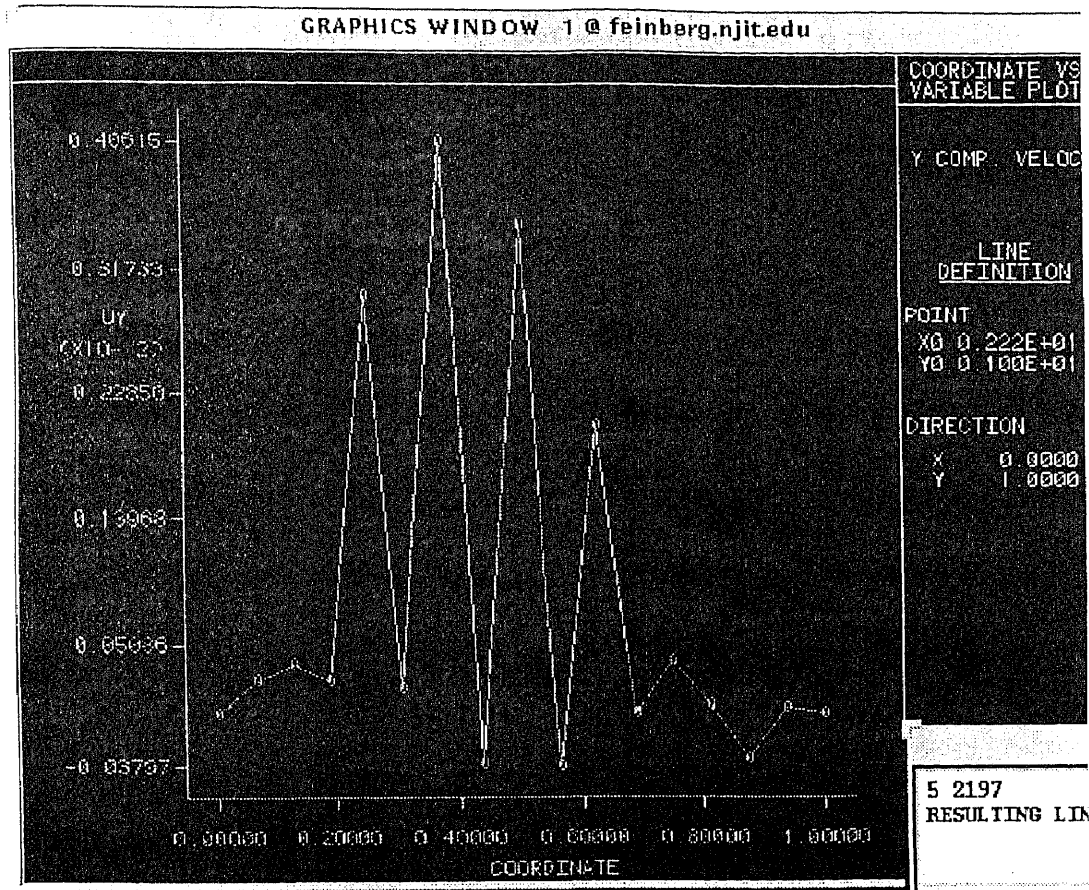
Figure 5.1.51
Y-Component Velocity Distribution for Line 5 2197
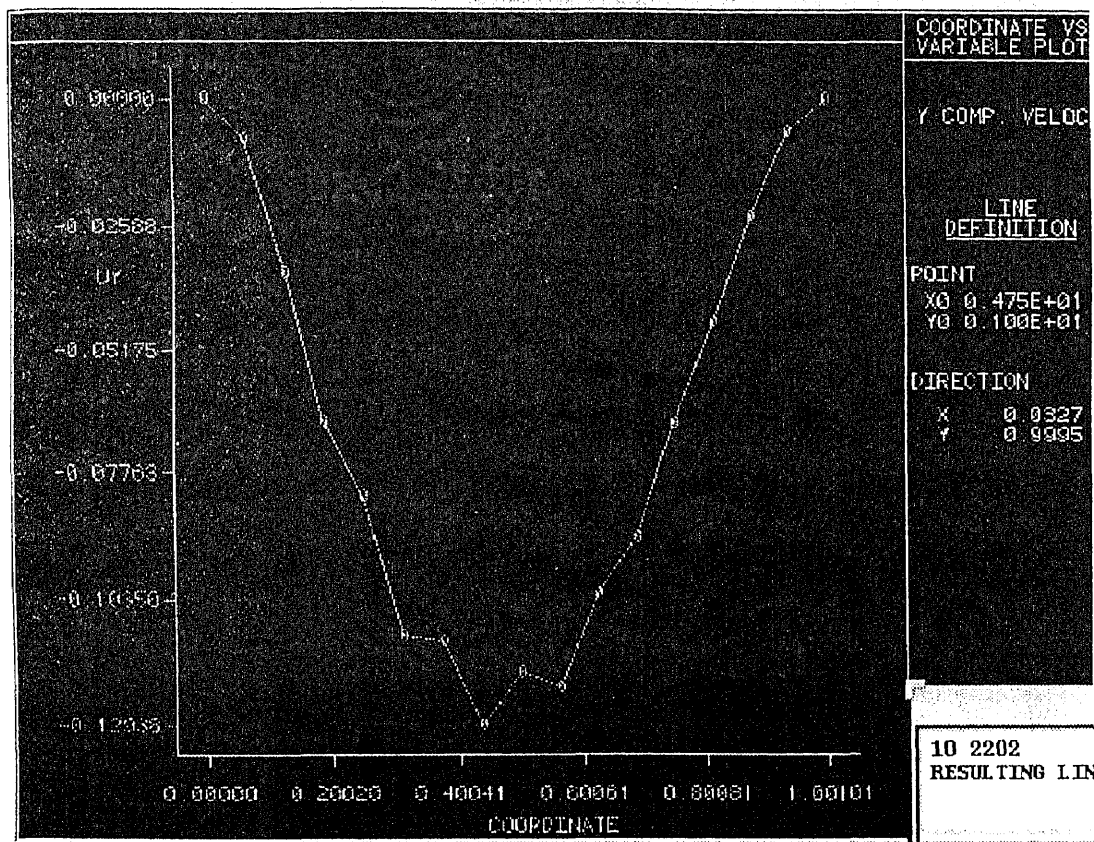
Figure 5.1.52
Y-Component Velocity Distribution for Line 10 2202
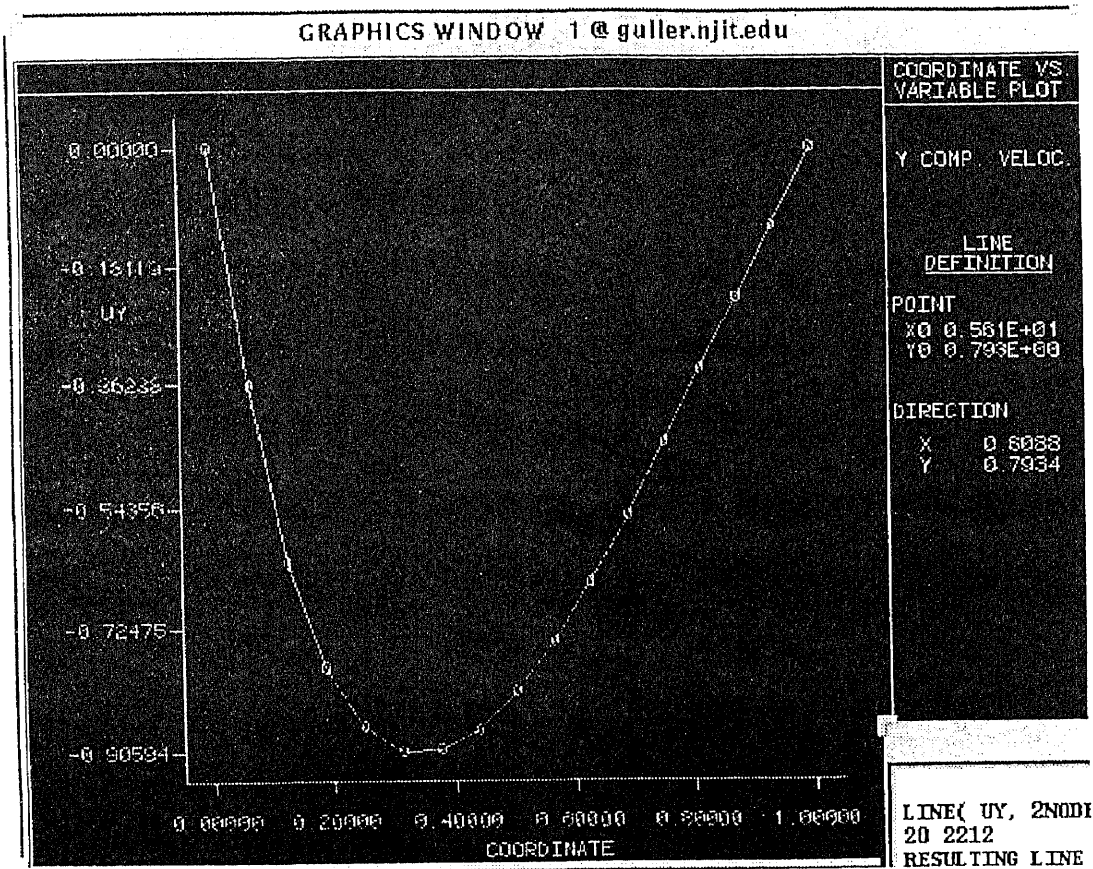
Figure 5.1.53
Y-Component Velocity Distribution for Line 20 2212
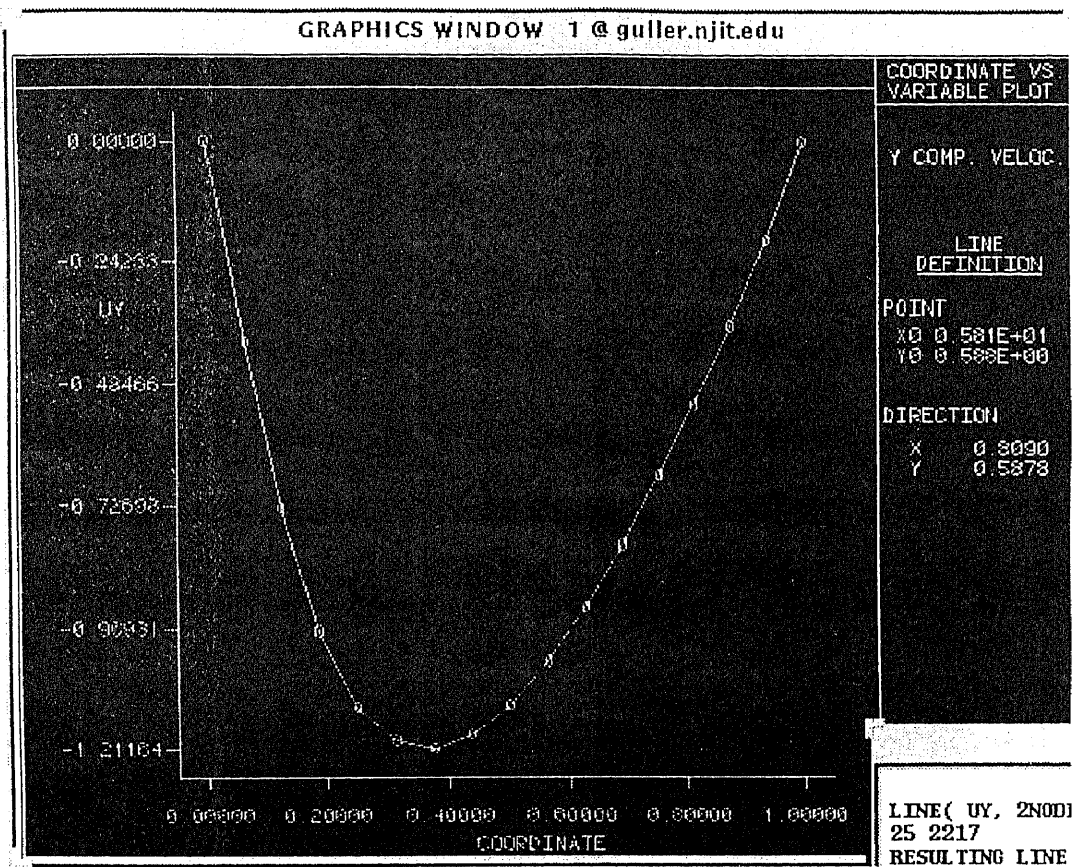
Figure 5.1.54
Y-Component Velocity Distribution for Line 25 2217
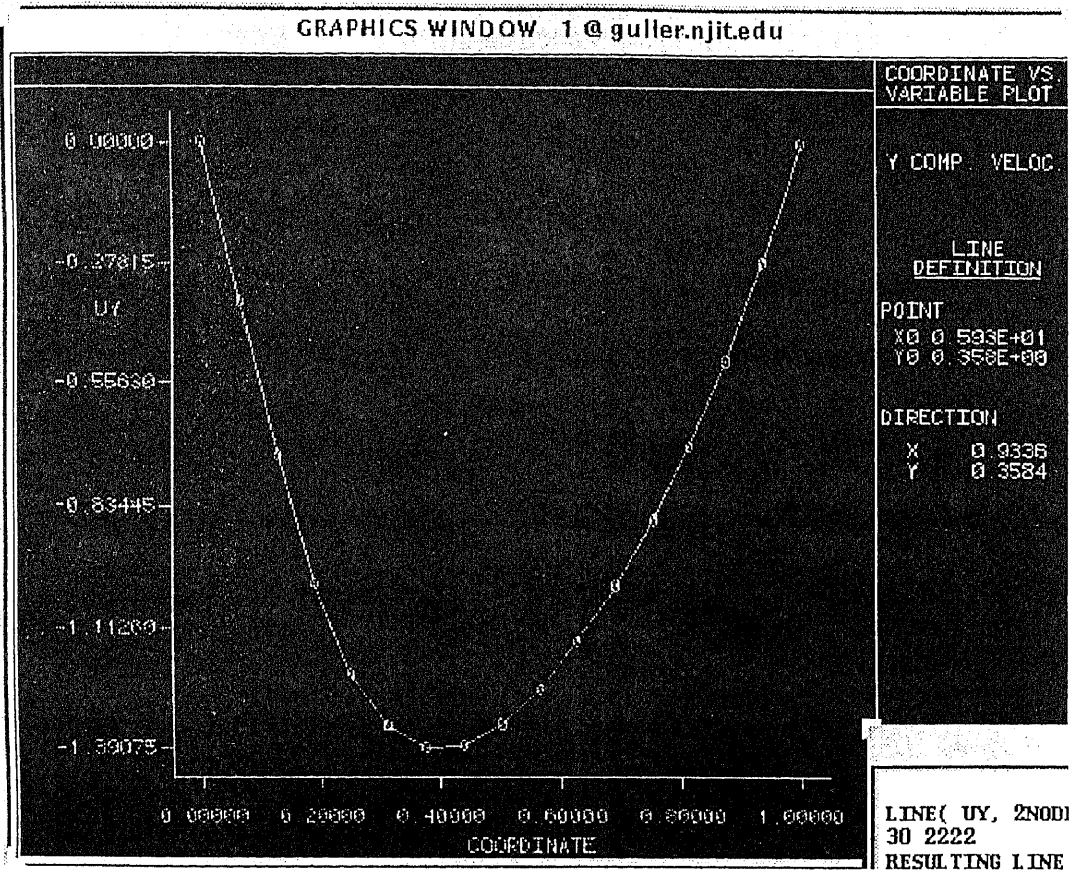
Figure 5.1.55
Y-Component Velocity Distribution for Line 30 2222
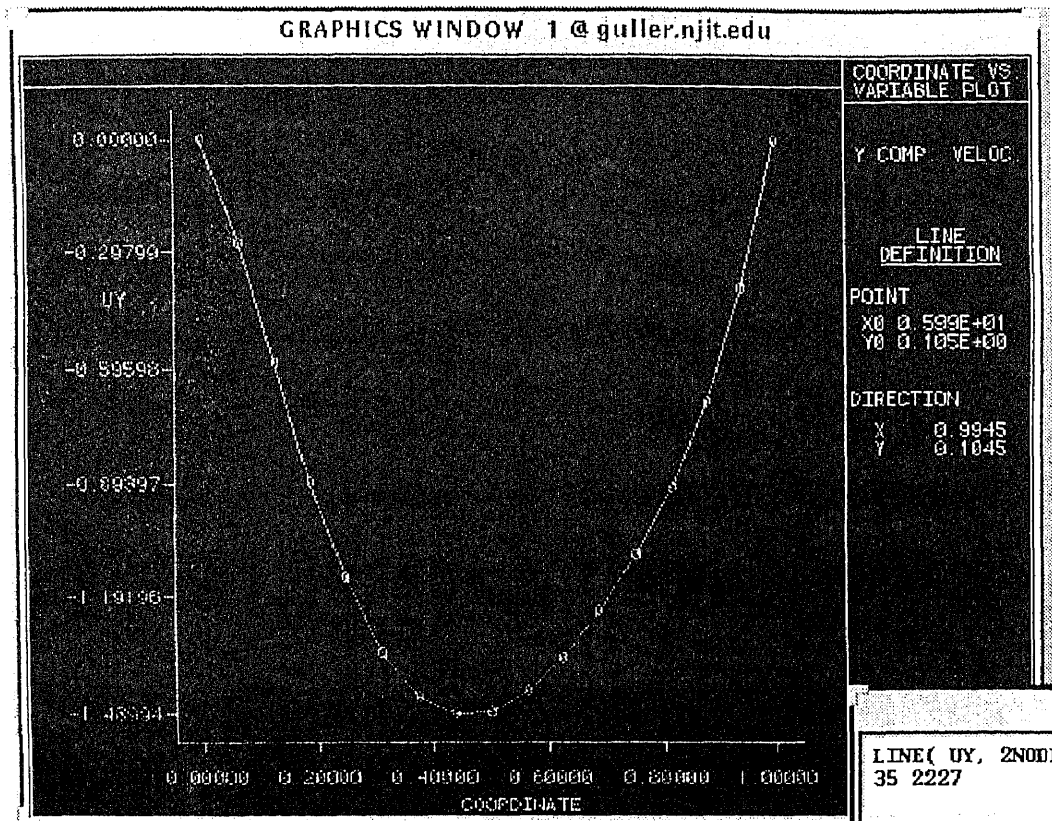
Figure 5.1.56
Y-Component Velocity Distribution for Line 35 2227
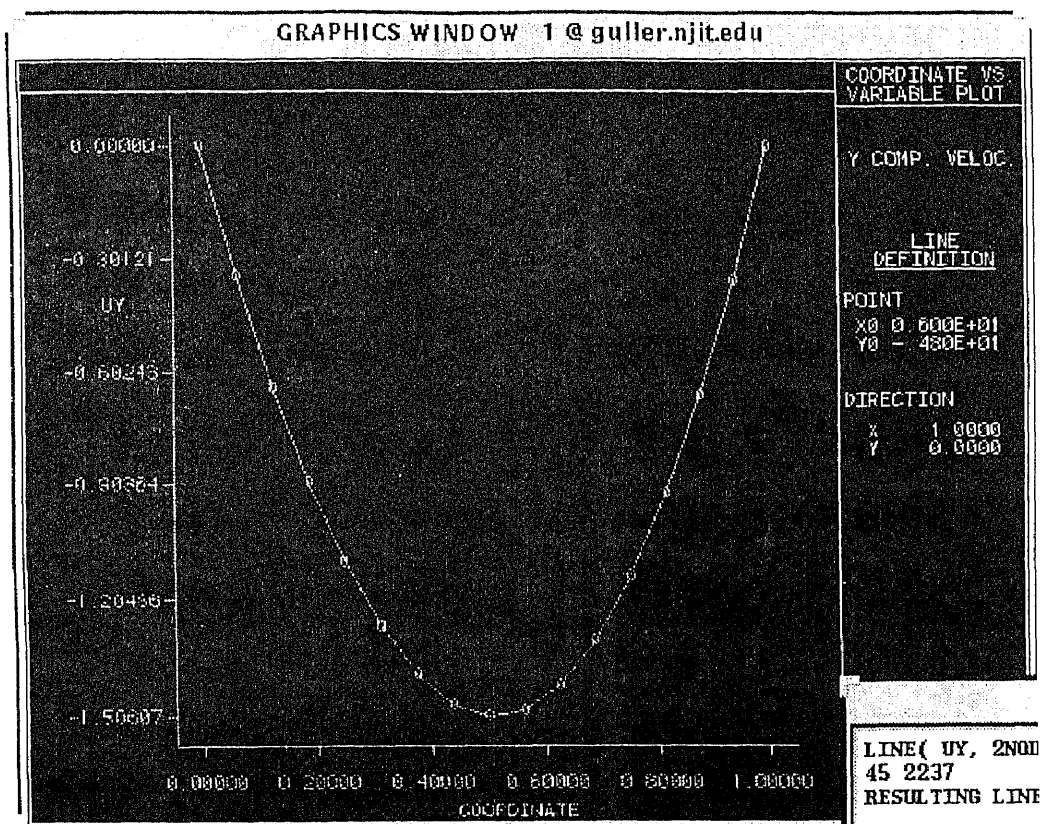
Figure 5.1.57
Y-Component Velocity Distribution for Line 45 2237
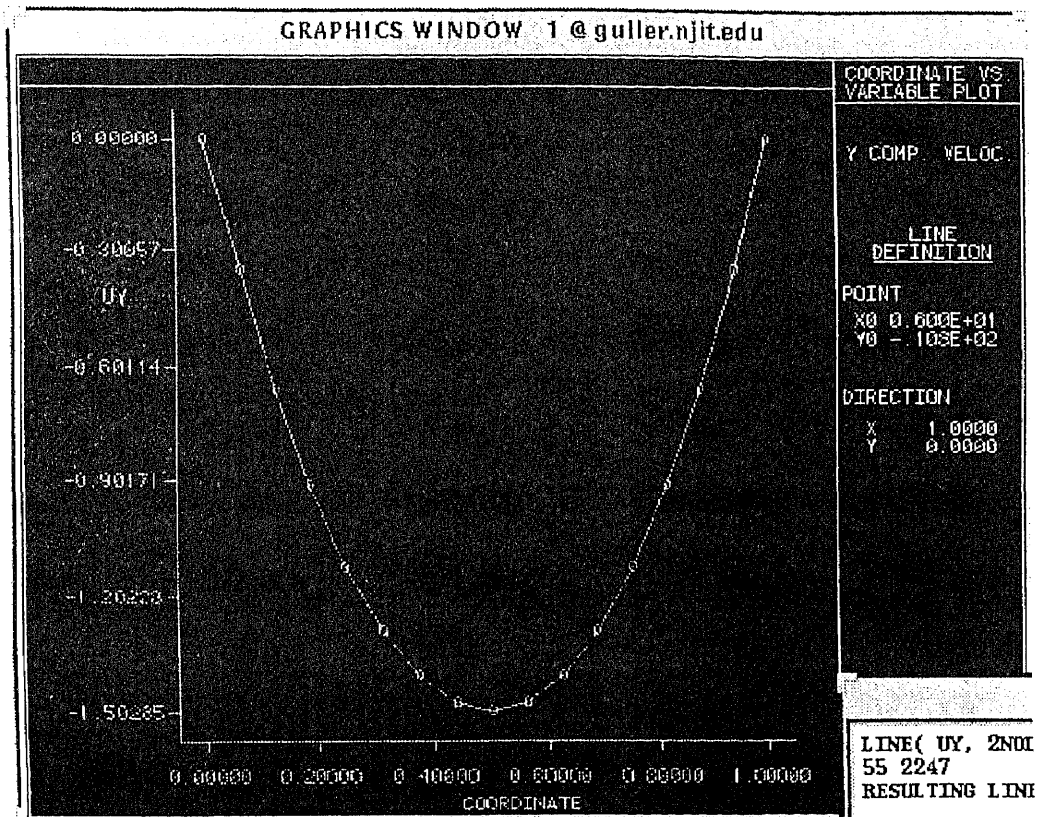
Figure 5.1.58
Y-Component Velocity Distribution for Line 55 2247
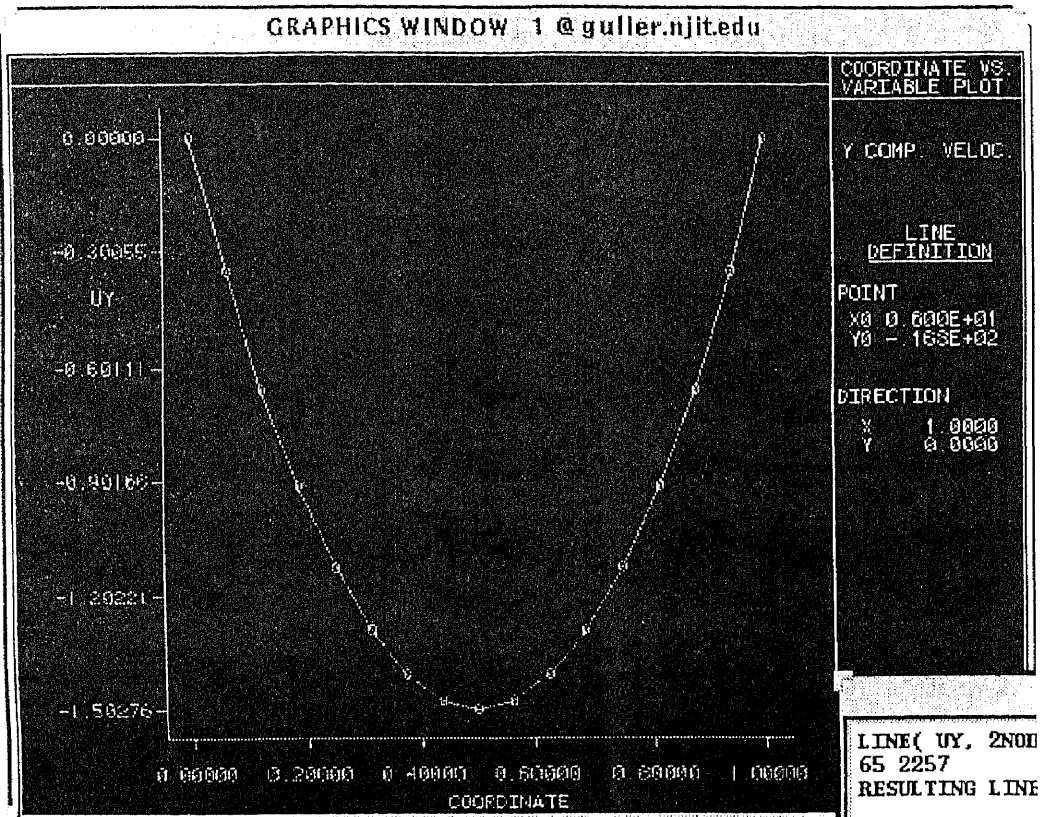
Figure 5.1.59
Y-Component Velocity Distribution for Line 65 2257
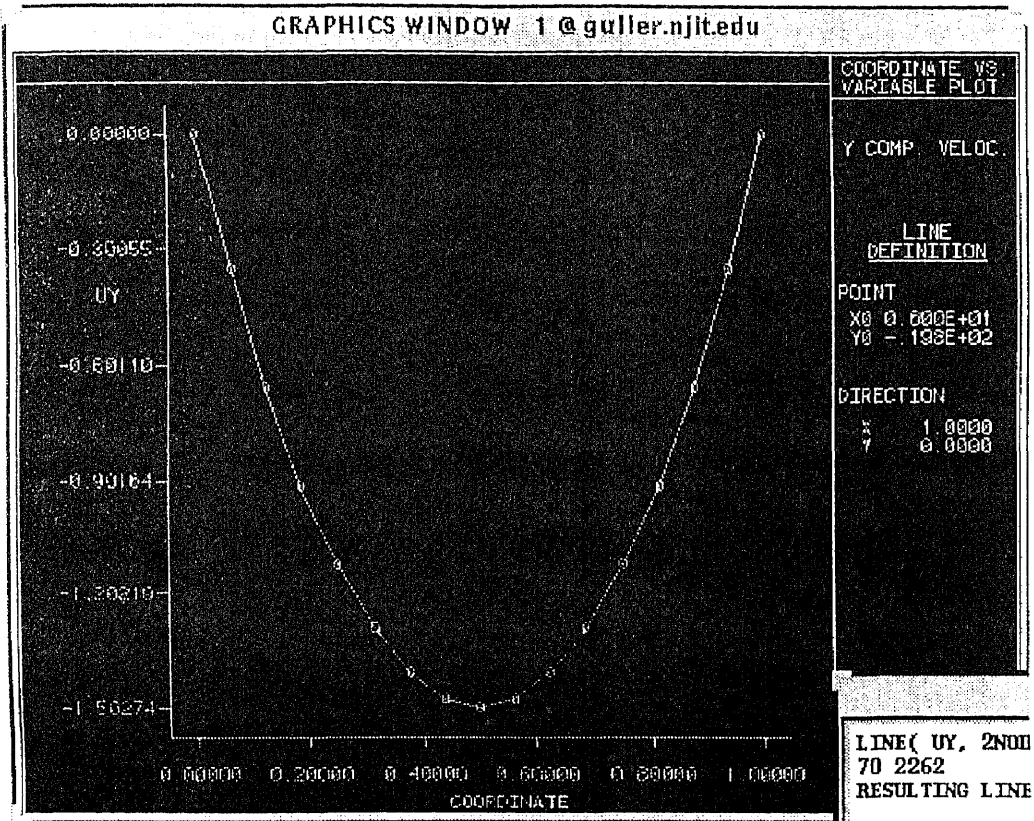
Figure 5.1.60
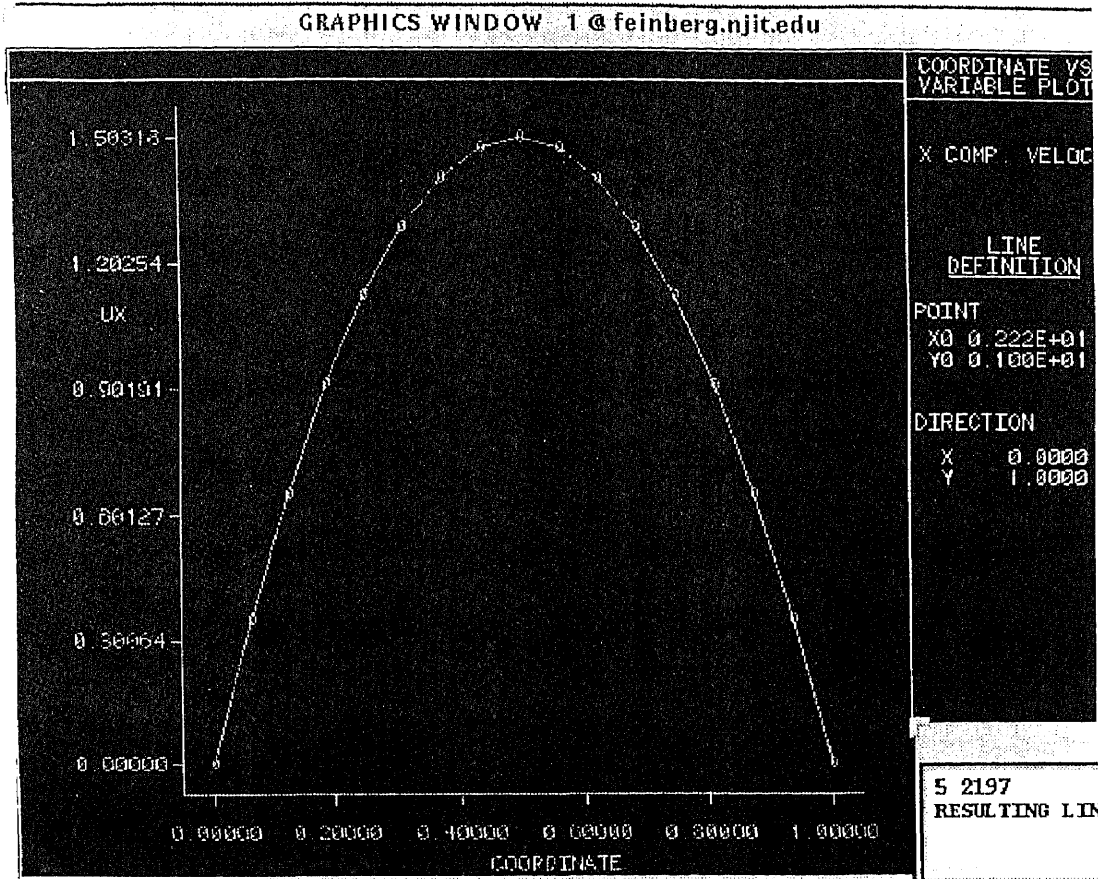**Y-Component Velocity Distribution for Line 70 2262**
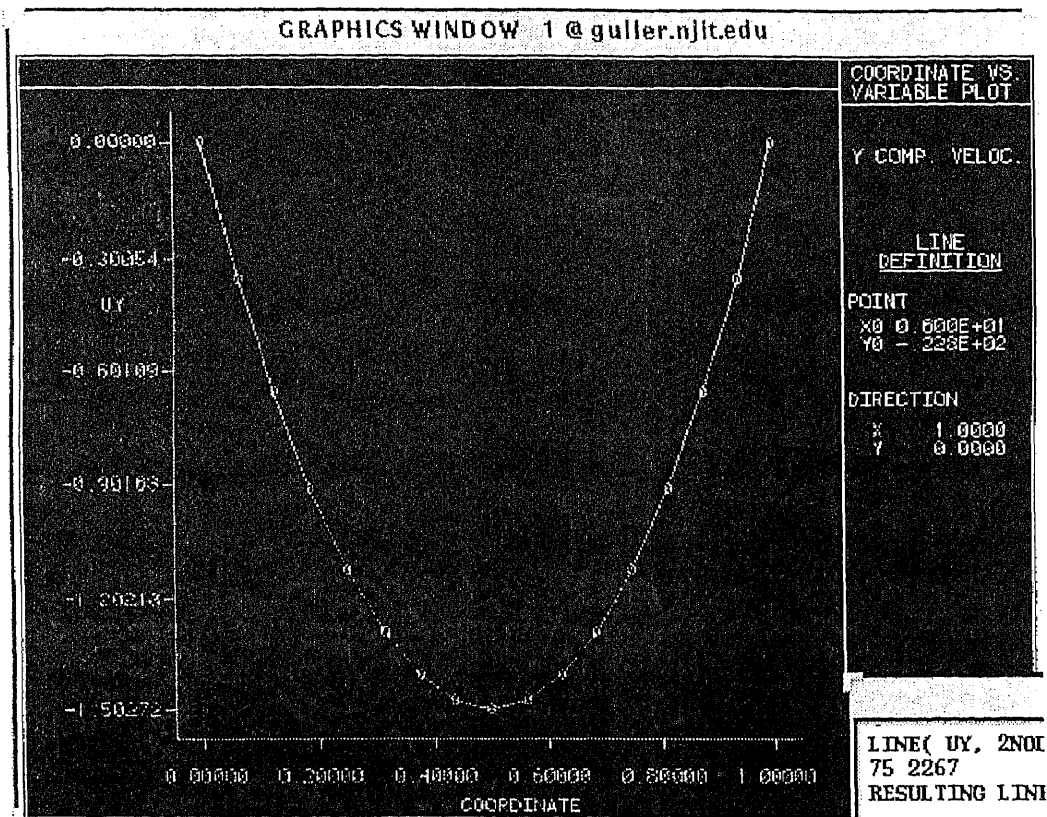
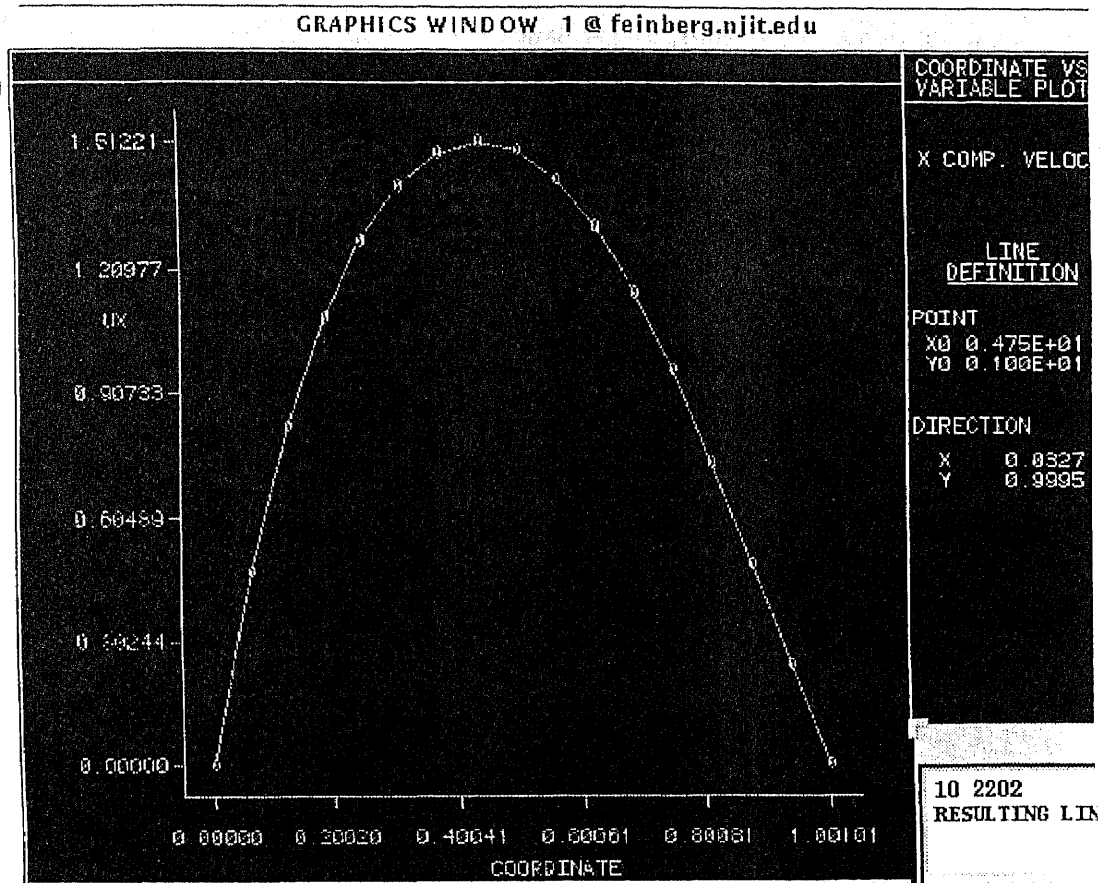Figure 5.1.61
Y-Component Velocity Distribution for Line 75 2267
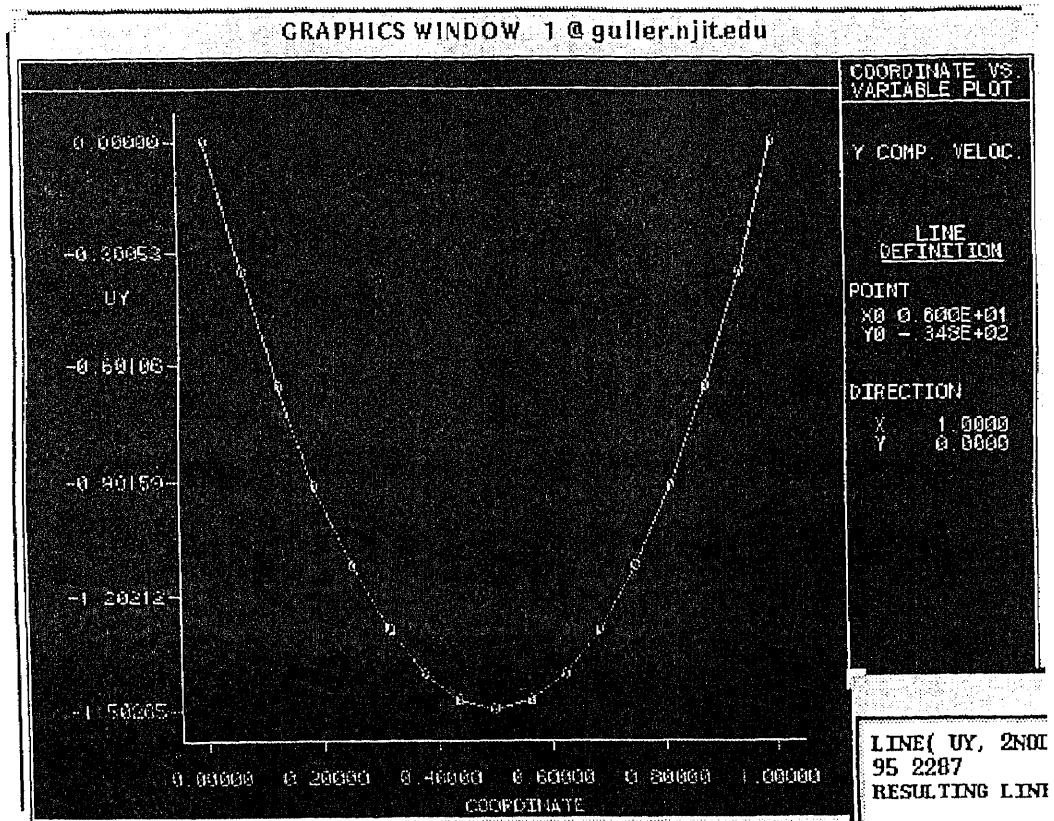
Figure 5.1.62
Y-Component Velocity Distribution for Line 95 2287
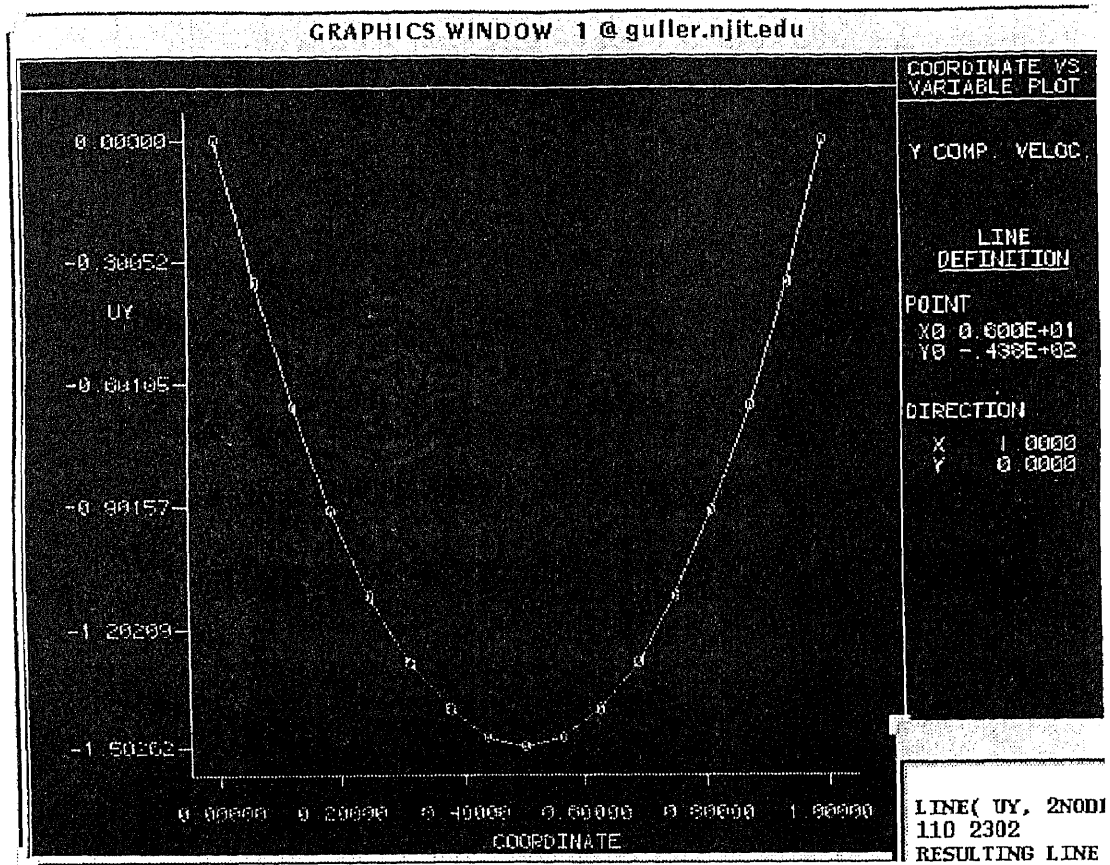
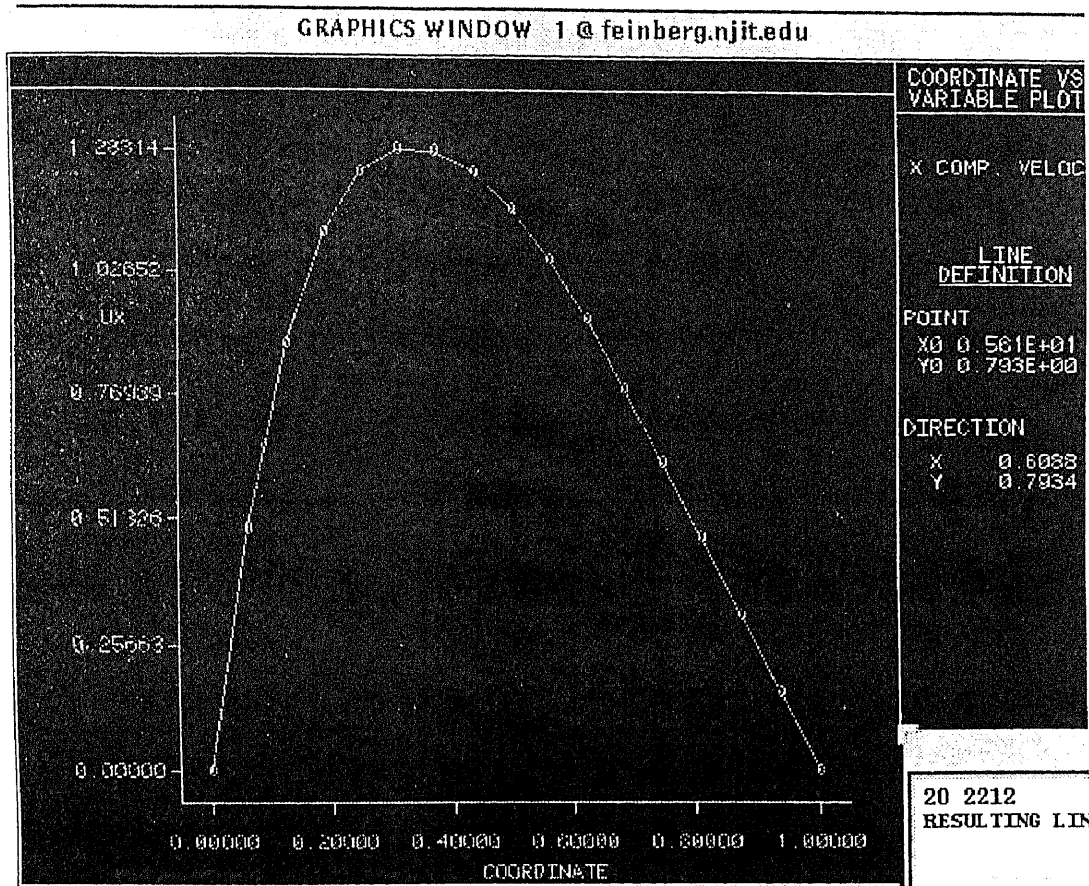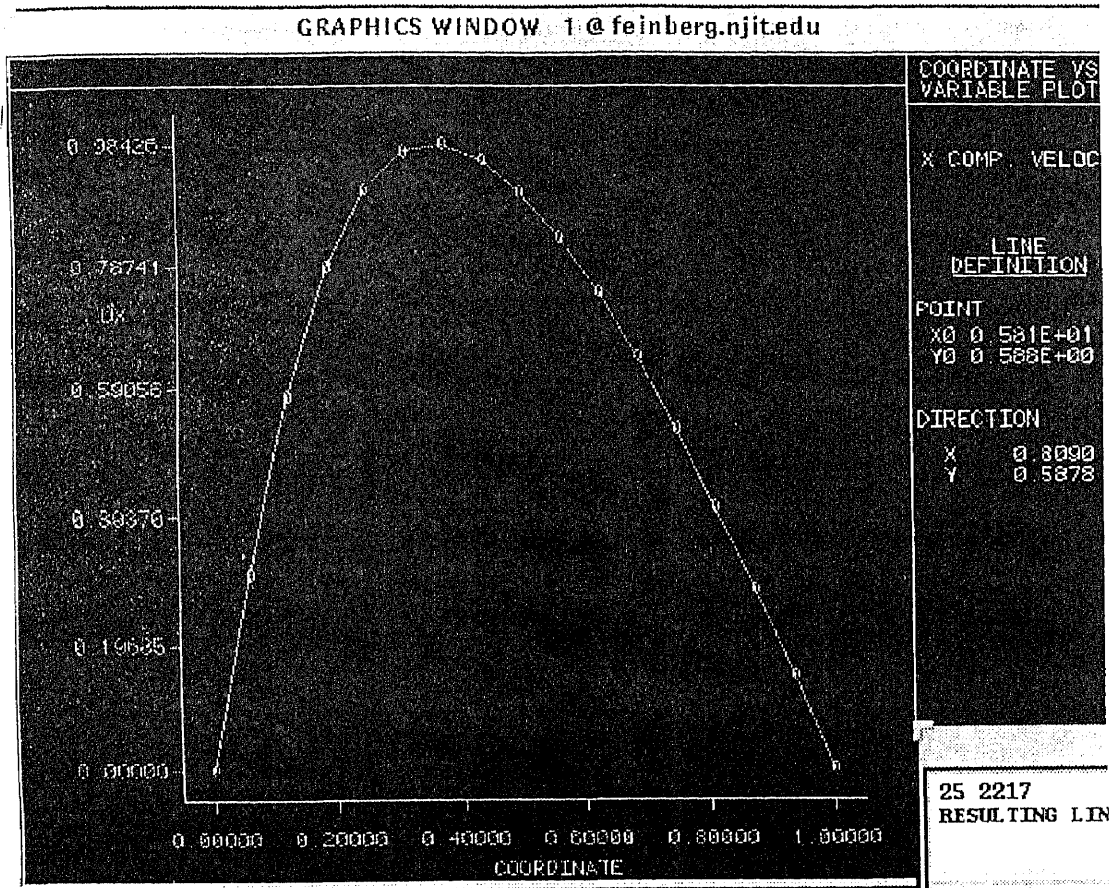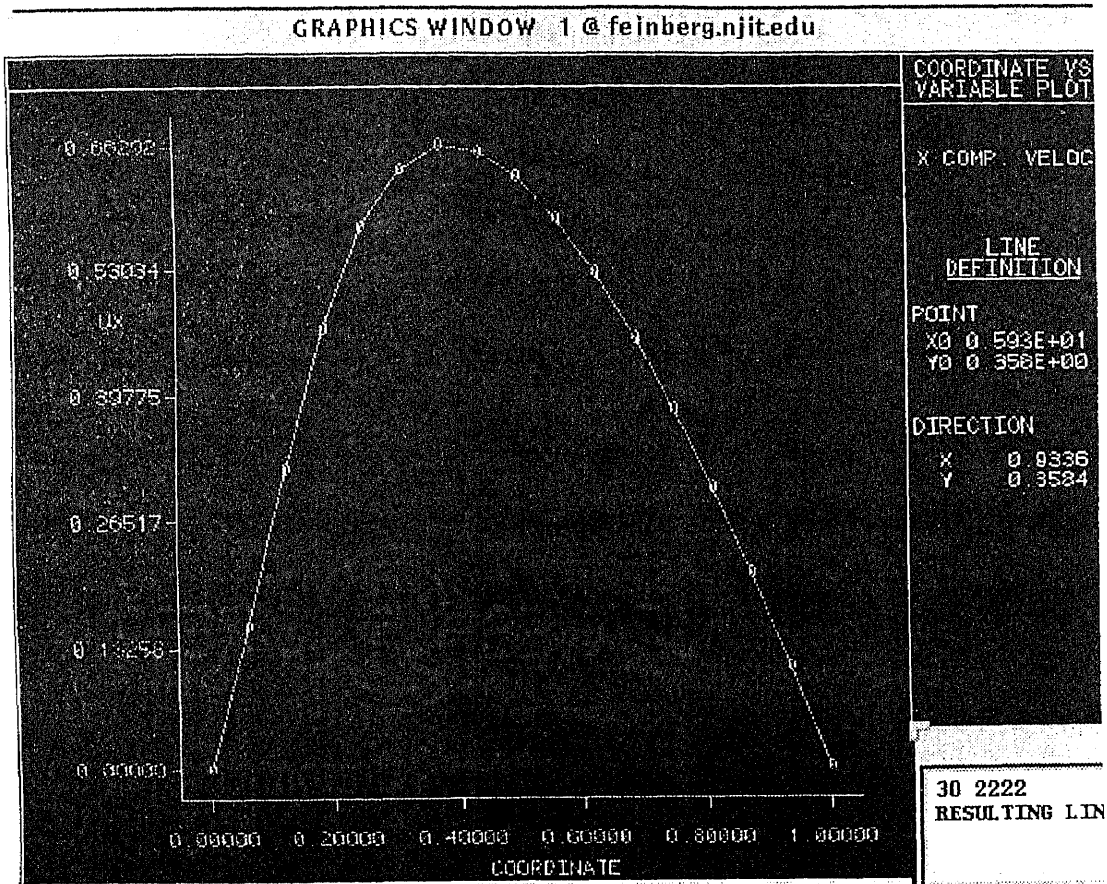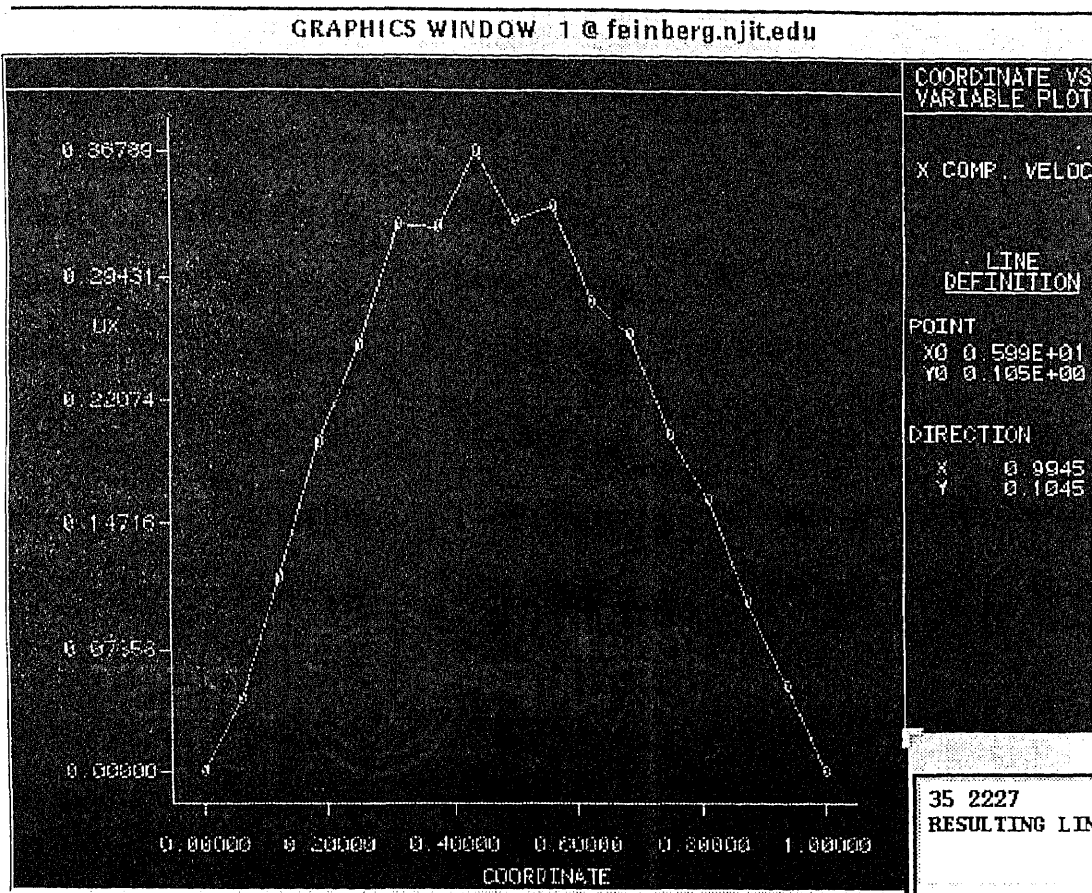**Figure 5.1.63**
Y-Component Velocity Distribution for Line 110 2302
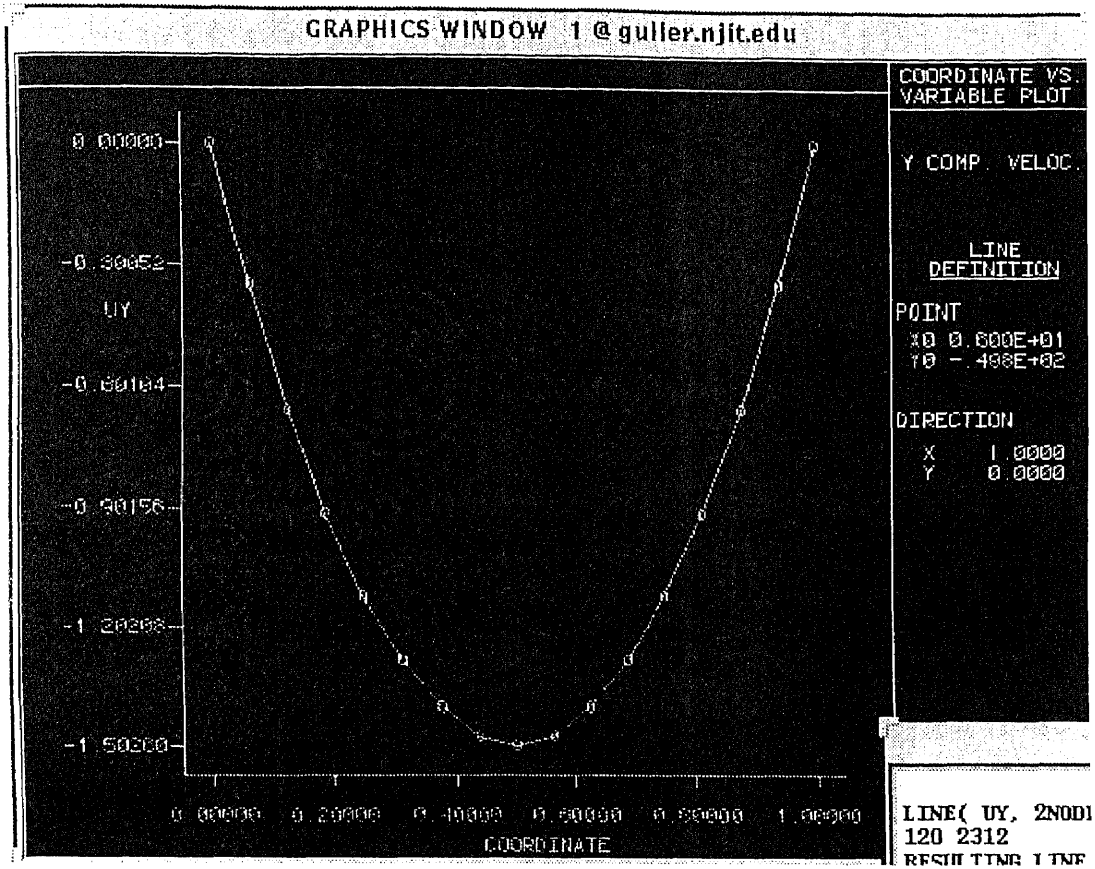
Figure 5.1.64
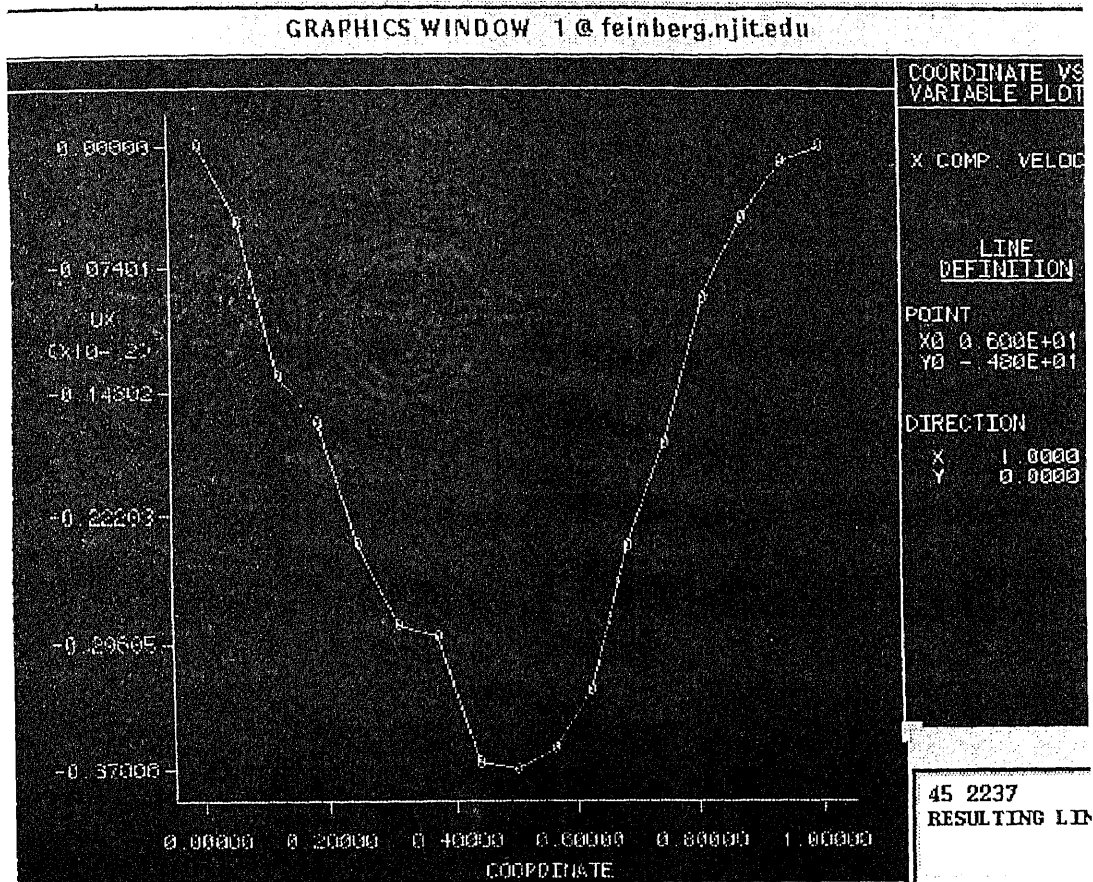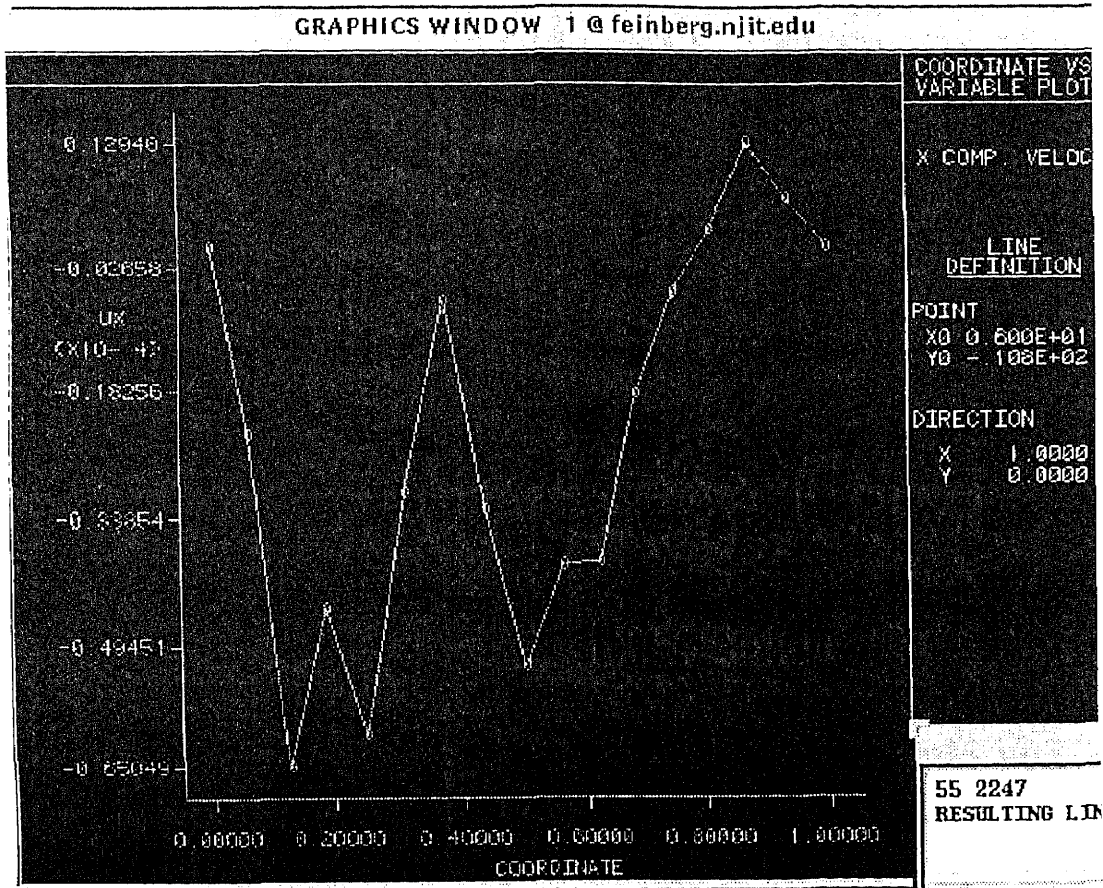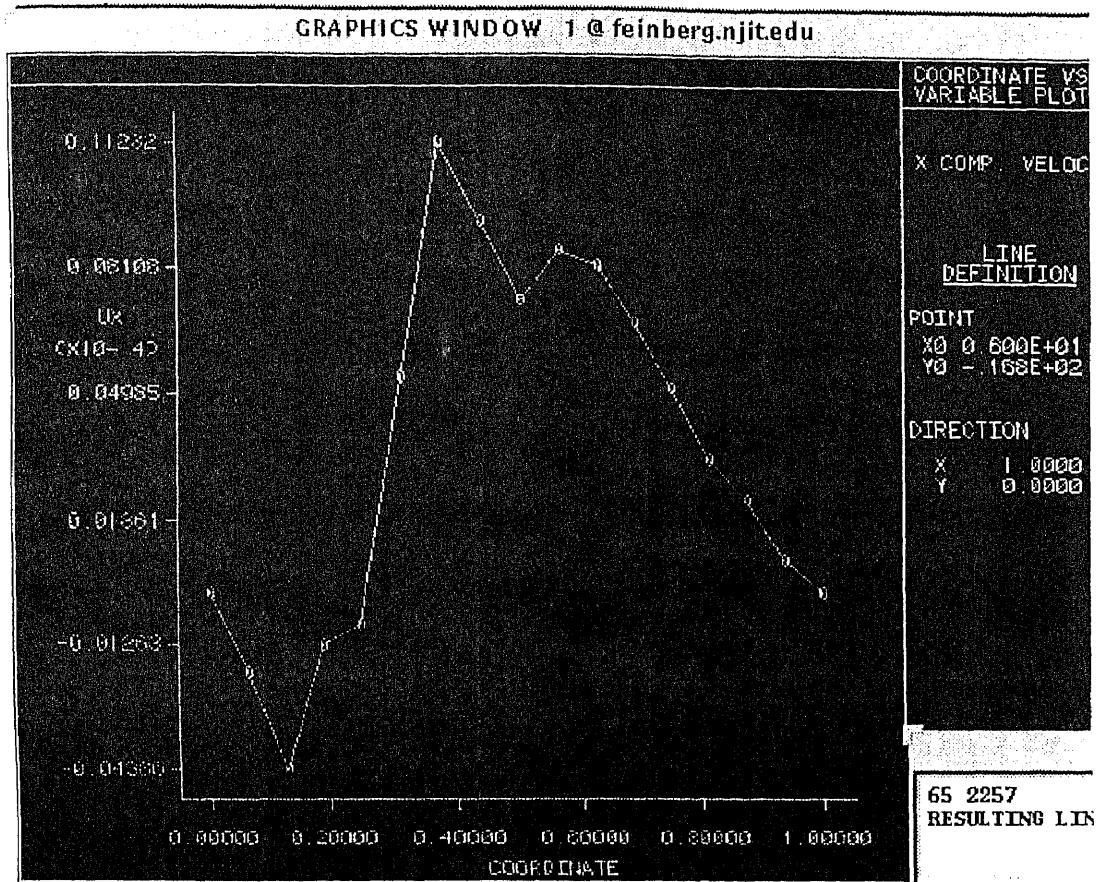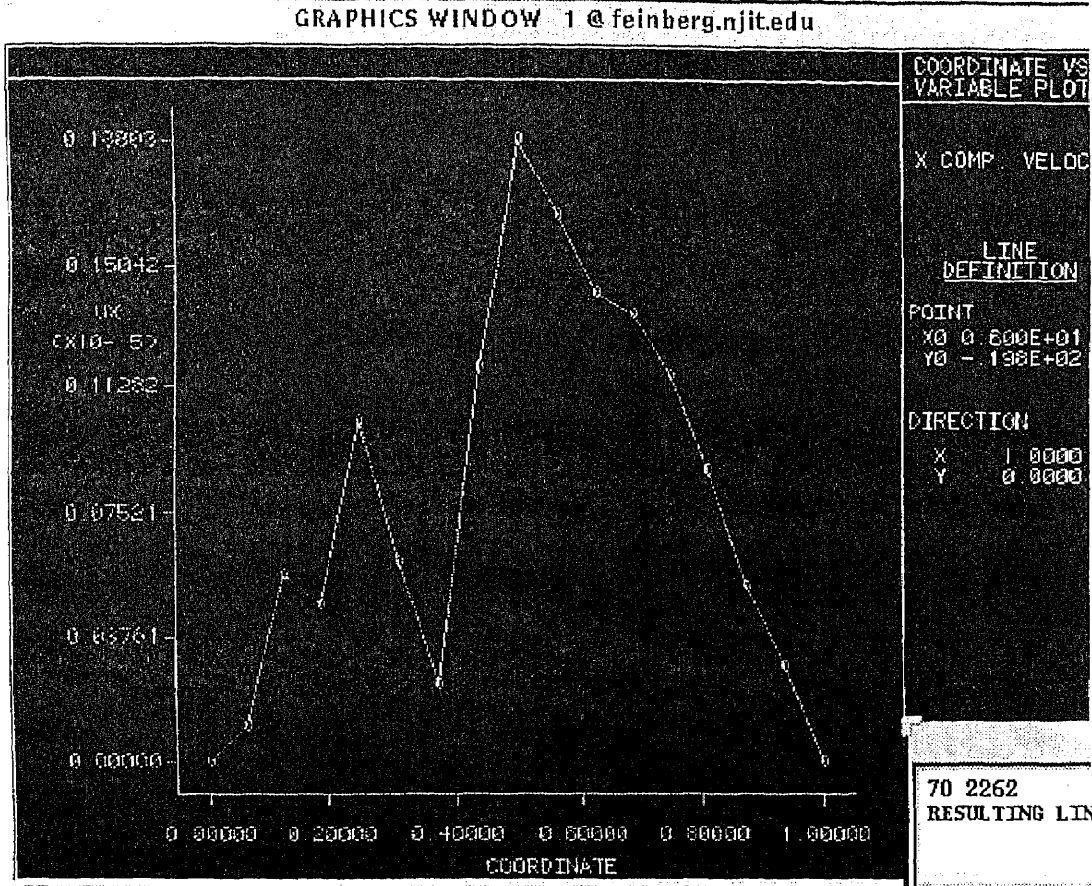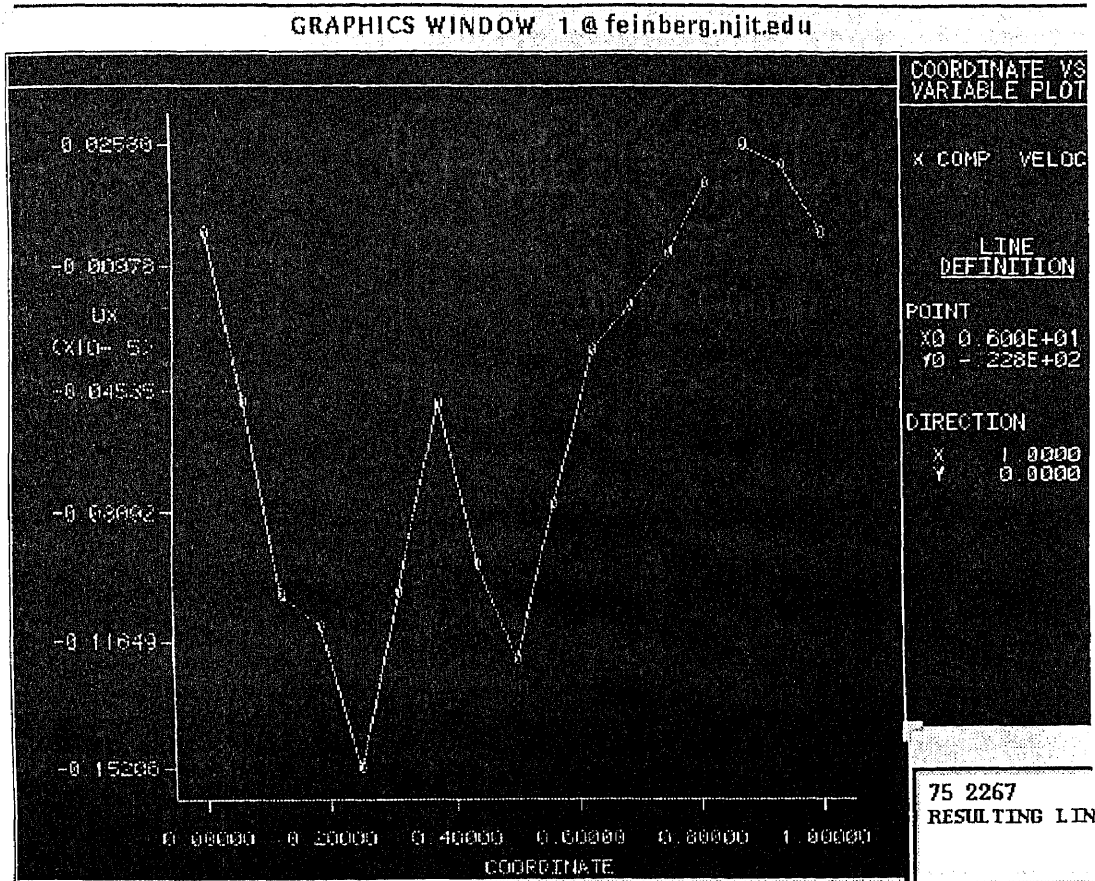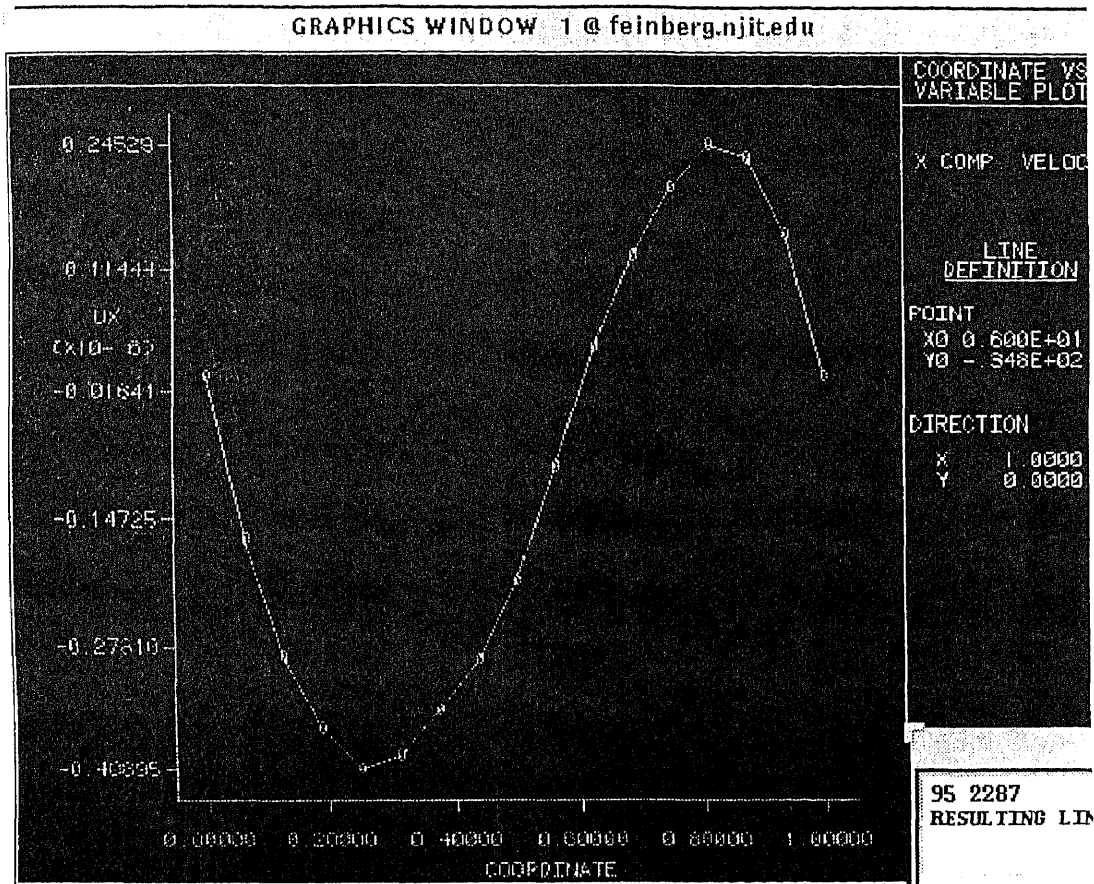**Y-Component Velocity Distribution for Line 120 2312**
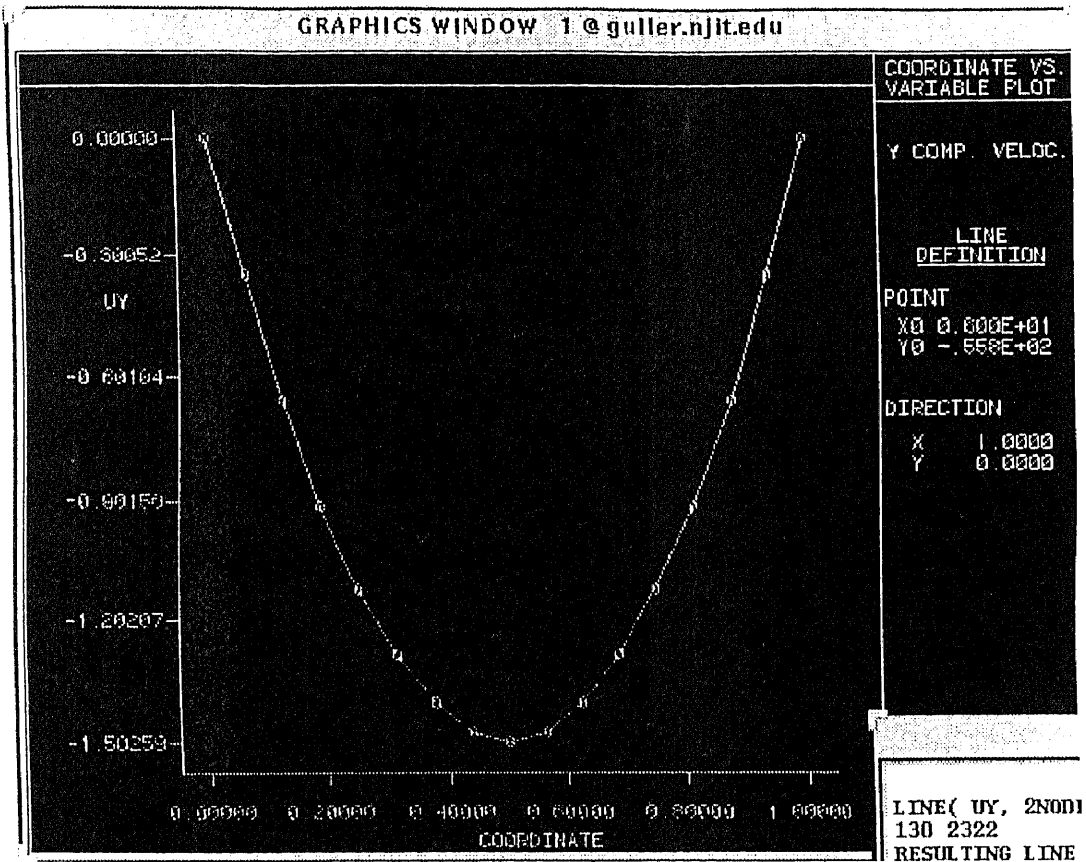
Figure 5.1.65
Y-Component Velocity Distribution for Line 130 2322

Table 5.1.2
Nodal Values for Pressure and Velocity from FIDAP

LINE	0	0.0625	0.125	0.1875	0.25	0.3125	0.375	0.4375	0.5
			PRESSURE						
1 2193	9.2607	9.2607	9.2613	9.2616	9.2610	9.2601	9.2591	9.2583	9.2568
5 2197	8.7206	8.7204	8.7204	8.7207	8.7200	8.7201	8.7195	8.7193	8.7193
10 2202	7.5440	7.5482	7.5553	7.6134	7.6729	7.7736	7.8337	7.9785	8.0690
20 2212	5.2855	5.4273	5.5833	6.0132	6.4371	6.8082	7.2927	7.6387	7.9155
25 2217	5.3335	5.4291	5.5285	5.8972	6.2784	6.6917	7.0652	7.5066	7.7783
30 2222	5.5466	5.6012	5.6482	5.9101	6.1912	6.5250	6.8919	7.1671	7.5646
35 2227	5.8191	5.8461	5.8598	5.9947	6.1479	6.3636	6.5864	6.9081	7.1556
45 2237	6.5217	6.5205	6.5195	6.5174	6.5152	6.5078	6.5029	6.4938	6.4869
55 2247	5.8767	5.8766	5.8764	5.8763	5.8761	5.8756	5.8754	5.8748	5.8744
65 2257	5.1810	5.1810	5.1809	5.1809	5.1808	5.1807	5.1806	5.1803	5.1802
70 2262	4.8257	4.8257	4.8257	4.8257	4.8257	4.8257	4.8257	4.8257	4.8257
75 2267	4.4682	4.4682	4.4682	4.4682	4.4682	4.4682	4.4682	4.4682	4.4682
95 2287	3.0293	3.0293	3.0293	3.0293	3.0293	3.0293	3.0293	3.0293	3.0293
110 2302	1.9476	1.9476	1.9476	1.9476	1.9476	1.9476	1.9476	1.9476	1.9476
120 2312	1.2263	1.2263	1.2263	1.2263	1.2263	1.2263	1.2263	1.2263	1.2263
130 2322	0.5050	0.5050	0.5050	0.5050	0.5050	0.5050	0.5050	0.5050	0.5050

Table 5.1.2
(Continued)
Nodal Values for Pressure and Velocity from FIDAP

0.5625	0.625	0.6875	0.75	0.8125	0.875	0.9375	1
9.2561	9.2556	9.2555	9.2563	9.2567	9.2569	9.2568	9.2568
8.7193	8.7200	8.7204	8.7215	8.7220	8.7225	8.7229	8.7228
8.0872	8.1957	8.2682	8.3768	8.3949	8.4129	8.4129	8.4129
8.1924	8.4000	8.5039	8.6423	8.7112	8.7462	8.7462	8.7462
8.0499	8.1858	8.2876	8.4235	8.4574	8.4914	8.4914	8.4914
7.7480	8.0844	8.1761	8.4146	8.4452	8.4819	8.4971	8.5124
7.4526	7.7249	7.7992	8.0442	8.1184	8.1679	8.1803	8.1952
6.4799	6.4716	6.4656	6.4594	6.4566	6.4538	6.4535	6.4521
5.8739	5.8733	5.8730	5.8728	5.8727	5.8726	5.8725	5.8724
5.1801	5.1799	5.1799	5.1799	5.1799	5.1799	5.1799	5.1799
4.8257	4.8257	4.8257	4.8257	4.8257	4.8257	4.8257	4.8257
4.4682	4.4682	4.4682	4.4682	4.4682	4.4682	4.4682	4.4682
3.0293	3.0293	3.0293	3.0293	3.0293	3.0293	3.0293	3.0293
1.9476	1.9476	1.9476	1.9476	1.9476	1.9476	1.9476	1.9476
1.2263	1.2263	1.2263	1.2263	1.2263	1.2263	1.2263	1.2263
0.5050	0.5050	0.5050	0.5050	0.5050	0.5050	0.5050	0.5050

Table 5.1.2
(Continued)
Nodal Values for Pressure and Velocity from FIDAP

LINE	0	0.0625	0.125	0.1875	0.25	0.3125	0.375	0.4375	0.5
			X-DIRECTION VELOCITY						
1 2193	0.00000	0.70453	1.31512	1.83178	2.25450	2.58328	2.81812	2.95903	3.00600
5 2197	0.00000	0.69960	1.31261	1.83351	2.25608	2.58901	2.82109	2.96203	3.00619
10 2202	0.00000	1.07434	1.77690	2.30899	2.64087	2.88139	3.00888	3.03676	2.97969
20 2212	0.00000	1.22020	2.05239	2.43154	2.59018	2.62915	2.58674	2.46855	2.28755
25 2217	0.00000	0.71612	1.36009	1.77667	1.97352	2.04128	2.02460	1.95455	1.82604
30 2222	0.00000	0.33115	0.74294	1.08326	1.30555	1.38865	1.41856	1.37557	1.31205
35 2227	0.00000	0.08762	0.25833	0.48645	0.60469	0.78047	0.75199	0.82591	0.72578
45 2237	0.00000	0.00403	0.01509	0.02734	0.03766	0.04405	0.04991	0.05053	0.05092
55 2247	0.00000	0.00046	0.00175	0.00356	0.00570	0.00755	0.00895	0.00948	0.00926
65 2257	0.00000	0.00016	0.00063	0.00130	0.00209	0.00283	0.00339	0.00363	0.00355
70 2262	0.00000	0.00010	0.00024	0.00081	0.00131	0.00178	0.00214	0.00231	0.00225
75 2267	0.00000	0.00006	0.00025	0.00051	0.00082	0.00111	0.00134	0.00145	0.00143
95 2287	0.00000	0.00001	0.00003	0.00007	0.00011	0.00015	0.00019	0.00020	0.00020
110 2302	0.00000	0.00000	0.00001	0.00001	0.00002	0.00003	0.00003	0.00004	0.00004
120 2312	0.00000	0.00000	0.00000	0.00000	0.00001	0.00001	0.00001	0.00001	0.00001
130 2322	0.00000	0.00000	0.00000	0.00000	0.00000	0.00000	0.00000	0.00000	0.00000

Table 5.1.2
(Continued)
Nodal Values for Pressure and Velocity from FIDAP

0.5625	0.625	0.6875	0.75	0.8125	0.875	0.9375	1
2.95903	2.81812	2.58328	2.25450	1.83178	1.31512	0.70453	0.00000
2.96203	2.82109	2.58901	2.25608	1.83351	1.31261	0.69960	0.00000
2.81521	2.57964	2.23961	1.83733	1.36624	0.87163	0.40055	0.00000
2.04568	1.75673	1.43210	1.09782	0.77422	0.48235	0.22509	0.00000
1.65498	1.44385	1.20536	0.95519	0.70651	0.46704	0.23540	0.00000
1.19725	1.06712	0.90591	0.73843	0.56362	0.38777	0.20317	0.00000
0.73225	0.60326	0.55821	0.42108	0.34267	0.21183	0.11118	0.00000
0.05039	0.04541	0.04095	0.03158	0.01948	0.01047	0.00189	0.00000
0.00811	0.00675	0.00481	0.00309	0.00159	0.00059	0.00011	0.00000
0.00314	0.00252	0.00180	0.00114	0.00060	0.00024	0.00005	0.00000
0.00200	0.00161	0.00116	0.00070	0.00040	0.00016	0.00004	0.00000
0.00127	0.00103	0.00075	0.00050	0.00030	0.00011	0.00002	0.00000
0.00018	0.00015	0.00011	0.00010	0.00001	0.00002	0.00000	0.00000
0.00001	0.00001	0.00000	0.00001	0.00000	0.00001	0.00000	0.00000
0.00000	0.00000	0.00000	0.00000	0.00000	0.00000	0.00000	0.00000
0.00000	0.00000	0.00000	0.00000	0.00000	0.00000	0.00000	0.00000

Table 5.1.2

(Continued)

Nodal Values for Pressure and Velocity from FIDAP

LINE	0	0.0625	0.125	0.1875	0.25	0.3125	0.375	0.4375	0.5
				Y-DIRECTION VELOCITY					
1 2193	0.00000	0.00000	0.00000	0.00000	0.00000	0.00000	0.00000	0.00000	0.00000
5 2197	0.00000	0.00285	0.00641	0.00019	0.01547	0.00412	0.01558	0.00617	0.01142
10 2202	0.00000	0.02318	0.08200	0.17078	0.18491	0.27049	0.24902	0.30695	0.26304
20 2212	0.00000	0.88739	1.44726	1.70638	1.81461	1.85478	1.82136	1.74614	1.61385
25 2217	0.00000	0.91276	1.66310	2.13591	2.37209	2.43900	2.43884	2.34582	2.20664
30 2222	0.00000	0.73726	1.54737	2.18898	2.58894	2.77120	2.81518	2.77462	2.64621
35 2227	0.00000	0.43189	1.08559	1.84255	2.42272	2.79501	2.99245	3.03051	2.98997
45 2237	0.00000	0.54047	1.02970	1.48982	1.93163	2.33962	2.68575	2.93699	3.08163
55 2247	0.00000	0.66210	1.23821	1.73307	2.15175	2.49636	2.76420	2.94807	3.03867
65 2257	0.00000	0.68865	1.28605	1.79395	2.22143	2.54837	2.79554	2.95336	3.01798
70 2262	0.00000	0.69480	1.29724	1.80839	2.22950	2.56136	2.80370	2.95505	3.01303
75 2267	0.00000	0.69861	1.30420	1.81744	2.22391	2.56965	2.80901	2.95629	3.01004
95 2287	0.00000	0.70377	1.31372	1.82991	2.25245	2.58140	2.81677	2.95844	3.00625
110 2302	0.00000	0.70434	1.31477	1.83131	2.25397	2.58276	2.81769	2.95873	3.00585
120 2312	0.00000	0.70442	1.31492	1.83151	2.25418	2.58295	2.81781	2.95876	3.00578
130 2322	0.00000	0.70444	1.31496	1.83156	2.25423	2.58299	2.81784	2.95876	3.00575

Table 5.1.2

(Continued)

Nodal Values for Pressure and Velocity from FIDAP

0.5625	0.625	0.6875	0.75	0.8125	0.875	0.9375	1
0.00000	0.00000	0.00000	0.00000	0.00000	0.00000	0.00000	0.00000
0.00000	0.00000	0.00582	0.00000	0.00230	0.00215	0.00000	0.00000
0.28416	0.22897	0.21068	0.15171	0.10445	0.05356	0.01422	0.00000
1.44527	1.23769	1.00869	0.77337	0.54794	0.34611	0.16565	0.00000
1.99877	1.75374	1.46990	1.17358	0.88193	0.59488	0.31089	0.00000
2.45640	2.20232	1.90719	1.58236	1.24609	0.89410	0.49425	0.00000
2.84900	2.64930	2.37565	2.06383	1.71439	1.30977	0.78343	0.00000
3.11755	3.04633	2.86196	2.54724	2.08480	1.48050	0.77446	0.00000
3.02706	2.90704	2.67589	2.33546	1.89153	1.35102	0.71959	0.00000
2.98538	2.85277	2.61929	2.28607	1.85541	1.32976	0.71098	0.00000
2.97510	2.83950	2.60566	2.27425	1.84668	1.32445	0.70869	0.00000
2.96870	2.83115	2.59701	2.26670	1.84104	1.32096	0.70716	0.00000
2.96000	2.81820	2.58482	2.25588	1.83283	1.31578	0.70482	0.00000
2.95902	2.81801	2.58340	2.25461	1.83185	1.31516	0.70454	0.00000
2.95887	2.81781	2.58319	2.25443	1.83172	1.31507	0.70449	0.00000
2.95876	2.81784	2.58299	2.25423	1.83156	1.31496	0.70444	0.00000

Table 5.1.2
(Continued)
Nodal Values for Pressure and Velocity from FIDAP

LINE	0	0.0625	VELOCITY 0.125	0.1875	0.25	0.3125	0.375	0.4375	0.5
1 2193	0.00000	0.70453	1.31512	1.83178	2.25450	2.58328	2.81812	2.95903	3.00600
5 2197	0.00000	0.69960	1.31263	1.83351	2.25613	2.58901	2.82113	2.96204	3.00621
10 2202	0.00000	1.07459	1.77879	2.31530	2.64734	2.89406	3.01917	3.05223	2.99128
20 2212	0.00000	1.50876	2.51135	2.97054	3.16257	3.21755	3.16363	3.02370	2.79954
25 2217	0.00000	1.16015	2.14843	2.77825	3.08571	3.18049	3.16969	3.05338	2.86421
30 2222	0.00000	0.80821	1.71648	2.44235	2.89949	3.09966	3.15239	3.09689	2.95363
35 2227	0.00000	0.44069	1.11590	1.90568	2.49704	2.90193	3.08549	3.14104	3.07680
45 2237	0.00000	0.54049	1.02981	1.49007	1.93200	2.34003	2.68621	2.93742	3.08205
55 2247	0.00000	0.66210	1.23821	1.73307	2.15176	2.49637	2.76421	2.94809	3.03868
65 2257	0.00000	0.68865	1.28605	1.79395	2.22143	2.54837	2.79554	2.95336	3.01798
70 2262	0.00000	0.69480	1.29724	1.80839	2.22950	2.56136	2.80370	2.95505	3.01303
75 2267	0.00000	0.69861	1.30420	1.81744	2.22391	2.56965	2.80901	2.95629	3.01004
95 2287	0.00000	0.70377	1.31372	1.82991	2.25245	2.58140	2.81677	2.95844	3.00625
110 2302	0.00000	0.70434	1.31477	1.83131	2.25397	2.58276	2.81769	2.95873	3.00585
120 2312	0.00000	0.70442	1.31492	1.83151	2.25418	2.58295	2.81781	2.95876	3.00578
130 2322	0.00000	0.70444	1.31496	1.83156	2.25423	2.58299	2.81784	2.95876	3.00575

Table 5.1.2

(Continued)

Nodal Values for Pressure and Velocity from FIDAP

0.5625	0.625	0.6875	0.75	0.8125	0.875	0.9375	1
2.95903	2.81812	2.58328	2.25450	1.83178	1.31512	0.70453	0.00000
2.96203	2.82109	2.58902	2.25608	1.83351	1.31261	0.69960	0.00000
2.82951	2.58978	2.24950	1.84358	1.37023	0.87328	0.40080	0.00000
2.50472	2.14895	1.75168	1.34287	0.94850	0.59368	0.27947	0.00000
2.59500	2.27163	1.90092	1.51317	1.13003	0.75631	0.38996	0.00000
2.73264	2.44723	2.11141	1.74618	1.36763	0.97457	0.53438	0.00000
2.94160	2.71711	2.44035	2.10635	1.74830	1.32679	0.79128	0.00000
3.11796	3.04667	2.86225	2.54744	2.08489	1.48054	0.77446	0.00000
3.02707	2.90705	2.67589	2.33546	1.89153	1.35102	0.71959	0.00000
2.98538	2.85277	2.61929	2.28607	1.85541	1.32976	0.71098	0.00000
2.97510	2.83950	2.60566	2.27425	1.84668	1.32445	0.70869	0.00000
2.96870	2.83115	2.59701	2.26670	1.84104	1.32096	0.70716	0.00000
2.96000	2.81820	2.58482	2.25588	1.83283	1.31578	0.70482	0.00000
2.95902	2.81801	2.58340	2.25461	1.83185	1.31516	0.70454	0.00000
2.95887	2.81781	2.58319	2.25443	1.83172	1.31507	0.70449	0.00000
2.95876	2.81784	2.58299	2.25423	1.83156	1.31496	0.70444	0.00000

Table 5.2.1.a

Complete Calculation Values for Loss Coefficient Determination for a 90° Channel
Bend with a Bend Radius to Duct Width Ratio of 1.5

REYNOLDS NUMBER	VELOCITY MEAN	FRICTION FACTOR	KF	DELTA P ST. LENGTH	INLET PRESSURE	OUTLET PRESSURE	DELTA P TOTAL	DELTA P BEND	KB R/D=1.5
50									
100					LINE 1 2193	LINE 130 2322			
150	0.251	1.92	58.33	1.82888	1.99805	0.12630	1.87175	0.04287	1.36733
200	0.501	0.96	29.17	3.65776	4.05561	0.25260	3.80301	0.14525	1.15817
250	0.752	0.64	19.44	5.48664	6.09842	0.37874	5.71968	0.23304	0.82585
300	1.002	0.48	14.59	7.31065	8.15992	0.50487	7.65505	0.34440	0.68743
400	1.253	0.38	11.67	9.13953	10.15403	0.63033	9.52370	0.38417	0.49063
500	1.503	0.32	9.73	10.96841	12.22630	0.75579	11.47052	0.50211	0.44523
600	2.004	0.24	7.30	14.62130	16.45275	1.00974	15.44302	0.82171	0.41004
700	2.505	0.19	5.84	18.27906	20.64790	1.26325	19.38465	1.10559	0.35299
800	3.006	0.16	4.86	21.93195	24.93582	1.51590	23.41992	1.48796	0.33000
900	3.507	0.14	4.17	25.58971	29.30706	1.76855	27.53851	1.94880	0.31748
1000	4.008	0.12	3.65	29.24260	33.63664	2.02120	31.61544	2.37284	0.29601
1100	4.509	0.11	3.24	32.90036	37.96220	2.27385	35.68835	2.78799	0.27477
1200	5.010	0.10	2.92	36.55325	42.25800	2.52650	39.73150	3.17825	0.25375
1400	5.511	0.09	2.65	40.21101	46.62380	2.77915	43.84465	3.63364	0.23973
1600	6.012	0.08	2.43	43.86390	50.87496	3.03180	47.84316	3.97926	0.22063
1800	7.014	0.07	2.08	51.17455	59.81412	3.53710	56.27702	5.10247	0.20785
	8.016	0.06	1.82	58.48520	68.66328	4.04240	64.62088	6.13568	0.19136
	9.019	0.05	1.62	65.80072	77.98244	4.54770	73.43474	7.63402	0.18809

Table 5.2.1.b

Complete Calculation Values for Loss Coefficient Determination for a 90° Channel
Bend with a Bend Radius to Duct Width Ratio of 1.0

REYNOLDS NUMBER	VELOCITY MEAN	FRICTION FACTOR	KF	DELTA P ST. LENG	INLET PRESSURE	OUTLET PRESSURE	DELTA P TOTAL	DELTA P BEND	KB R/D=1.0
50					LINE 1 2193	LINE 130 2322-			
100	0.125	1.92	47.01	0.36848	0.42560	0.02632	0.39928	0.03080	3.92892
150	0.251	0.96	23.50	0.73697	0.87119	0.05263	0.81856	0.08159	2.60234
200	0.376	0.64	15.67	1.10545	1.30679	0.07895	1.22784	0.12239	1.73489
250	0.501	0.48	11.75	1.47393	1.86159	0.21053	1.65106	0.17712	1.41229
300	0.627	0.38	9.40	1.84241	2.35854	0.26306	2.09548	0.25307	1.29142
400	0.751	0.32	7.84	2.20894	2.81352	0.31558	2.49794	0.28900	1.02597
500	1.002	0.24	5.88	2.94590	3.85706	0.42091	3.43614	0.49024	0.97853
600	1.253	0.19	4.70	3.68287	4.89965	0.52624	4.37341	0.69054	0.88190
700	1.503	0.16	3.92	4.41984	5.98736	0.63157	5.35579	0.93596	0.82994
800	1.754	0.14	3.36	5.15680	7.03654	0.73676	6.29978	1.14298	0.74452
900	2.004	0.12	2.94	5.89181	8.16534	0.84195	7.32339	1.43158	0.71437
1000	2.255	0.11	2.61	6.62877	9.32654	0.94728	8.37926	1.75048	0.69007
1100	2.505	0.10	2.35	7.36574	10.49381	1.05261	9.44119	2.07545	0.66265
1200	2.756	0.09	2.14	8.10270	11.70243	1.15780	10.54462	2.44192	0.64428
1400	3.006	0.08	1.96	8.83771	12.85988	1.26300	11.59689	2.75918	0.61193
1600	3.507	0.07	1.68	10.31164	15.26927	1.47366	13.79561	3.48397	0.56757
1800	4.008	0.06	1.47	11.78361	17.71626	1.68404	16.03222	4.24861	0.53002
	4.509	0.05	1.31	13.25755	20.20657	1.89470	18.31187	5.05432	0.49813

REFERENCES

Hawthorn, W.R. *Fluid Mechanics of Internal Flow*. Elsevier Publishing Company, NY (1967): 205-207

Smith, A.J. *Pressure Losses in Ducted Flows*. Ward, J.W. Arrowsmith Ltd, Bristol England (1971): 76-77

Benedict, Robert P. *Fundamentals of Pipe Flow*. John Wiley & Sons, NY (1980): 145-148

Ward-Smith, A.J. *Internal Fluid Flow: The Fluid Dynamics of Flow in Pipes and Ducts*. Clarendon Press, Oxford, England (1980): 110-111

Ninomiya, H. *Flow Analysis Using a PC*. CRC Press, Inc., Boston, MA (1991): 87-88:101-110

Johnson, Frederick *FIDAP User's Manual*. Fluid Dynamics International, Inc. (1993)

Jackson, Mike L.*Fluid Mechanics*. Genium Publishing (1984)

White, Frank M. *Fluid Mechanics*. McGraw-Hill Book Company, New York, NY (1986):215-218.

White, Frank M. *Viscous Fluid Flow*. McGraw-Hill Book Company, New York, NY (1991):189-191.

General Electric Co. *Fluid Flow: Data Book*. Husmer R. Norris Schenectady, NY (1970): 101-105

Ding Sun 1995 "Particle Deposition on Surfaces in Divergant Channel Flow." Ph.D. Dissertation Department of Mechanical Engineering, New Jersey Institute of Technology, Newark, NJ.

Crane Co., "Resistance of Bends" *Flow of Fluids Through Valves, Fittings & Pipes* New York, NY (1969): 2.12-2-14.

TRW Systems Group "Pressure Losses in Hoses, Bends, and Ducts", *Aerospace Fluid Component Designer's Handbook* Glen W. Howell Rodondo Beach, CA (1970):86-87.